Estimation of Magnetic Anisotropy in Ferromagnetic Elements and Their Alloy Powders by the Law of Approach to Saturation (LAS)

by

Alex A. Paul

A thesis in partial fulfillment
of the requirements for the degree of
Master of Science in Engineering
(Mechanical Engineering)
in the University of Michigan-Dearborn
2020

Master's Thesis Committee:

Assistant Professor Tanjore V. Jayaraman, Chair
Professor Pravansu Mohanty
Associate Professor German Reyes-Villanueva

Acknowledgements

There is an old saying in Sanskrit “Matha, Pitha, Guru, Deivam” which translates to Mother, Father, Teacher, God; an indication to how important the people who play these roles are in an individuals life. So, I would like to start by acknowledging my parents, Mrs. Lyla Paul and Mr. Paul Abraham for their unfailing love and constant motivation for pushing me towards goals I thought were impossible to achieve.

On the note of ‘Guru’ I would like to thank my thesis advisor Prof. Tanjore Jayaraman who has been guiding, mentoring and teaching me since day one of my Master’s journey. ‘Patience’ is the word most apt to describe Dr. Jay, always eager and happy to help, being just a call/email away to clear doubts and frustrations from an overly persistent student. He has been a constant support, even during these tough times, always making sure that I am are doing well and on track to achieve my academic goals.

On the same note of ‘Gurus’ I would also like to thank my thesis committee members Prof. Pravansu Mohanty and Prof. German Reyes-Villanueva for attending my thesis defense and imparting me with helpful feedback and knowledge. I would also like to thank the University of Michigan-Dearborn and the Mechanical Engineering Department for their support and help in completing my thesis.

And lastly, I would like to thank God. May God bless us all.

Table of Contents

List of Figures

List of Tables

Abstract

This thesis work proposes to characterize the magnetic properties of elemental ferromagnetic powders (Fe, Ni, and Co) and their alloys, evaluate them by the law of approach to saturation, and establish correlations between magnetic anisotropy constant (K) of the alloy powders and their constituent elemental powders. The characterization of their magnetic properties, their dependence on temperature and milling time, the effect of shape anisotropy will be investigated.

The curve fitting of experimental data of magnetization (M) vs. the applied field (H) to several variants of the law of approach to saturation will be analyzed. The dependency and effect of different parameters in the equations and their fit based on statistical linearity, variations to the known M_S values from the M-H curves as well as known trends based on variations in temperatures are studied to infer the behavior of the material in the high field region.

The first order magnetocrystalline anisotropy constant (K_1) was estimated for the elemental powders and their alloys. A correlation between the anisotropy constant (K_1) of the elemental powders and their alloys was established. The dependence of magnetic anisotropy on composition, temperature and milling time is studied. The findings are likely to establish quality control of magnetic alloy powders in additive manufacturing.

Chapter 1. Introduction

The origins of magnetic materials can be traced back to some 2500 years ago when the mineral magnetite was discovered [1]. In 1820 Hans Christian Oersted discovered an electric current produces much stronger magnetic fields than magnetite [1]. Since the discovery, magnets have been used for numerous applications ranging from heavy industrial machinery to commercial handheld electronics. They are considered as one of the fundamental technologies necessary for decreasing the carbon footprint of human society as a whole [2]. Materials can be classified based on the type of magnetism they exhibit as either diamagnetic, paramagnetic, ferromagnetic, antiferromagnetic or ferrimagnetic. Both diamagnetic and paramagnetic materials are essentially considered nonmagnetic as they require an external magnetic field, and the magnitude of the induced moment is minimal for all practical purposes [1]. Ferromagnetism occurs when there is an incomplete cancellation of electron spin or orbital magnetic moment, and these materials possess an intense magnetic moment even in the absence of an external field. Ferromagnetic materials are mostly transition metals with incomplete electron shells. Antiferromagnetism occurs in materials with the opposite alignment of electron spins, which results in zero net magnetic moments; this is exhibited by certain ceramics such as manganese oxide, iron oxide and so on. Ferrimagnetism occurs in ceramics with cubic ferrite structure, which leads to a net magnetic moment due to aligned magnetic moments of Fe atoms. The figure below gives a graphical representation of the different types of magnetization.

For most practical purposes, ferromagnetic materials are the focus of research, and they form the base for modern magnetic materials [3] [4]. The word hysteresis means “to lag”. Hysteresis loops commonly represent the magnetic behavior of ferromagnetic materials. A hysteresis loop is a plot of magnetization (M) against the applied magnetic field (H). The applications of ferromagnets are highly dependent on the characteristics portrayed by its hysteresis loops. The hysteresis loop helps to understand two essential aspects, (i) the magnitude of saturation magnetization (M_s), and (ii) the path of the hysteresis loop to attain M_s [5] [4]. Several factors

affect the shape of the hysteresis loop, and the factors help us understand why some materials are soft magnets while others are hard magnets.

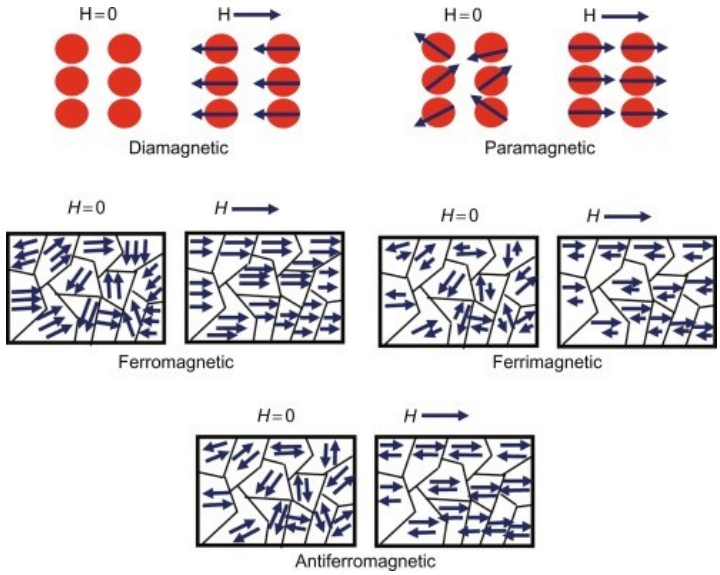

Figure 1.Allignment of moments in different types of magnetic materials [6]

A factor that strongly affects the shape of the hysteresis curve is magnetic anisotropy (K) [1]. Knowledge and understanding of the path taken by material to reach M_s and its dependence on K are essential for developing material compositions with enhanced magnetic properties in general. The Law of Approach to Saturation, first introduced by Akulov in 1932, helped in understanding and quantifying the effect of rotation of the magnetization vector of ferromagnetic materials near saturation. Later, researchers have modified and improved Akulov's original equation and have applied them to different ferromagnetic materials. Studies of how the different variants of Law of Approach to Saturation apply to different magnetic materials have been conducted to find the first order magnetocrystalline anisotropy constant (K_1) values, which help us understand the hysteresis loops of a particular magnetic material or the theory behind how magnetic saturation is achieved in a specific material.

This investigation deals with the magnetic properties, including magnetocrystalline anisotropy constant (K_1) of elemental ferromagnetic powders (Fe, Co, Ni), their ternary alloys, and some of their alloys. Estimation of the K_1 values of these powder materials accompanied with deeper insights on their hysteresis loops and its dependence on magnetic anisotropy using the law of approach to saturation is the main aim of this investigation. The K_1 value can be manipulated and

modified to achieve better suited magnetic properties from future magnetic materials while also serving as a functional characteristic for quality control of magnetic powders used in upcoming additive manufacturing methods.

Chapter 2. Literature Review and Background

2.1. Basic Concepts of Magnetism

2.1.1. Origins

The laws governing the forces between the poles were discovered by John Mitchell in 1750 and by Charles Coulomb in 1785. A magnetic pole creates a magnetic field around it and exerts a force on a second pole located nearby. Later, Michael Faraday represented the magnetic field by using "lines of force" [1]. Outside the magnet, the lines of force originate from the north pole and end at the south pole. Macroscopic magnetic properties are a result of magnetic moments of individual electrons in an atom. Magnetic moments in an electron occur due to two reasons one is due to the orbital motion around the nucleus, and the second is due to the spin of the electron around its own axis [3]. Each electron in an atom may be considered as a small magnet having orbital and spin magnetic moments. The most fundamental magnetic moment is called the Bohr magneton μ_B, having a magnitude of 9.27×10^{-24} Am^2.

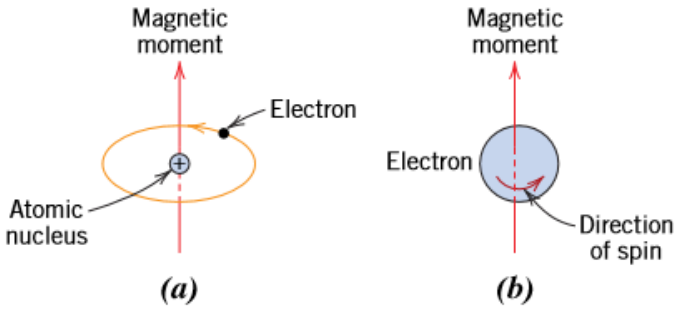

Figure 2.Illustration of magnetic moment associated with (a) an orbiting electron and (b) a spinning electron [3]

Generally, there is some orbital moment cancellation among electron pairs and spin moment cancelation depending on the direction of spin, up or down. So, the effective magnetic moment can be said as the sum of the orbital magnetic moment, spin moment and then accounting for this moment cancellation. Elements such as inert gases having atoms with filled electron shells have

complete cancelation of the magnetic moment. These principles can be classified based on the kind of magnetism they exhibit as diamagnetic, paramagnetic, ferromagnetic, antiferromagnetic, and ferrimagnetic.

2.1.2. Domain Theory

In 1906 Pierre Weiss [7] formulated the Weiss theory wherein he put forward two important postulates for ferromagnetic materials i) Spontaneous magnetization and ii) Division into domains. He stated that a molecular field acts in ferromagnetic materials below as well as above its curie temperature (The temperature at which a ferromagnetic material acts as a paramagnetic material) and that the field is so strong that it can magnetize the material to saturation even in the absence of an external field, hence spontaneously magnetized. He then postulated that when demagnetized ferromagnetic material is divided into small regions called domains. Each domain is spontaneously magnetized to saturation, but the direction of magnetization is such that the net magnetization is zero, so when an external magnetic field is applied, the multi-domain system is converted into a single domain system, magnetized in the same direction as the applied field. The figure below illustrates the process of magnetization in a ferromagnet based on domain theory.

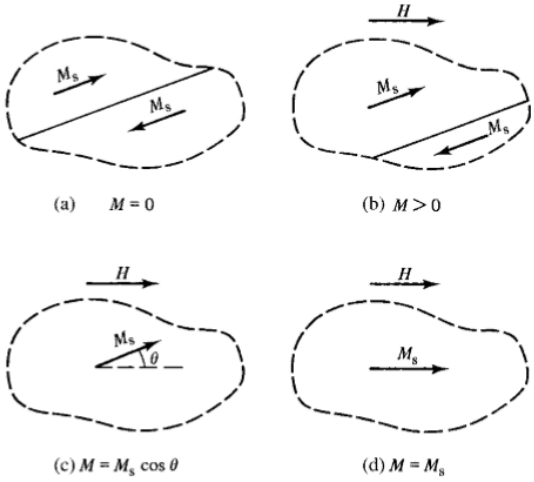

Figure 3.Magnetization in ferromagnets [1]

2.1.3. Magnetic Hysteresis

Magnetic Hysteresis was first observed in iron by Warburg [1]. The word hysteresis means: to lag, and it was introduced by Ewing [5], who was the first to investigate it scientifically. Magnetic properties of ferromagnetic materials can be easily represented using hysteresis loops. Hysteresis loops are nothing but the plots of magnetization *M* against the applied magnetic field *H*. When the

applied magnetic field is increased the ferromagnetic material starts to get magnetized, as the field H is increased, the magnetization reaches a saturation value, after which there is no significant increase in this value. This value is called magnetic saturation M_S of that particular ferromagnetic material. Once the value of magnetic saturation is achieved and the applied field is decreased, it is noticed that at zero fields there is some amount of remaining magnetization; this is called remanence M_R. This magnetization can be brought back to zero by applying a negative field of a certain strength. This field strength is called coercivity H_C. The applications of ferromagnets are highly dependent on the characteristics portrayed by its hysteresis loops.

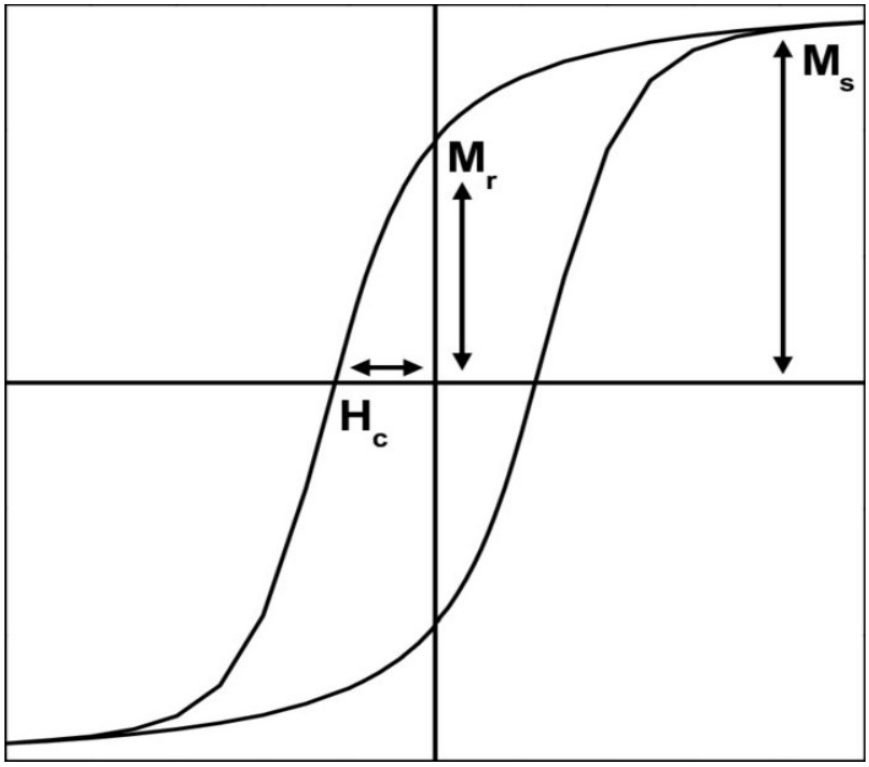

Figure 4.Hysteresis curve of ferromagnetic material [8]

2.1.4. Soft Magnets

In simple terms, materials that are easy to magnetize and demagnetize are called soft magnets. Coercivity is the term that distinguishes materials as either soft magnets or hard magnets. Materials with coercivity less than 1000 A/m (1 kA/m) are considered soft magnets [5]. One of the most important applications for soft magnets is electromagnets and relays. Other important applications include transformers, motors and generators [9]. Examples of soft magnetic materials include Iron

silicon alloys, Iron aluminum alloys, Nickel-Iron alloys (Permalloy) etc. [4]. The figure below represents the narrow hysteresis curve behavior of soft magnetic materials.

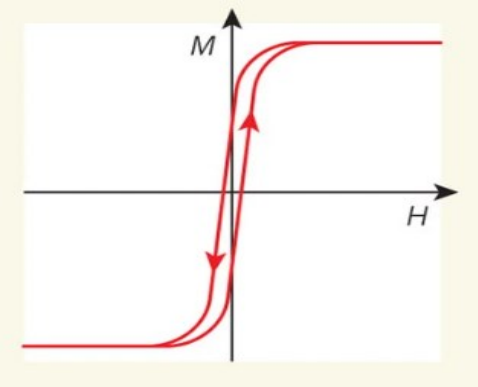

Figure 5.Hysteresis curve of a soft-magnetic material [10]

2.1.5. Hard Magnets

Materials that are difficult to magnetize and demagnetize are called as hard magnetic materials. Materials with coercivity greater than 10 kA/m are considered hard magnets [5]. Hard magnets are generally used as permanent magnets to generate magnetic fields without continuous application of electrical energy. Their most important application is electric motors, where electrical energy is converted into mechanical energy, electric generators, where mechanical energy is converted to electrical energy [9]. They also find use in a variety of commercial electronics such as loudspeakers, TV sets etc. Examples of hard magnetic materials include neodymium iron boron, alnico alloys, samarium cobalt etc. [4]. The figure below represents the broad hysteresis curve behavior of hard magnetic materials.

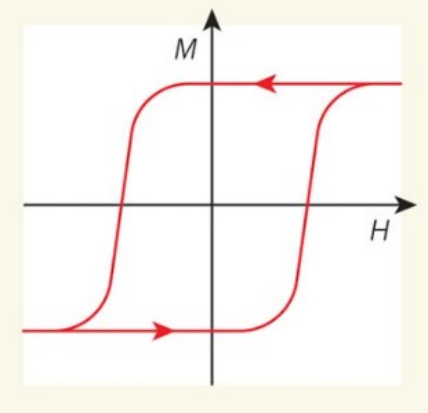

Figure 6.Hysteresis curve of a hard-magnetic material [10]

2.2. Magnetic Anisotropy

The hysteresis loops for ferromagnetic materials can be viewed to understand two extremely important factors, i.e., The magnitude of saturation magnetization and the path it takes on a hysteresis loop to reach this value. There are several factors that affect the shape of the hysteresis loops, and these help us understand why some materials act as soft magnets and some as hard magnets. One factor that strongly affects the shape of the hysteresis curve is magnetic anisotropy. Magnetic anisotropy is nothing but the dependence of magnetic properties in certain preferred directions [1].

2.2.1. Cubic Crystal

Both iron and nickel are cubic crystals. In iron, saturation can be achieved at quite low fields in the [100] crystallographic direction, and this is called the easy direction or easy axis for iron [1] [3].

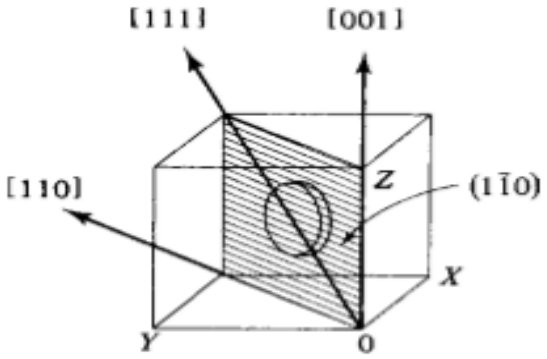

Figure 7.Principal crystallographic directions in a cubic crystal [1]

So, domains in demagnetized iron, when under an applied field in [100] direction, will grow in volume by domain wall motion, and continued application will lead to the elimination of all but the favored domain [3].

Nickel has [111] as the direction of easy magnetization, and the same is the case for all cubic ferrites except cobalt ferrite or ferrites containing a large amount of cobalt. Domain rotation for single-crystal iron in the [010] (one of the six easy directions by the convention of symmetry) easy direction is shown below in Fig.9.

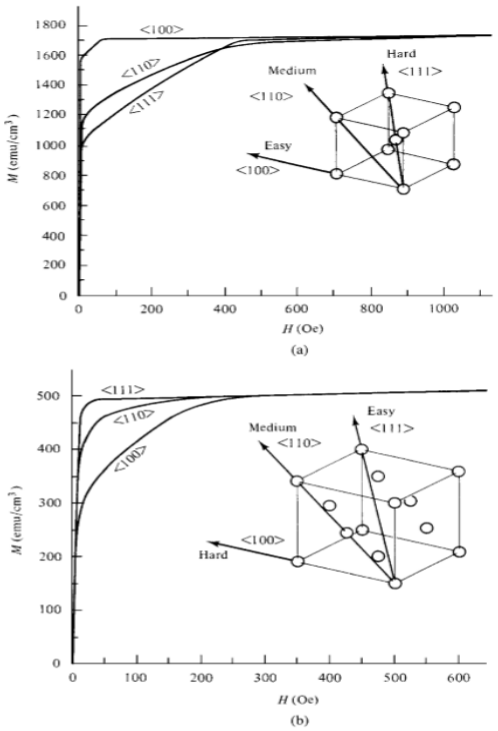

Figure 8.Magnetization curves for single crystal(a) iron and (b) nickel [1]

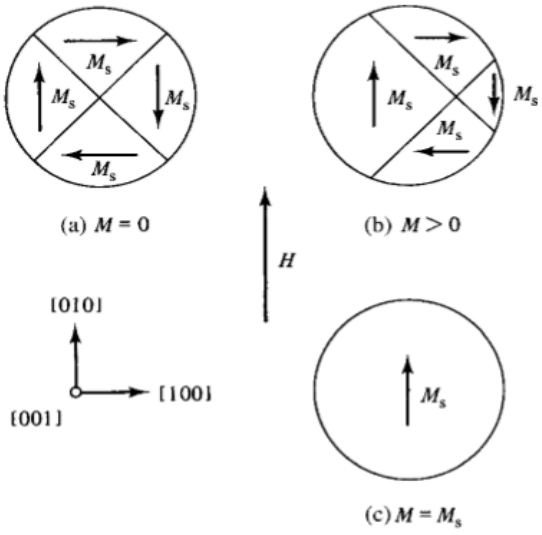

Figure 9.Domain rotation in single-crystal iron in the easy direction [1]

Mixed ferrites with a large amount of cobalt have [100] as an easy direction. To saturate iron in [110] (hard direction) it has been found that a fairly high strength field is required in the order of several hundred oersteds. In such a case, domain wall motion occurs until there are only two domains left with equal potential energy and are aligned in the easy direction. Now the only way

for the magnetization to increase is by rotation of the M_S vector of each domain until it is parallel with the applied field. This is called domain rotation. Domain rotation for single-crystal iron in the [110] hard direction is shown below.

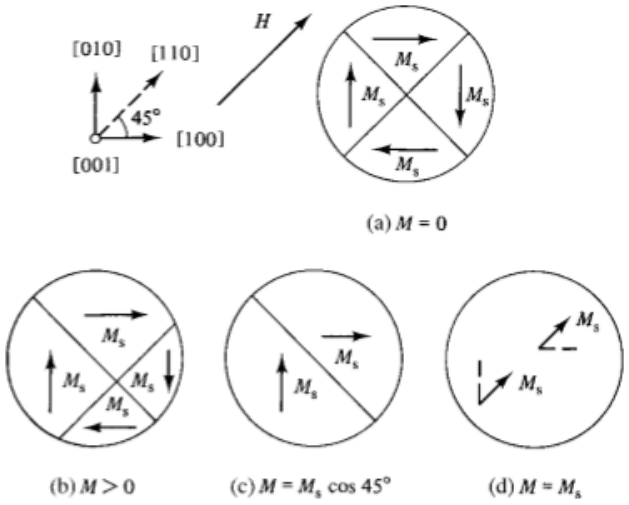

Figure 10.Domain rotation in single-crystal iron in the hard direction [1]

The domain, which is a collection of atoms, does not rotate; rather, the magnetic moment of the atoms rotate. Domain rotation occurs only when a high strength field is applied because it must act against the force of crystal anisotropy. Crystal anisotropy can hence be defined as the force which holds the magnetization in certain crystallographic directions in a crystal. Once the rotation is complete, the crystal is saturated. As the applied field must do work against the anisotropy forces to turn the magnetization vectors in the non-easy direction this must mean there is energy stored in any crystal in which M_S points in the non-easy direction. This energy is called the crystal anisotropy energy E [1] [3] [5]. In 1929 the Russian physicist Akulov [11] showed that E can be expressed as a series expansion of the direction cosines of M_S relative to the crystal axes.

$$E=K_0+K_1(\alpha_1^2+\alpha_2^2+\alpha_2^2+\alpha_3^2+\alpha_3^2+\alpha_1^2)+K_2(\alpha_1^2\alpha_2^2\alpha_3^2)+\ldots \quad (1)$$

where $K_0, K_1, K_2\ldots$ are constants for particular materials at a particular temperature and has a unit of J/m^3. $\alpha_1, \alpha_2, \alpha_3$ are the cosines of the angles made by M_S vector with the crystallographic axes. It has been found that higher powers are generally not required and even K_2 is so small that it can be neglected. Similarly, K_0 term is neglected as it is independent of angle and we are concerned with the change in energy E due to domain rotation.

2.2.2. Hexagonal Crystal

Cobalt has a hexagonal close-packed structure, and the hexagonal c axis is the direction of the easy axis for cobalt. The magnetization curve for a cobalt single-crystal is shown below. Hence the anisotropy energy E for cobalt only depends on a single angle between the M_S vector and the c axis.

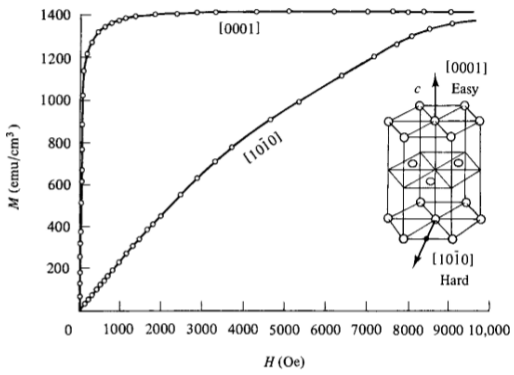

Figure 11.Magnetization curve for a cobalt single crystal [1]

The anisotropy energy E can be given as,

$$E = K_0 + K_1 \sin^2\theta + K_2 \sin^4\theta + \ldots. \quad (2)$$

Where $K_0, K_1, K_2 \ldots$ are constants for particular materials at a particular temperature and has a unit of J/m^3. A crystal with a single-axis is referred to as a uniaxial system. A uniaxial system can have magnetization in only two directions, either up or down [1] [3]. Elemental cobalt, barium ferrite and many rare earth transitional metal intermetallic compounds behave in a similar manner.

2.2.3. Physical Nature of Magnetic Anisotropy

The physical nature of magnetism, as discussed in section 2.1.1, arises from the electron spin as well as the orbital motion. The origins of magnetic anisotropy can also be assessed in a similar manner. Two adjacent electrons will have a type of spin coupling, which will maintain the motion of the electrons to be parallel [1]. This will not cause them to have a similar direction as it depends on the angle of the spins rather than the direction; any contribution from this coupling to magnetic anisotropy would be negligible. Similarly, there would be an orbit lattice coupling, which would be strong as the orientations of the orbit will be fixed to the lattice. Now the spin-orbit coupling, when under the influence of the field, the spin will try to reorient itself, but the orbit will resist this

reorientation as it is fixed to the lattice the energy required to rotate the spin to overcome the spin-orbit coupling is called the anisotropy energy [3] [1]. While there is scientific consensus on the fact that the major contribution to the anisotropy constants $K_0, K_1, K_2\ldots$ are the spin-orbit coupling. There is no clear or general way of calculating their values from these principals as it is greatly influenced by the crystal structure. Since anisotropy is strongly dependent on the structure as expected, with an increase in temperature, anisotropy decreases. Anisotropy contributes significantly to the coercive field, and just like how coercivity tends to zero as the temperature approaches the curie temperature T_C, anisotropy vanishes at curie temperature.

2.2.4. Magnetic Anisotropy in Polycrystals

In the case of polycrystals, if the constituent crystals are oriented randomly in space, then the anisotropy of the individual grains will average out, and the body as a whole will not exhibit anisotropy [12]. Most of the time, the crystals will have a preferred orientation called crystallographic texture, and the polycrystals will exhibit anisotropy dictated by the weighted average of the individual crystals. Control over the easy axis orientation is possible to a lesser extent in polycrystals. The control of easy axis orientation is quite simple when the magnet is manufactured using a process of compaction and sintering as one can apply a field to orient individual grains to align the powders based on their respective easy axis.

2.2.5. Shape Anisotropy in Polycrystals

It has been found that in polycrystals with their grains oriented in random direction, if it has a spherical shape, an applied field will have the same magnetization effect in any direction. In case it is not spherical in shape, then it was found that the easier direction for magnetization was along the long axis rather than the short axis. This was due to the fact that the demagnetizing field along the short axis is stronger. An applied field along the short axis would need to be stronger to work against the demagnetizing field and attain the same level of magnetization than it would require in the long axis. E.P. Wohlfarth et al [13] studied this effect and gave obtained the difference between the demagnetizing fields as a function of c/a where c is the major axis (in the basal plane) and a is the minor axis (normal to the basal plane).

2.2.6. Measurement of Magnetic Anisotropy

There are several methods that can be used to estimate magnetic anisotropy, such as using torque curves generated by a torque magnetometer or by a torsion pendulum method. However,

the application of these methods in the case of polycrystals is not an easy proposition. Instead, the use of magnetization curves to calculate anisotropy, which is a rather uncommon method for bulk materials, can be used to a greater extent in the case of polycrystals. The calculation of magnetic anisotropy involves fitting a calculated magnetization curve to an experimentally observed one. In the estimation of magnetic anisotropy using magnetization curves, we only consider crystal anisotropy and neglect any other source of anisotropy also; we assume that the M_S vector can be rotated out of the easy direction by applying a strong field that can overcome anisotropy forces [1].

'Magnetization curves for ferromagnetic single crystals' by H. Lawton et al [14] published in 1947 put forward expressions for magnetization curves for single crystal iron. They explained that when a field is applied in [110] direction wall motion occurs until there are only two domains left of [100] directions i.e. [010] and [100] directions as these are the two easy directions closest to the direction of the field. The expression for magnetization is then given by

$$M=M_S\times \cos 45^0 \tag{3}$$

The direction cosines of Ms relative to the crystal axes are then $\alpha_1=\cos\delta$, $\alpha_2=\cos(90-\delta)$, $\alpha_1=0$.

The anisotropy energy is then given by,

$$E_a=K_0+(K_1/4)\times\sin^2 2\delta \tag{4}$$

The magnetic potential energy is,

$$E_p=-M_SH\cos(45-\delta) \tag{5}$$

Larger the value of δ the larger is the anisotropy energy and smaller the potential energy. The angle δ will therefore be such as to minimize the total energy Et,

$$E_t=K_0+(K_1/4)\times\sin^2 2\delta- M_SH\cos(45-\delta) \tag{6}$$

To minimize E_t,

$$dE_t/d\delta= [K_1 \sin^2\delta\cos^2\delta]-[M_SH\sin(45-\delta)]= 0 \tag{7}$$

When thought in terms of torque instead of energy, the first term is the torque exerted by the crystal on M_S and the second term is the torque exerted by the field on M_S. The terms are equal and opposite to each other. M_S in the field direction of measured magnetization is,

$$M=M_S(\cos 45- \delta) \quad (8)$$

Using Eq 7 and 8 and eliminating δ we get,

$$H= (4K1/M_S)\times(M/M_S)\times[(M/M_S)^2-0.5] \quad (9)$$

This equation gives the field required to reach any given level of magnetization. This field is directly proportional to K_1 and independent of K_2. The field required to make $M=M_S$, i.e., to saturate the magnetization in the [110] direction is,

$$H= (2K_1/M_S) \quad (10)$$

Similarly, magnetization curves in the case of a uniaxial crystal-like cobalt were given by Y. Barnier, R. Pauthenet, and G. Rimet [15]. For iron, nickel and cobalt single crystals, the calculated magnetization curves duplicate the features of experimental magnetization curves.

2.3. Magnetization in the High Field Region

A magnetization curve can be divided into different regions based on the strength of the applied field as the low, intermediate and high field regions. The low field region is considered to be from about zero to one oersted or 80 A/m and is called the Rayleigh region, named after Lord Rayleigh [1], who first investigated it. The intermediate region consists of the largest section of the magnetization curve. The shape of this region varies widely from material to material. A simple relation between the magnetization M and applied field H for this region is not possible. In the case of the high field region, magnetization proceeds due to the domain rotation mechanism. The change in magnetization is relatively small, and a relation between the magnetization M and applied field H can be observed. This relation is called the Law of Approach to Saturation (LAS).

2.3.1. Law of Approach to Saturation (LAS)

In 1931, Akulov and Gans [16] calculated the effect of rotation of magnetization vector, the magnetization field and the crystalline anisotropy torques on the variation of magnetization of ferromagnets near saturation. They put forward the law of approach to saturation (LAS),

$$M=Ms(1-(b/H^2)) \quad (11)$$

where M is the Magnetizing field, M_S is the saturation magnetization, H is the coercive field, and b is a constant that is proportional to the square of the crystalline anisotropy constant given as,

$$b = 8 K_1^2/M_S^2 \quad (12)$$

However, the result of this derivation did not closely match the experimental values. In 1940, Holstien and Primakoff [17] published their work on magnetization near saturation in polycrystalline ferromagnets. They realized that Akulov and Gans had in their derivation neglected the internal magnetic field h, the torque term $M_S \times h$ caused by this would be similar in order to the $M_S \times h$ for the external fields in which experiments were conducted and neglecting it with the observation that $|h| << |H|$ is not possible as H and M_S are parallel while h has a totally different direction from H and M_S. They improved Akulov's equation by taking into account the internal magnetic field h. This resulted in equations which more closely matched the experimental values. Holstien and Primakoff [18] as well as W.F Brown [19] in his Theory of approach to magnetic saturation, also published in 1940, found that experimental values can be fitted to the empirical formula,

$$M = M_S(1 - (a/H) - (b/H^2)) + \chi H \quad (13)$$

It has been found that the χ term is independent of the metallurgical history of the materials and seems to arise from the variation in the intrinsic domain magnetization with the field and may be proportional to $H^{0.5}$ as suggested by Holstein. The a and b term are dependent on the metallurgical history of the material, while b is mostly associated with the crystalline properties of the material. The value of b was found to be in agreement with the value of b found using Eq.(3).The equation for the b/H^2 constant for a cubic crystal is given as,

$$b = (8/105) (K_1^2/M_S^2) + \lambda_2 (\sigma^2/M_S^{0.5}) \quad (14)$$

The first part is due to the crystalline anisotropy, and the second part was derived by Becker and Polley [20] and considered to be due to the effect of internal strain on the approach to magnetic saturation. Here, K_1 is the magnetic anisotropy constant, M_s is the saturation magnetization, λ_2 is the magnetostriction constant, and σ is the internal stress. Magnetostriction is the property of ferromagnetic materials due to which they expand or contract under the influence of a magnetic field. Similarly, the equation for the constant b for a uniaxial system given by Gans [21],

$$b = (4/15) (K_1^2/M_S^2) \quad (15)$$

Here, K_1 is the magnetic anisotropy constant; M_s is the saturation magnetization.

J.F Herbst and F.E Pinkerton [22] analyzed the approach to saturation in polycrystalline ferromagnets from the remnant state. They considered the generic law of approach to saturation,

$$M = M_S (1 - (\beta K_1^2 / M_S^2 H^2)) \quad (16)$$

Where M is the magnetization, M_S is the saturation magnetization, and K is the anisotropy constant that depends on constant β. The constant $\beta = 8/105$ for cubic systems and 4/15 for uniaxial systems. Herbst et al. found that β changes when the initial state is the remnant state, i.e., when the magnet has been saturated, causing the magnetic moment of each crystal to have their configuration in the easy direction closest to the direction of the applied field. They also found that β not only depends on the direction of the easy axis but also on the angle ρ, which is the angle between the initial field applied and the second saturating field. They concluded by deriving expressions for β for {100} and {111} easy directions for a cubic system; they also proved that in the case of a uniaxial system $\beta = 4/15$ holds a true event in the case of an initial remnant state.

2.3.2. Origin of the a/H Term

While the other terms were at least partially understood, the mechanism behind the *1/H* term could not be explained theoretically. W.F Brown [19], in his theory of approach to magnetic saturation, tried to explain this; according to him, the $1/H$ term was due to the presence of line concentrations of force. This was explained using Kaufmann's measurement on nickel subjected to various degrees of plastic deformation. He found that the coefficient increases with an increase in plastic deformation. Plastic deformation is explained as the flow of dislocations through the lattice, and according to Taylor's theory of hardening, the application of shearing stress greater than the yield value will cause new dislocations, which will propagate a certain distance until they are stopped by a flaw. This process continues until there are numerous stopped dislocations and their stress field starts opposing the applied stress. This creates a stable condition with a new yield value. It compared the line concentrations of the force responsible for the *a/H* term with dislocation lines. It was found a is proportional to the number of dislocations per unit volume and in turn to plastic deformation. W.F brown concluded by suggesting maybe a dislocation caused the breaking up of exchange forces and deviation from magnetic saturation.

In 1948 Neel [23] put forward his theory attributing the origin of *1/H* term due to nonmagnetic inclusions which in the high magnetic field region would cause irregular internal disturbing forces or stray fields.

Takasi Huzimura [24] tried to correlate the theory put forward by W.F Brown using experimental results. He tested the magnetic susceptibility of polycrystalline nickel rods, which were stretched using a tensile testing machine. The magnetic susceptibility was measured in the unloaded state. He also inserted the specimen in a magnetizing solenoid and twisted the specimen to measure magnetic susceptibility in the loaded state. W.F Brown had found the following expressions for *a* and *b*,

$$a = nf_1 \times 9(\lambda G \lambda_0)^2 (3X^2+5Y^2)/128\pi c(1-\nu)^2 M_S \quad (17)$$

$$b = nf_2 \times 9(\lambda G \lambda_0)^2 (lnR+C_0)/4\pi c(1-\nu)^2 M_S^2 \quad (18)$$

Where *X* and *Y* are the components of *R*, the mean distance between paired dislocations, *G* is the modulus of rigidity, ν is the Poisson's ratio and λ_0 is the Burger's vector. The calculations are classified into two groups according to $R_{ij} <> (c'/H M_S)^{0.5}$, where *c'* is a constant related to change the energy of spins and *Rij* is the distance between two dislocations, nf_1 and nf_2 are the average number of dislocations of the first and second group, respectively, and *n* represents the total number of dislocations. Both *a* and *b* are proportional to the number of dislocations, and it may be considered that both are proportional to the amount of deformation. Huzimura concluded that Brown's result qualitatively agreed with his experimental results.

Dennis Grady [25], in his paper 'Origin of the linear term in the expression for the approach to saturation in ferromagnetic materials' published in 1971, found that when investigating a slightly porous polycrystalline material subjected to external hydrostatic pressure, it experiences non-hydrostatic strain in the vicinity of the pores. The non-hydrostatic strain regions along with other magnetoelastic properties of the material, will drastically affect the magnetization curve. He concluded by saying that the origin of the *a/H* term was due to the residual internal strain of the magnetic material and that it is only valid in a limited field range.

H. Zhang et al. [26] in 2010 tried to explain the origins of the aH^{-1}, bH^{-2} and χH terms. These researchers have theorized that in the case of ferromagnetic materials magnetization will follow the Law of Approach to Saturation (LAS) independent of the whether direction of the applied field

is in the easy axis or hard axis. If the field is in the direction of the easy-axis magnetic anisotropy would aid in magnetization. No paramagnetism like phenomenon occurs and that all the terms aH^{-1}, bH^{-2} and χH are all originating from the magnetocrystalline anisotropy.

2.3.3. Curve Fitting

The use of curve fitting for analyses and comparison with different forms of Law of Approach to Saturation was done by R.Grossinger [27]. In his paper published in 1982, he generated data using the equation using the formula,

$$M = M_S\,(1 - a/H - b/H^2 - c/H^3) + \chi H + d\sqrt{H} \tag{19}$$

This data was then fitted to a set of different forms of Law of Approach to Saturation as given below.

$$M = M_S\,(1 - (a/H)) + \chi H \tag{20}$$

$$M = M_S\,(1 - (a/H) - (b/H^2) - (c/H^3)) \tag{21}$$

$$M = M_S\,(1 - (b/H^2) - (c/H^3)) \tag{22}$$

$$M = M_S\,(1 - (a/H) - (b/H^2)) + \chi H \tag{23}$$

$$M = M_S\,(1 - (a/H) - (b/H^2)) + d\sqrt{H} \tag{24}$$

Here, M_S is the saturation magnetization, a is an inhomogeneity parameter, b is a factor proportional to K_2 and c is the factor proportional to K_3, both b and c depend on the shape of the anisotropy function as well as the symmetry of lattice, χ is the susceptibility, D is the spin wave factor as shown by the calculation done by Holstein and Primakoff. d is proportional to the spin-wave stiffness and the spin-wave stiffness can be determined by the temperature dependence of M which should be proportional to $T^{3/2}$.The reliability of such a computer fit was compared to other graphical methods. To determine the reliability, an expression for mean error per point was applied,

$$\text{Error per point} = (1/n)\sum[M_{exp}(H) - M_{calc}(H)/M_{exp}(H)]^2 \tag{25}$$

where $M(H)$ is the magnetization at a certain field H and n is the number of measuring points. Application of this procedure in the case of cobalt found that there was very little deviation between the various law of approach to saturation.

Similarly, researchers [28] [29] have tried to understand the dependence of the parameters based on statistical indicators. The dependence of magnetization on the applied field in the case of Mn-Zn and Mn-Ni nanoparticles using different variations of the law of approach to saturation (LAS) was studied. Using statistical parameter to analyze different compositions of Mn-Zn nano ferrites they established that based on goodness of fit indicators such as R^2 and χ^2 values Eq.23 was best among the other variations in explaining the dependence of the parameters.

2.3.4. Application of Law of Approach to Saturation (LAS) in Various Magnetic Materials

In 1962 J.Sternberk [30] analyzed samples of polycrystalline Mn-Mg ferrite to find an internal field H so that the Law of Approach to saturation $M=M_S(1-b/H^2)$ is satisfied. They found that in the case of Mn-Mg ferrites most samples had linear dependence while the other samples could achieve a linear dependence when a small correction field smaller than the Lorentz field was introduced.

The effect of stress on the Law of Approach to Saturation in the case of carbon steels have been studied by researchers [31]. They used LAS having the form,

$$M=M_S(1-(b/H^2)-(c/H^3)) \tag{26}$$

where M is the magnetization, M_S is the saturation magnetization and b and c are constants proportional to the magnetocrystalline anisotropy. When stresses are applied additional contribution to magnetic anisotropy occurs which can be measured based on how the coefficients b and c vary and can be used as a form of non-destructive testing. Researchers also deduced that the square root of $2b$ varied linearly based on the applied stress and the calculated values of K agreed with standard values with certain variations based on composition and heat treatments.

Extensive research has been done on the applicability of Laws of Approach to Saturation in amorphous alloys as well. The law of approach to saturation in amorphous alloys was first investigated by Kronmuller et al. [32] in 1977. They analyzed the fluctuations in spontaneous magnetization due to inhomogeneities using the micromagnetic theory and found that the origin of the aH^{-1} term was a result of dislocation dipoles. They concluded that in amorphous materials,

short-range dipole stresses exist, which can be described as large dense dislocations. Further, in their research work, Kronmuller et al [33] developed a phenomenological description of the law of approach to saturation by considering the exchange and magnetic dipole interaction of magnetic inhomogeneities. It was found that the dipolar and exchange interactions in most materials was minimal but the magnetocrystalline and magnetostrictive fluctuations gave rise to a $H^{-1/2}$ term in materials with huge magnetocrystalline field. Later they also investigated the magnetization in amorphous ferromagnets and found that in the low field regions magnetization was described by the term H^{-1} and H^{-2} [34]. In 1980 Kronmuller et al [35] studied the magnetic polarization in amorphous $Fe_{40}Ni_{40}P_{14}B_6$. They studied the law of approach to saturation on quenched, annealed and plastically deformed specimens using the H^{-n} power series. In 1982 V.A Ignatchenko et al. studied the law of approach to saturation in amorphous alloys by experimental analysis on microcrystalline Co-P alloys. They also studied the effect of change in concentration by varying the concentration of P. Instead of using the traditional form of the Law of Approach to Saturation they made use of the knowledge of correlation radius which is the region of orderliness of a corresponding parameter to understand the structure of an amorphous magnet and obtaining a more rigorous and analytical expression for Law of approach to saturation. They found that the local magnetic anisotropy was not affected by the transition into the amorphous state. Magnetic anisotropy in Co-P is primarily caused by magneto crystalline anisotropy with minor contributions from elastic stresses. Nakai in his paper investigated the Law of Approach to Saturation in a series of alloys of Gd_2T where T= Co, Ni and Cu. He found that magnetization approaches saturation as a power of $H^{-1/2}$ rather than H^{-2} as stated in Akulov's theory.

Z.Q. Jin et al [36] investigated the magnetic properties of nanocrystalline Nd-Fe-Ti-N. Using the LAS they found that the $1/H^2$ term has the maximum contribution in this compound and calculated the Keff value. They also found that the absorption of nitrogen increased the compounds unit cell volume, magnetic saturation as well as magnetocrystalline anisotropy constant.

In 2009 N. Ranvah et al [37] studied the temperature dependence of magnetocrystalline anisotropy in the case of germanium/cobalt substituted cobalt ferrite. They realized that increasing the content of germanium at any temperature decreased the first order magnetocrystalline anisotropy K_1 value. Another important finding was the increase in the K_1 value with the decrease in temperature.

2.3.5. Summary

The development of the Law of Approach to Saturation has been worked upon by researchers for well over half a century. The physics behind the Law of Approach to Saturation does not seem to have a consensus in the scientific community, with the origin of the *a/H* term not being clear. Some researchers have attributed it to internal stress, while others have attributed it to inhomogeneities. Experimental data suggest that both the terms *a* and *b* vary similarly in response to stress. This makes it difficult to understand and explain the physicality of the *a/H* term. Researchers suggest the *a/H* term existing only in certain field ranges without which it would lead to the infinite energy of magnetization. Some researchers also suggest that the relevance of the *a/H* term has been overestimated. Application of the Law of Approach to Saturation in different materials has also led to possibilities of the existence of $1/H^{1/2}$ and $1/H^{3/2}$ terms as well. While all this might suggest that the understanding of the physics behind the law of approach to saturation is in disarray, this has no consequence for its use and application in the field of engineering. The practical usage of the Law of Approach to saturation has been proven by researchers for a wide range of materials.

Chapter 3. Motivation

Understanding the magnetic behavior of materials as it reaches saturation is critical to the development of new magnetic materials with enhanced properties. Magnetic anisotropy is a significant contributor to the magnetic behavior of a material in the high field region. The coercivity of a magnet is an important parameter when it comes to deciding the application of a magnet. Magnetic anisotropy greatly influences coercivity. Knowledge and understanding of how magnetic anisotropy can be exploited and tuned to manufacture magnets with upcoming manufacturing methods such as additive manufacturing wherein layer by layer consolidation of metal powders is possible will prove to be critical in developing magnets with superior magnetic properties. Manufacturing of magnets using additive manufacturing is still in its infancy, the use of functional magnetic properties such as magnetic anisotropy along with other structural properties can be used to ensure fabrication of high-quality magnets. In this thesis work, we propose to investigate the magnetic properties of elemental ferromagnetic powders (Fe, Co, Ni) and some of their alloys ($Fe_xCo_yNi_z$), and gain deeper insights on their hysteresis loops and its dependence on magnetic anisotropy by modeling with the Law of Approach to saturation.

Chapter 4. Experimental Procedure

4.1. Procedure of Synthesis

Pure Elemental Powders: The elemental powders having compositions $Fe_{33.33}Ni_{33.33}Co_{33.33}$, $Fe_{30}Ni_{40}Co_{30}$, $Fe_{40}Ni_{30}Co_{30}$ and $Fe_{30}Ni_{30}Co_{40}$ were mechanically alloyed in a SPEX SamplePrep 8000 Dual Mill shown in Fig.12 for ~9 h to ~12 h.

Figure 12.SPEX Sample Prep 8000D Mixer/Mill high energy ball mill

The milling media (cylindrical vial and balls) (Fig.13) used for the study were made of stainless steel (SPEX 8007). A 8:1 ball to powder ratio was used for the mechanical alloying. To decrease cold welding between the powder particles and the wall of the vial, stearic acid (~3 wt.%) was added as a process control agent (PCA).

Figure 13.SPEX 8007 stainless steel vial and balls.

In order to prevent any oxidation of powders, loading, sealing, and unloading of powders into and from the vial were performed in a high purity Ar atmosphere. To avoid damage to the mill motor during mechanical alloying intermittent stoppages were provided. The macroscopic temperature of the vial was measured using a thermocouple during the intermittent stoppages and at the end of mechanical alloying.

4.2. Physical Characterization

The pure elemental powders and the mechanically alloyed powders were analyzed using a Rigaku Miniflex 600 Diffractometer shown in Fig.14 with Ni filter and CuKα radiation to find phase evolutions that occurred during the milling process. The lattice parameter was estimated using Cohen's method, and the crystallite size and lattice strain were estimated by the Williamson Hall method.

Figure 14.Rigaku Miniflex 600 Diffractometer

The powders were then analyzed in a JEOL IT500 Scanning Electron Microscope shown in Fig.15 for EDX mapping. The images were taken in secondary electron mode and the ImageJ software was used to analyze the image and calculate the particle size.

Figure 15.JEOL IT500 Scanning Electron Microscope

4.3. Magnetic Characterization

The magnetic properties were tested on a Quantum Design Versa Lab Vibrating Sample Magnetometer (VSM) (Fig.16). Properties such as Magnetic saturation (M_S), Intrinsic coercivity (H_C) and Magnetic Remanence (M_R) were estimated from hysteresis loops generated using the VSM.

Figure 16.Quantum Design's Vibrating Sample Magnetometer (VSM)

The tests were conducted for both ambient and sub-ambient temperatures with hysteresis loops being generated at every 30 K temperature interval from 300 K to 60 K. Magnetic saturation (M_S),

Intrinsic coercivity (H_C) and Magnetic Remanence (M_R) were estimated through the hysteresis loops. From these hysteresis loops, further K_1 analysis was conducted.

4.4. Magnetocrystalline Anisotropy Constant (K_1) Analysis

K_1 analysis was conducted for all the samples by using the curve fitting method. Hysteresis loop data generated using the Vibrating Sample Magnetometer (VSM) was imported into the commercial statistical software 'Origin' for nonlinear curve fitting. The data was fit to four different variations of the Law of Approach to Saturation (LAS). The Equations and their abbreviations which will be used for future reference are mentioned below.

LAS A: $M=Ms(1-(b/H^2))$ (27)

LAS B: $M=Ms(1-(b/H^2))+\chi H$ (28)

LAS C: $M=Ms(1-(a/H)-(b/H^2))$ (29)

LAS D: $Ms(1-(a/H)-(b/H^2)) +\chi H$ (30)

Experimental data is first curve fit to LAS A. Data points in the high field region i.e. above 40 kA/m are fit to the LAS equation. The figure below shows the LAS A curve fit in the case of Fe elemental powders at 300 K.

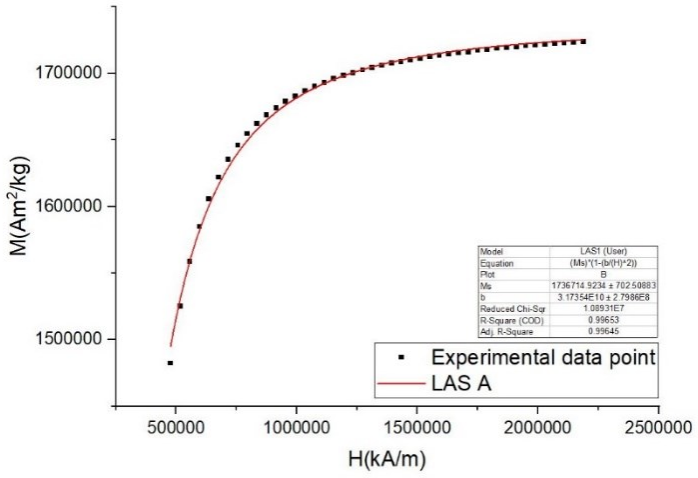

Figure 17.Curve fitting of elemental Fe powders for the case of LAS A

This is followed by plotting for LAS B. The figure below shows the LAS B curve fit in the case of Fe elemental powders at 300 K.

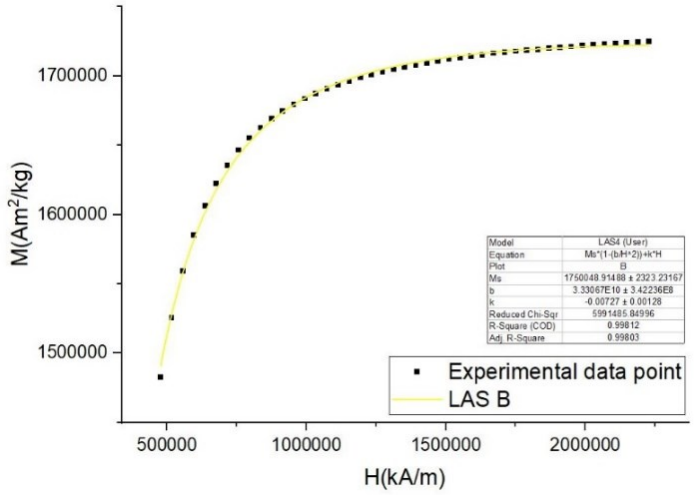

Figure 18. Curve fitting of elemental Fe powders for the case of LAS B

In the case of LAS C, we initialize the M_S parameter using values obtained from LAS A to obtain convergence of fit. The figure below shows the LAS C curve fit in the case of Fe elemental powders at 300 K.

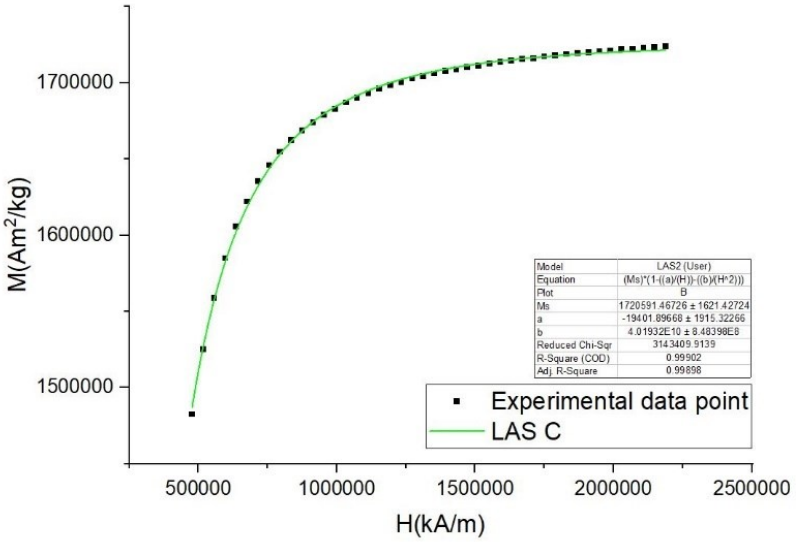

Figure 19. Curve fitting of elemental Fe powders for the case of LAS C

Similarly, for the case of LAS D we initialize parameters M_S as well as b using values from LAS A to attain convergence of the fit. The figure below shows the LAS D curve fit in the case of Fe elemental powders at 300 K.

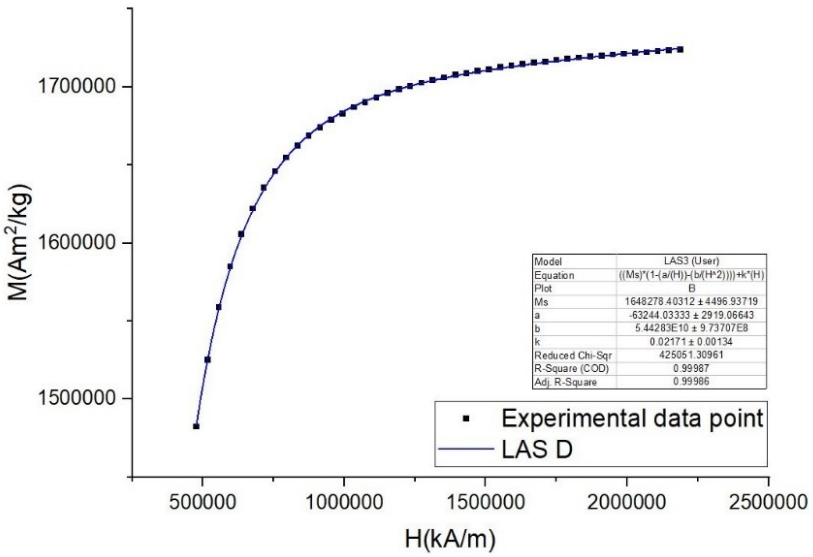

Figure 20. Curve fitting of elemental Fe powders for the case of LAS D

Chapter 5. Results

5.1. Physical Characterization of the Magnetic Powders

5.1.1. Pure Elemental Powders and Their Alloys

The scope of physical characterization in this study is limited to making sure that the powders are synthesiszed according to the right composition and alloy formation occurs. The unalloyed mixture of equiatomic elemental powders and the mechanically alloyed powders were analyzed in a Rigaku Miniflex 600 Diffractometer in order to discern the phase evolution during mechanical alloying. The source of the x-ray radiation was Cu Kα (the wavelength of Kα1 and Kα2 is 0.15406 nm and 0.15444 nm, respectively) and a monochromator was used to filter the Kβ radiation. The x-ray diffraction patterns were collected for the 2 θ values ranging from 20° to 100° at a step-size of 0.02°. Fig.21 presents the x-ray diffraction patterns of the unalloyed ferromagnetic powders and their alloys ($Fe_xCo_yNi_z$).

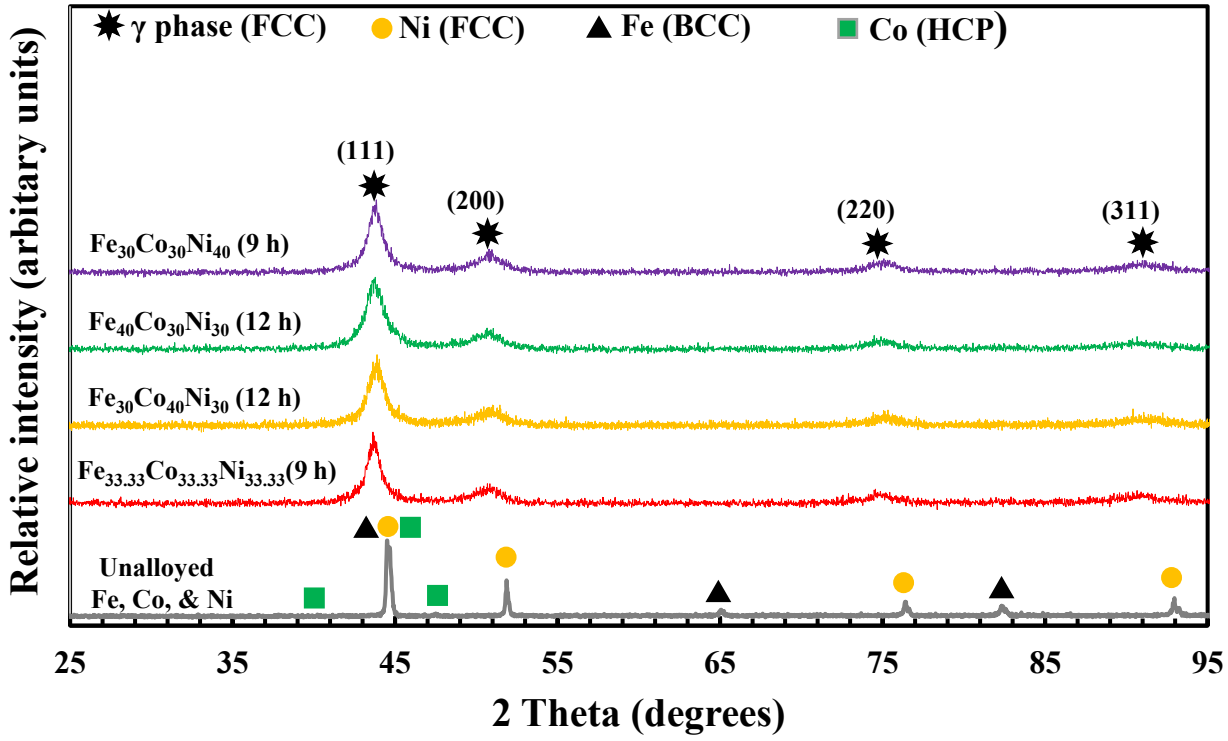

Figure 21.X-ray diffraction patterns of elemental ferromagnetic powders and their alloys

Observation of the patterns shows disappearance of Co peaks and a shift in Ni peaks to lower angles which suggests to a probable formation of a solid solution (alloy). We can also notice an increase in the XRD peak widths suggesting decrease in crystallite size combined with a an increase in lattice strain. During mechanical alloying, the elemental powders were subjected to heavy deformation and the observed peak broadening probably corresponds to lattice strain induced by heavy deformation. At up to ~3 h of mechanical alloying, no noticeable disappearance of any existing peaks or appearance of any new peaks was observed. After mechanical alloying, the Co peaks disappeared and the Ni peaks shifted to lower 2 θ values suggesting probable diffusion of Co into the Ni lattice and formation of a substitutional solid solution of Co and Ni. During mechanical alloying, the increased amount of cold working is known to introduce a large number of crystal defects such as dislocations, grain boundaries, vacancies, etc that provide the diffusion paths for alloy formation. At the end of mechanical alloying for 9 h, the Fe peaks also disappeared and the remnant shifted diffraction peaks of Ni correspond to the diffraction. At the end of mechanical alloying for 9 h, the Fe peaks also disappeared and the remnant shifted diffraction peaks of Ni correspond to the diffraction peaks of the equiatomic $Fe_xCo_yNi_z$ alloy—a substitutional solid solution of Fe, Co and Ni. Further mechanical alloying for 6 h didn't show any signs of a phase change. The XRD patterns suggest that the formation of the $Fe_xCo_yNi_z$ alloy from the constituent elemental powders was complete by 9 h of mechanical alloying and the alloy was comprised of the γ-phase only [38]. The γ- phase also forms during equilibrium cooling e.g. as in conventional melting and casting of the equiatomic $Fe_xCo_yNi_z$ alloy. The particle size distribution (D_{90}) for the alloy powders was estimated using an SEM [39] [40] [41] [42]. The alloys $Fe_{33.33}Co_{33.33}Ni_{33.33}$, $Fe_{30}Co_{30}Ni_{40}$, $Fe_{40}Co_{30}Ni_{30}$, $Fe_{30}Co_{40}Ni_{30}$ had a particle size distribution of ~16, 8.7, 8.9 and 5 μm respectively.

5.1.2. Maraging Steel Powders

Fig.22 shows the XRD patterns for maraging steel As Received powders and milled powders (5 h & 56 h). The As Received powders consists predominantly of martensite (α) phase and traces of some austensite (γ) phases.

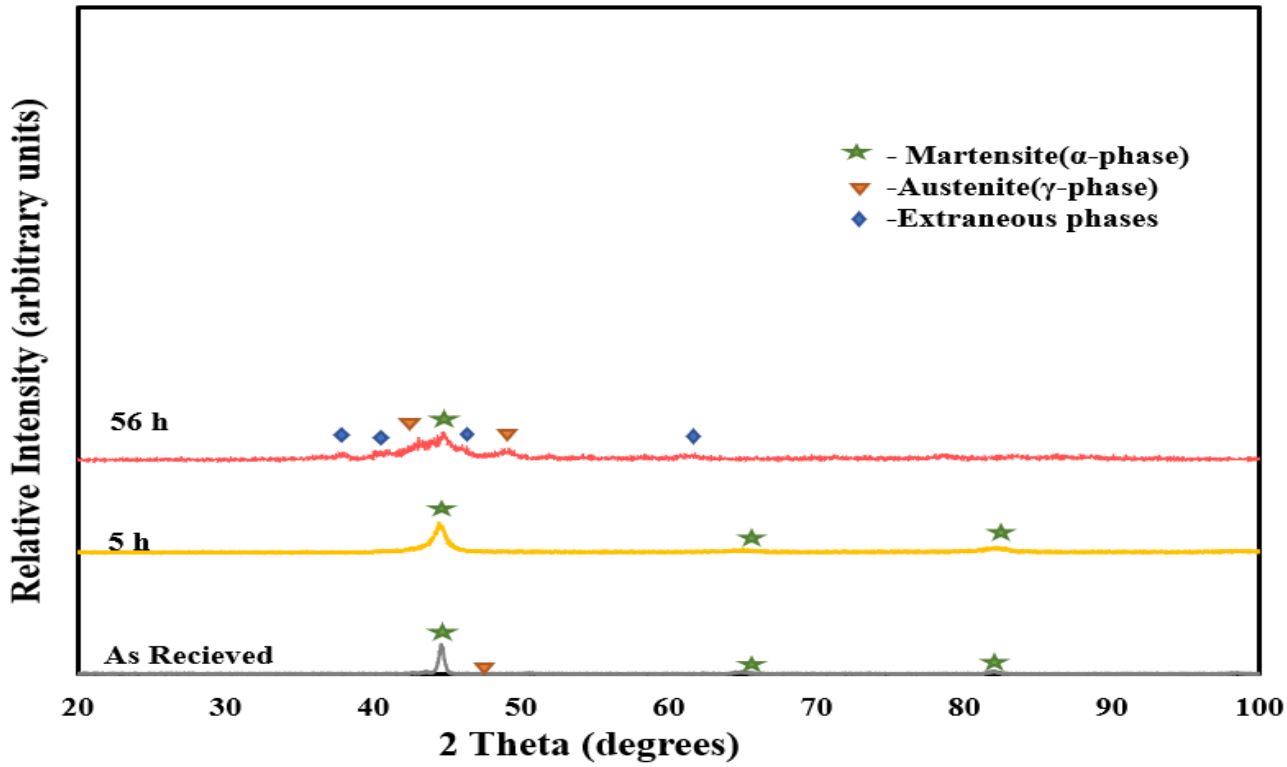

Figure 22. X-ray diffraction patterns of Maraging steel powders

Milling the powders for upto 5 h shows the presence of predominantly the martensite (α) phase having broadened peaks indicating the presence of nanocrystalline grains, or lattice strain, or both. It is seen that continued milling till upto 56 h and beyond the peak broadening further increases with the evolution of some extraneous phases present along with the austenite (γ) and martensite phases (α). The particle size distribution (D_{90}) of the As Received powders were estimated using an SEM [43] and was estimated to be ~21 µm. The particle size initially decreased with an increase in milling time and was ~8.9 µm after milling for 5 h. Later with increase in milling time the particle size increased and is most likely due to agglomeration of the powder caused due to cold welding.

5.2. Magnetic Properties of Elemental Powders

5.2.1. Iron (Fe)

Figure 21 shows the magnetization (M) versus the applied magnetic field (H) curve for elemental Fe powders at ambient temperature. The inset shows the M-H curves in the low magnetic field realm of about ±10 kA/m. The M_S was estimated to be 217 ± 4 Am^2/kg. The H_C and M_R were calculated to be about 1 ± ~1% kA/m and 1 ± ~9% Am^2/kg, respectively.

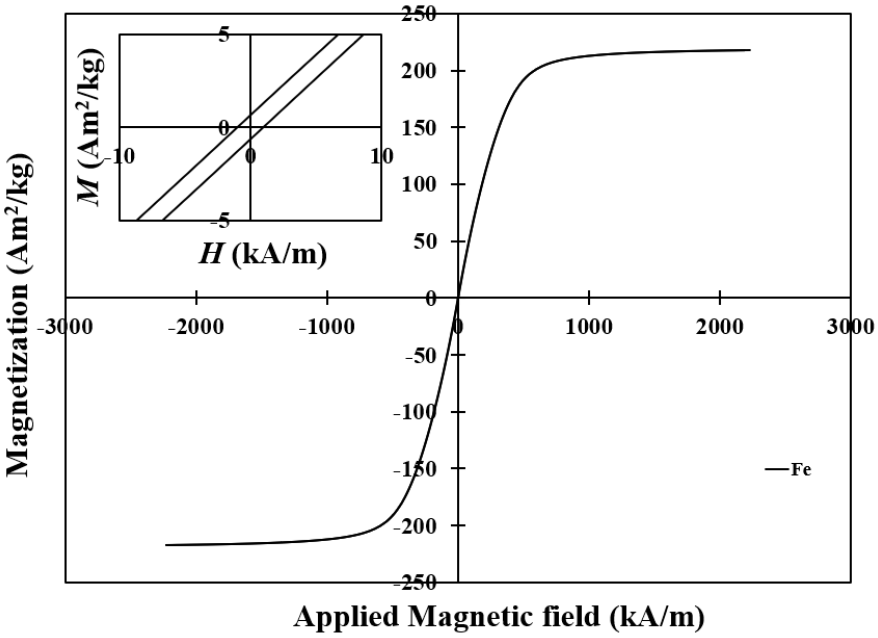

Figure 23. Magnetization (*M*) vs. Applied magnetic field (*H*) curves for elemental Fe powders at ambient temperature

The magnetization (*M*) versus the applied magnetic field (*H*) curves observed for Fe elemental powders at sub-ambient temperatures as low as 60 K are shown below in Figure 22.

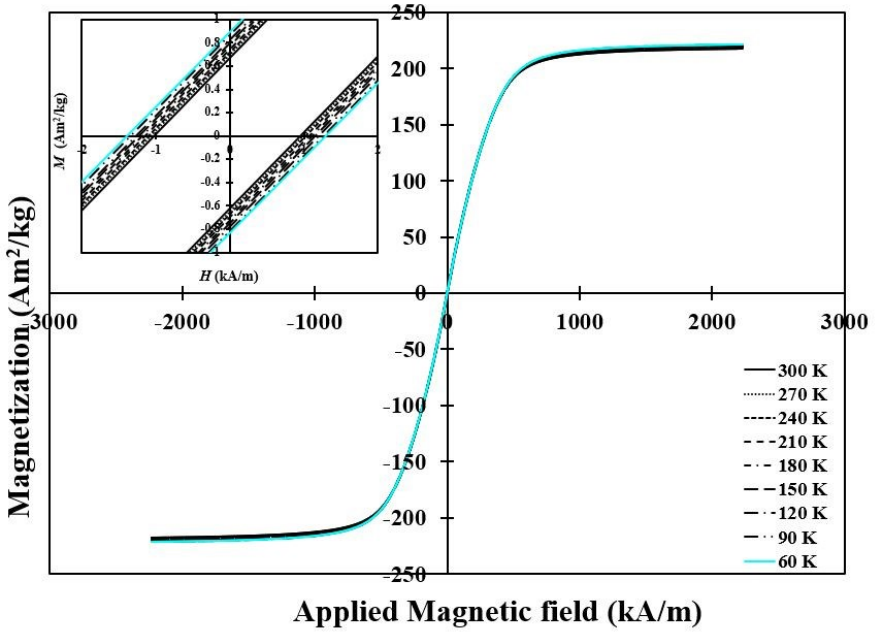

Figure 24. Magnetization (*M*) vs. Applied magnetic field (*H*) curves for elemental Fe powders at sub-ambient temperatures

Variation of M_S, H_C and M_R with respect to decreasing temperature is shown below in Figure 23.

(a)

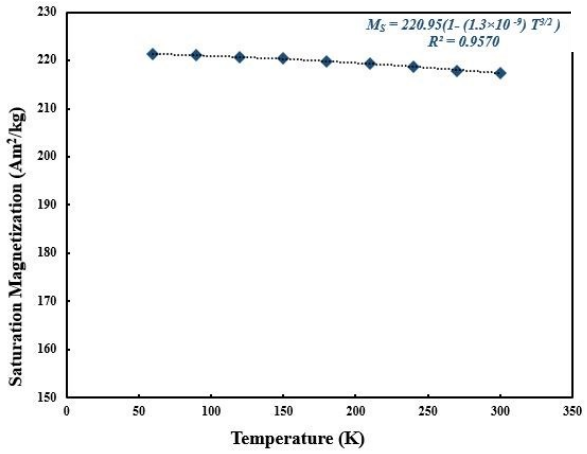

(b)

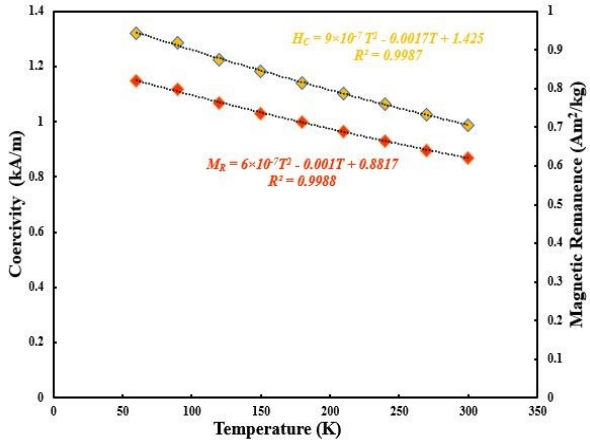

Figure 25.a)Magnetic saturation (M_S) vs Temperature (T) b) Coercivity (H_C) & Magnetic remanence (M_R) vs Temperature (T)

A trend of increasing M_S, H_C and M_R with decreasing temperature is evident from Figure 23. This increment is expected as the temperature drops interactions between the magnetic moments of the neighbouring atoms decreases [44]. The M_S increased by about ~2% from ~217 ± 4 Am^2/kg to ~221 ± 4 Am^2/kg, H_C increased by about ~34% from 0.98 kA/m to 1.32 kA/m and M_R increased by ~32% from ~0.62 Am^2/kg to ~0.81 Am^2/kg .

The dependence of M_S on the temperature at sub-ambient temperatures is given by Bloch's law [45]:

$$M_S(T) = M_S(0)\,[1-AT^{3/2}] \tag{31}$$

Where $M_S(0)$ is the saturation magnetization at absolute (0 K), A is a constant, and T is the temperature. From the sub-ambient runs the $M_S(0)$ and A was estimated to be ~220.95 Am^2/kg and 1.3×10^{-9} K$^{-3/2}$. At 0 K the magnetic moment per atom (μ_H) and saturation magnetization $M_S(0)$ are related as :

$$M_S(0) = \mu_H\,(N/A_W) \tag{32}$$

Where N is the Avogadro's number, A_W is the atomic weight. In the case of Fe taking the atomic weight as 55.845 g/mol the μ_H is estimated to be ~2.1 μ_B .

Magnetocrystalline anisotropy constant (K_1) analysis:Table 1 below shows the analysis of the different variants of the Law of Approach to Saturation for elemental Fe powders. Curve fitting of

the experimental data to the LAS variants was conducted using the commercial statistical software "Origin". Evaluation of the different variations of the LAS are done on a case by case basis based on statistical variation, variation of Magnetic saturation (M_S) from the known M_S values obtained from hysteresis loops and known metallurgical history of the powders.

Among the different variants of the Law of Approach to Saturation (LAS), LAS A has the least variation in the magnetocrystalline anisotropy constant (K_1) values. It is also evident that there is increasing variation in the constants as we go from left to right in the table. Constant *b* which is associated with crystal structure varies by ~35% in both LAS C and LAS D relative to ~25% in both LAS A and LAS B. Constant *a* which is associated to plastic deformation has ~70% variation in LAS C and about 35% variation in LAS D. It is also noticed that the M_S values in the case of LAS D have drastically deviated from known ~217 Am^2/kg inferred from the hysteresis loops. There is slight deviation in the M_S values for both LAS B and LAS C while LAS A reports a value consistent with the value observed through hysteresis loops.

Table 1. Evaluation of different variants of Law of Approach to Saturation in Fe powders

	LAS A				**LAS B**					**LAS C**					**LAS D**				
Temperature (K)	Magnetic saturation M_S (Am^2/kg) ±3	Constant $b\times10^{10}$ ±25%	Magnetocrystalline Anisotropy Constant K_1 (J/m^3) $\times10^6$ ±13%		Magnetic saturation M_S (Am^2/kg) ±5	Constant $b\times10^{10}$ ±28%	Constant χ	Magnetocrystalline Anisotropy Constant K_1 (J/m^3)$\times10^6$ ±16%		Magnetic saturation M_S (Am^2/kg) ±2	Constant $b\times10^{10}$ ±36%	Constant $a\times10^4$ *±69%*	Magnetocrystalline Anisotropy Constant K_1 (J/m^3)$\times10^6$ ±18%		Magnetic saturation M_S (Am^2/kg) ±2	Constant $b\times10^{10}$ ±32%	Constant $a\times10^4$ *±35%*	Constant χ	Magnetocrystalline Anisotropy Constant K_1 (J/m^3)$\times10^6$ ±15%
300	217.5	3.38	1.43		219.6	3.58	0.010	1.48		215.1	4.41	2.3	1.60		203.7	8.71	10	0.025	2.15
270	217.9	3.47	1.45		220.2	3.68	0.010	1.50		215.4	4.56	2.5	1.62		204.9	8.72	10	0.025	2.17
240	218.7	3.51	1.46		221.0	3.73	0.011	1.52		216.0	4.63	2.5	1.64		206.0	8.72	10	0.023	2.18
210	219.3	3.55	1.47		221.8	3.77	0.011	1.53		216.7	4.68	2.6	1.65		207.0	8.72	9.9	0.023	2.19
180	219.9	3.58	1.48		222.4	3.8	0.011	1.54		217.2	4.73	2.6	1.67		207.9	8.71	9.7	0.022	2.20
150	220.4	3.61	1.49		222.9	3.84	0.011	1.55		217.6	4.78	2.6	1.68		208.7	8.71	9.6	0.021	2.21
120	220.7	3.63	1.50		223.3	3.87	0.011	1.56		217.9	4.82	2.7	1.69		209.4	8.70	9.4	0.020	2.21
90	221.1	3.66	1.51		223.7	3.89	0.012	1.57		218.2	4.86	2.7	1.70		210.0	8.69	9.3	0.019	2.22
60	221.3	3.66	1.51		224.1	3.9	0.012	1.58		218.4	4.90	2.8	1.71		210.3	8.71	9.3	0.019	2.23

Note: R^2 values for all the above variants of Law of approach to saturation are >0.996.

Also, these Elemental Fe powders are commercially acquired and do not have a metallurgical history of them having undergone any plastic deformation. The effect of constant a should be negligible in this case. LAS C and LAS D, as suggested by the variation in data, seem to be a forced fit in this case. Among LAS A and LAS B, close similarities within the K_1 and constant b values are observed. The constant χ seems to have a negligible effect on the K_1 values in this case. Even with similar values, LAS A seems to have a consistent M_S value and less data variation in comparison, and we consider it to be the right fit for the case of elemental Fe powders.

The K_1 values, as shown in Table 1 for iron, is estimated to be ~1.43×10^6 J/m^3. It is also evident from the table that the K_1 values increase with a decrease in temperature and this is graphically illustrated in Figure 24 below.

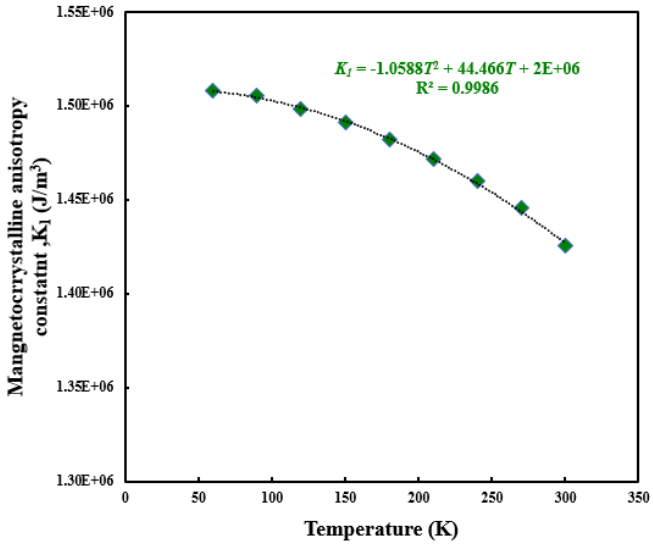

Figure 26. Magnetocrystalline anisotropy constant (K_1) vs Temperature (T)

K_1 increases from ~ 1.43×10^6 J/m^3 at 300 K to ~1.51×10^6 J/m^3 at 60 K an increase of ~5%. Increase in K_1 with respect to decreasing temperature is expected as K_1 is related to both M_S and H_C and is similar trend is noticed in both M_S and H_C.

5.2.2 Cobalt (Co)

Figure 25 below shows the magnetization (M) versus the applied magnetic field (H) for elemental cobalt powders. The M_S, H_C and M_R were estimated to be 160 ±1 Am^2/kg, ~12 kA/m and 7 ± ~10% Am^2/kg, respectively.

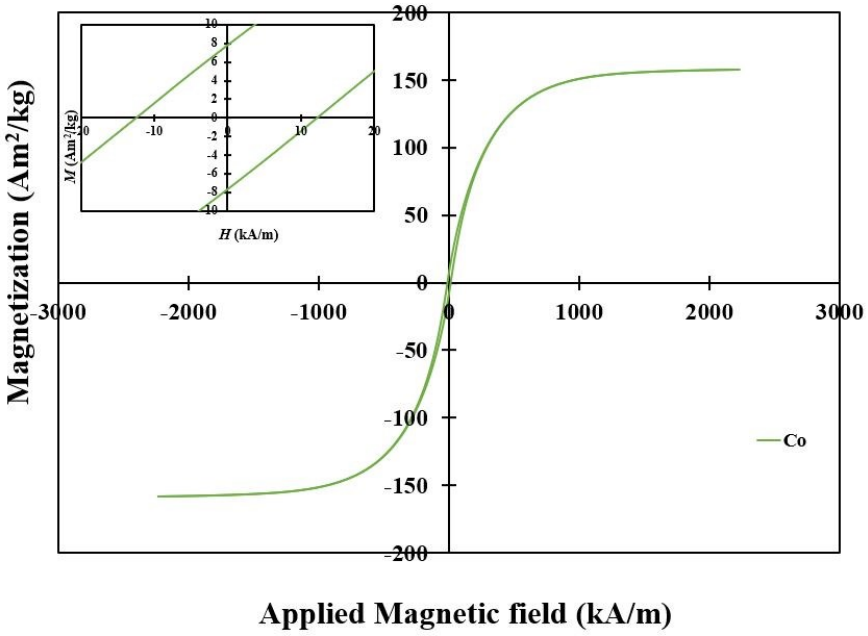

Figure 27.Magnetization (*M*) vs Applied magnetic field (*H*) curves for elemental Co powders at ambient temperature

The magnetization (*M*) versus the applied magnetic field (*H*) for cobalt at sub ambient temperatures are shown below in Figure 26.

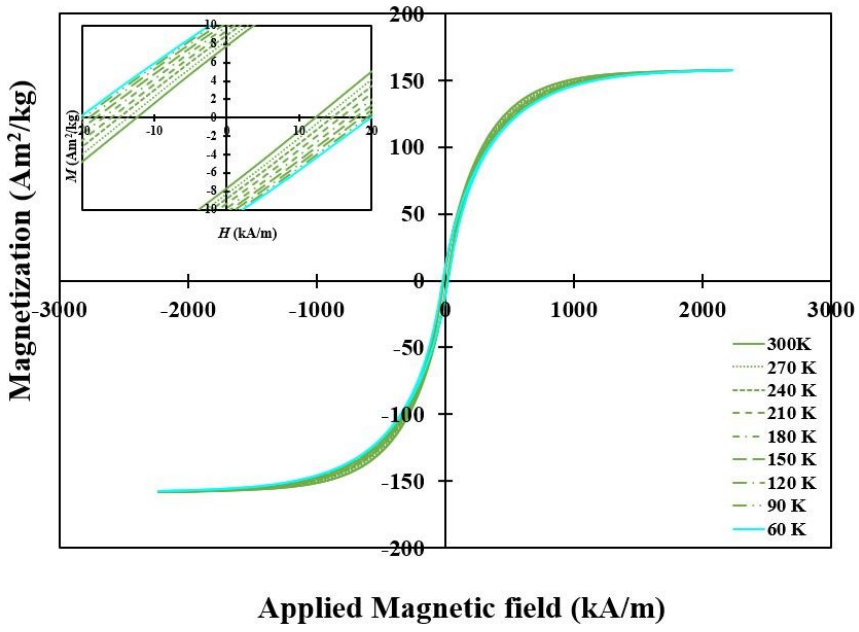

Figure 28.Magnetization (*M*) vs Applied magnetic field (*H*) curves for elemental Co powders at sub-ambient temperatures

Variation of M_S, H_C and M_R with respect to decreasing temperature is shown below in Figure 27.

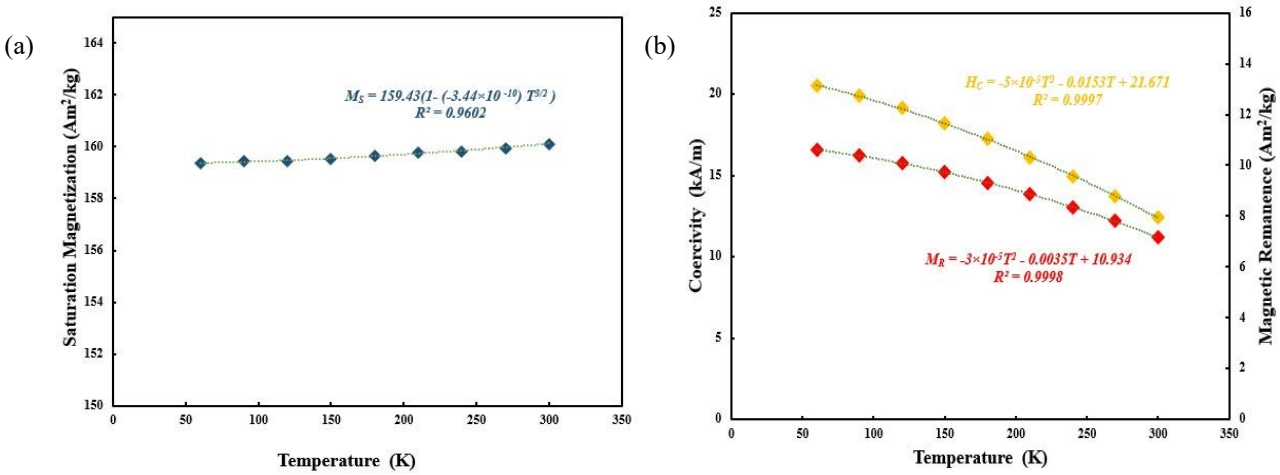

Figure 29.a)Magnetic saturation (M_S) vs Temperature (T) b) Coercivity (H_C) & Magnetic remanence (M_R) vs Temperature (T)

In the case of cobalt, the variation of M_S with respect to temperature seems to be negligible. An increase in H_C of about ~65% from ~12 kA/m to ~20 kA/m and M_R by 48% from ~7 Am^2/kg to ~11 Am^2/kg from 300 K to 60 K is noted.

The dependence of M_S on temperatures in the sub-ambient range are plotted with respect to Bloch's law as given by Eqn 31.Using Bloch's law $M_S(0)$ and A were estimated to be ~159.43 Am^2/kg and ~-3.44×10^{-10} $K^{-3/2}$. Estimating magnetic moment per atom (μ_H) using Eqn 32 taking A_W for nickel as 58.933 g/mol we get the value to be ~1.56 μ_B .

Table 2.Evaluation of different variants of Law of Approach to Saturation in Co powders

	LAS A				**LAS B**					**LAS C**					**LAS D**				
Temperature (K)	Magnetic saturation M_S (Am^2/kg) ±0.5	Constant $b\times10^{10}$ ±7%	Magneto crystalline Anisotropy Constant K_1 (J/m^3)×10^5 ±4%		Magnetic saturation M_S (Am^2/kg) ±0.4	Constant $b\times10^{10}$ ±7%	Constant χ	Magneto crystalline Anisotropy Constant K_1 (J/m^3)×10^5 ±3%		Magnetic saturation M_S (Am^2/kg) ±1.3	Constant $b\times10^{10}$ ±4%	Constant $a\times10^5$ *±13%*	Magneto crystalline Anisotropy Constant K_1 (J/m^3)×10^5 ±2%		Magnetic saturation M_S (Am^2/kg) ±4	Constant $b\times10^{10}$ ±34%	Constant $a\times10^5$ *±9%*	Constant χ	Magneto crystalline Anisotropy Constant K_1 (J/m^3)×10^5 ±20%
300	160.1	5.50	8.09		158.1	5.25	0.010	7.80		162.9	3.94	0.35	6.97		182.3	0.459	1.4	-0.051	2.45
270	160.0	5.79	8.29		156.8	5.41	0.016	7.86		163.8	3.56	0.49	6.67		185.9	0.286	1.6	-0.058	1.88
240	159.8	6.12	8.52		155.4	5.60	0.022	7.92		165.0	3.16	0.65	6.33		189.4	0.946	1.8	-0.064	3.94
210	159.8	6.41	8.72		154.2	5.75	0.028	7.97		166.1	2.79	0.80	5.98		192.2	1.50	2.0	-0.069	5.06
180	159.7	6.65	8.87		153.1	5.88	0.033	8.00		167.0	2.46	0.92	5.65		194.3	1.93	2.2	-0.072	5.80
150	159.5	6.86	9.00		152.1	6.00	0.037	8.03		167.7	2.20	1.0	5.37		196.0	2.27	2.3	-0.074	6.35
120	159.4	7.02	9.11		151.4	6.09	0.040	8.05		168.3	2.01	1.1	5.14		197.4	2.53	2.4	-0.077	6.77
90	159.5	7.15	9.19		150.9	6.17	0.042	8.08		168.8	1.88	1.2	4.98		198.5	2.72	2.5	-0.078	7.05
60	159.4	7.23	9.23		150.6	6.22	0.044	8.10		168.9	1.82	1.2	4.90		199.2	2.83	2.5	-0.080	7.22

Note: R^2 values for all the above variants of Law of approach to saturation are >0.992

Magnetocrystalline anisotropy constant (K_1) analysis:

Table 2 (page 39) shows the analysis of different variants of LAS on elemental Co powders. It is observed that the percentage variation in the magnetocrystalline anisotropy constant (K_1) in the case of LAS D is higher in comparison to the other variants. A higher variation of ~35% in the constant *b,* which is known to be related to the crystal structure, is also noticed in LAS D while this variation is >7% in the other variants. Constant *a,* which is related to internal stresses caused by plastic deformation, shows a of variation ~10% in both LAS A and LAS D. From the table, it is also evident that K_1 values in the case of LAS C seem to be decreasing with decreasing temperature this trend seems unlikely as both M_S and H_C increase with decreasing temperatures and K_1 influences both these factors. Similarly, M_S values seem to drastically vary from the M_S value of ~160 Am^2/kg inferred from the hysteresis loops in the case of LAS D. This leads us to believe that the experimental data is being forced fit to both LAS C and LAS D. LAS A and LAS B show similar K_1 values. This indicates that the effect of χ term is negligible. The fact that these elemental powders have no metallurgical history of plastic deformation or applied stress leads us to believe that Akulov's original equation, i.e. LAS A is the correct fit for Co Elemental powders.

From table 2, K_1 value for elemental cobalt powders at room temperature (300 K) is estimated to be ~8.09×10^5 J/m^3. The figure below shows the dependence of K_1 value on decreasing temperature. K_1 increases with a decrease in temperature. K_1 increases from ~8.09×10^5 J/m^3 at 300 K to ~9.23×10^5 J/m^3 at 60 K an increase of ~14%.

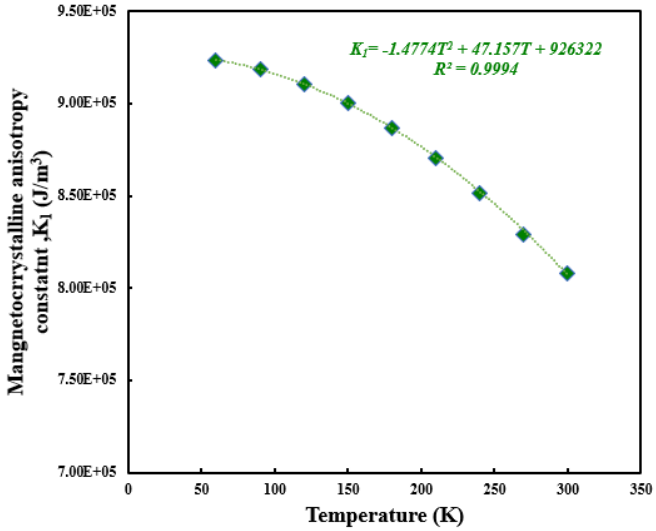

Figure 30.. Magnetocrystalline anisotropy constant (K_1) vs Temperature (T)

5.2.3. Nickel (Ni)

5.2.3.1. Nickel Spherical Powders

The Magnetization (*M*) versus applied field (*H*) for nickel is shown below in Figure 29. The M_S, H_C and M_R were estimated to be ~55 Am^2/kg, 3 ± ~1% kA/m and 2 ± ~10% Am^2/kg respectively.

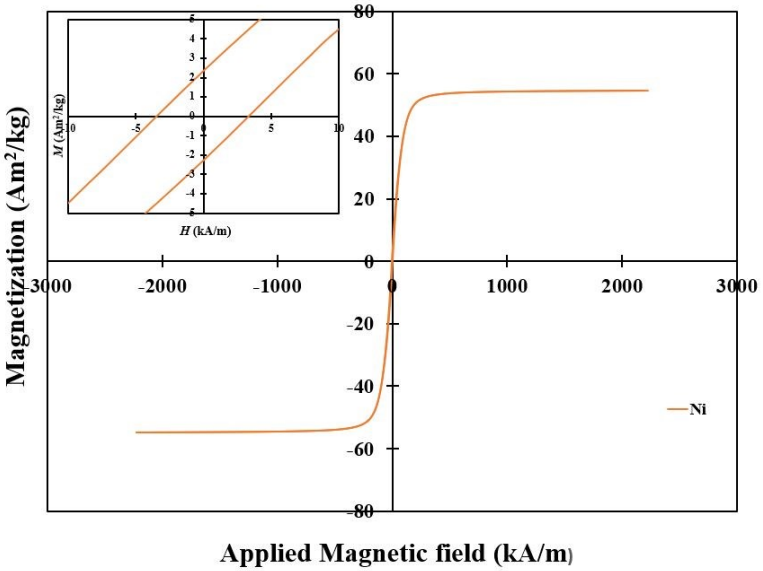

Figure 31.Magnetization (*M*) vs Applied magnetic field (*H*) curves for elemental Ni powders at ambient temperature

The inset illustrates the magnetization (*M*) versus the applied magnetic field (*H*) behavior at low fields of about ±5 kA/m. The magnetization (*M*) versus the applied magnetic field (*H*) curves for the case of Ni elemental powders at sub-ambient temperatures are shown below in Figure 30.

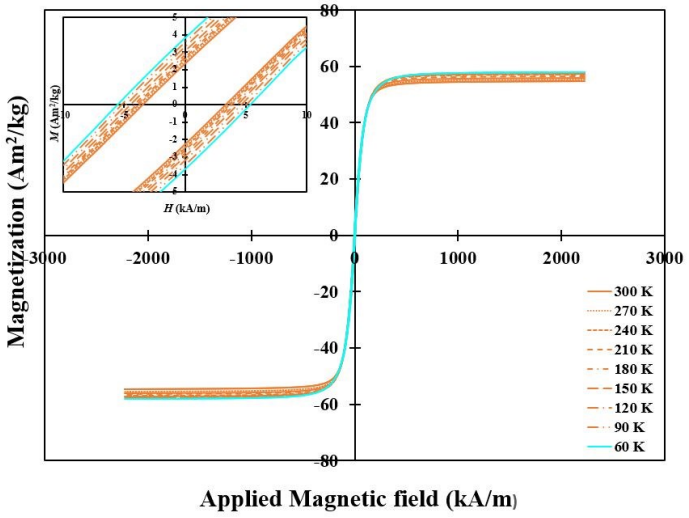

Figure 32. Magnetization (*M*) vs Applied magnetic field (*H*) curves for elemental Ni powders at sub-ambient temperatures

Variation of M_S, H_C and M_R with respect to decreasing temperature is shown below in Figure 31.

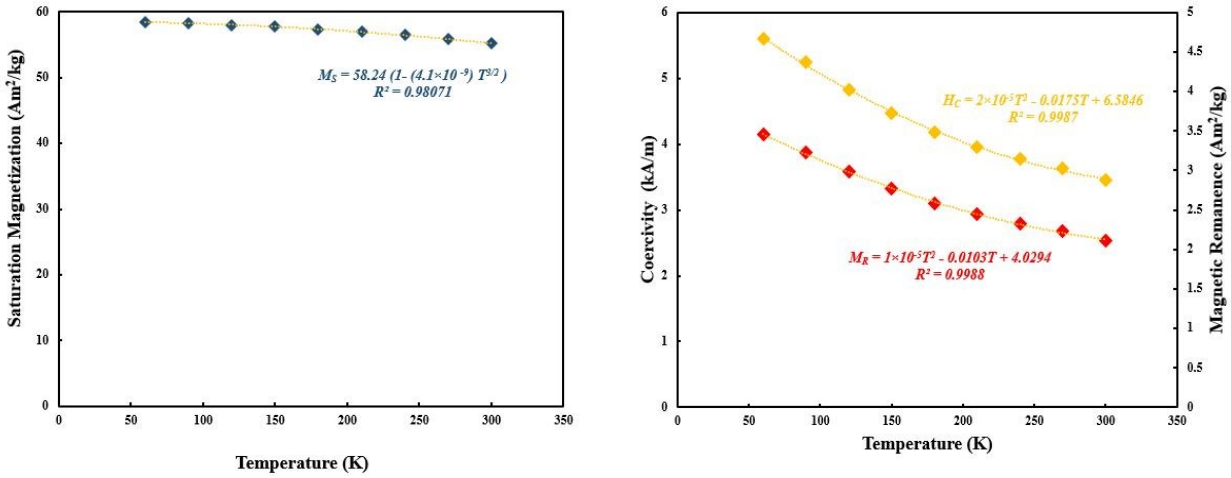

Figure 33.a)Magnetic saturation (M_S) vs Temperature (T) b) Coercivity (H_C) & Magnetic remanence (M_R) vs Temperature (T)

From Figure 31, it is evident that there is an increase in M_S, H_C and M_R with a decrease in temperature. While M_S increases by a modest ~6% from ~55 Am^2/kg to ~58 Am^2/kg, H_C increased by ~62% from ~3.4 kA/m to ~5.6 kA/m and M_R increase by ~64% from ~2.1 Am^2/kg to ~3.4 Am^2/kg. The dependence of M_S on temperatures in the sub-ambient range is plotted with according to Bloch's law as given by Eqn 31.Using Bloch's law $M_S(0)$ and A were estimated to be ~58.24 Am^2/kg and ~4.1×10^{-9} $K^{-3/2}$. Estimating magnetic moment per atom (μ_H) using Eqn _ taking A_W for nickel as 58.68 g/mol we get the value to be ~0.567 μ_B .

Table 3.Evaluation of different variants of Law of Approach to Saturation in Ni spherical powders

	LAS A				**LAS B**					**LAS C**					**LAS D**				
Temperature (K)	Magnetic saturation M_S (Am^2/kg) ±0.4	Constant $b\times10^9$ ±5%	Magneto crystalline Anisotropy Constant K_1 (J/m^3)×10^5 ±3%		Magnetic saturation M_S (Am^2/kg) ±0.4	Constant $b\times10^9$ ±6%	Constant χ	Magneto crystalline Anisotropy Constant K_1 (J/m^3)×10^5 ±4%		Magnetic saturation M_S (Am^2/kg) ±0.4	Constant $b\times10^9$ ±15%	Constant $a\times10^3$ *±11%*	Magneto crystalline Anisotropy Constant K_1 (J/m^3)×10^5 ±8%		Magnetic saturation M_S (Am^2/kg) ±0.4	Constant $b\times10^9$ ±14%	Constant $a\times10^3$ *±43%*	Constant χ	Magneto crystalline Anisotropy Constant K_1 (J/m^3)×10^5 ±7%
300	55.2	4.30	1.46		55.0	3.31	0.001	1.28		55.4	1.15	7.95	0.751		55.2	2.70	3.75	0.001	1.15
270	55.8	4.13	1.45		55.7	3.32	0.001	1.30		56.0	1.39	6.45	0.845		55.8	2.61	2.33	0.001	1.15
240	56.5	4.12	1.47		56.3	3.40	0.001	1.33		56.6	1.70	5.69	0.944		56.4	2.84	1.85	0.001	1.22
210	57.0	4.14	1.49		56.8	3.51	0.001	1.36		57.1	2.01	5.03	1.03		56.9	2.99	1.72	0.001	1.26
180	57.4	4.23	1.51		57.3	3.67	0.001	1.41		57.5	2.35	4.43	1.13		57.4	3.22	1.53	0.000	1.32
150	57.7	4.39	1.55		57.6	3.91	0.001	1.46		57.9	2.77	3.81	1.23		57.7	3.60	1.08	0.000	1.40
120	58.0	4.68	1.61		57.9	4.27	0.000	1.53		58.1	3.30	3.25	1.35		58.0	4.05	1.00	0.000	1.49
90	58.3	5.12	1.69		58.2	4.76	0.000	1.63		58.4	3.91	2.84	1.48		58.2	4.68	0.855	0.000	1.61
60	58.5	5.61	1.77		58.4	5.32	0.000	1.73		58.5	4.64	2.26	1.61		58.4	5.27	0.906	0.000	1.72

Note: R^2 values for all the above variants of Law of approach to saturation are >0.981

Magnetocrystalline anisotropy constant (K_1) analysis:

Table 3 shows the results obtained from curve fitting with the different variation of LAS for elemental Ni (spherical powders). Analyzing the results for K_1 indicates a higher variation in values for both LAS C and LAS D relative to LAS A and B. A closer look at the constant *b,* which is related to the crystal structure, indicated a higher degree of variation in LAS C and LAS D. A considerable variation in constant *a,* which is related to plastic deformation in the case for LAS D, is evident. Comparing the K_1 values for all different variants of LAS, it is evident that LAS C relatively lower values while the values are similar in LAS A, LAS B and LAS D. A higher K_1 value in the case of LAS D and a lower value in the case of LAS C indicates that the large variation in the constant *a* in LAS D counteracts the change in value due to the variation in constant *b*. M_S values for all the different variants are a close match to the M_S value of ~55 Am^2/kg inferred from the hysteresis loops. The effect of constant χ which is arises due to the internal magnetic fields seems negligible in the case of elemental Ni powders. Knowing the metallurgical history of these pure gas atomized elemental powders helps us know that the effect of constant *a* should be negligible, and the large variations counteracting the effect on K_1 due to constant *b* seems to indicate a force fit. Based on the analysis of this data, we are led to believe LAS A is the right fit for elemental nickel powders as well.

Using LAS A, K_1 is estimated to be ~1.46×10^5 J/m^3 at room temperature (300 K). The figure below shows the dependence of K_1 on varying temperature. K_1 increases with a decrease in temperature. K_1 increases from ~1.46×10^5 J/m^3 at 300 K to ~1.77×10^5 J/m^3 at 60 K, an increase of ~21%.

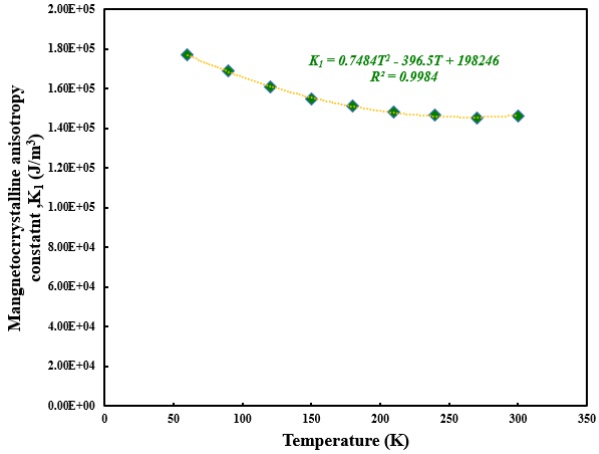

Figure 34.Magnetocrystalline anisotropy constant (K_1) vs. Temperature (T)

5.2.3.2. Nickel Flake Powders

Figure 33 shows the magnetization (M) versus the applied magnetic field (H) curves for Ni flake powders. The inset shows the M-H curves at the low magnetic field realm of about ±10 kA/m.

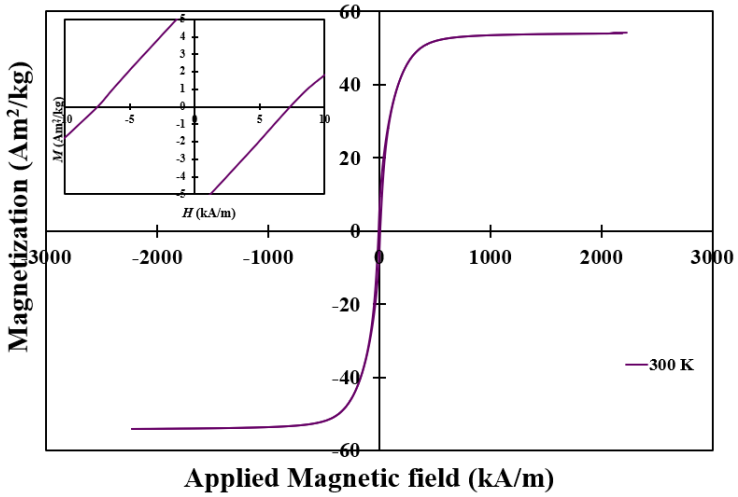

Figure 35.Magnetization (M) vs. Applied magnetic field (H) curves for elemental Ni-Flake powders at ambient temperature

The M_S, H_C and M_R were estimated from the M-H curves above. The M_S was estimated to be ~54 Am^2/kg. The H_C and M_R were estimated to be ~9 ±1% kA/m and ~6 ±3% Am^2/kg.

Figure 34 shows the M-H curves at sub-ambient temperatures. A closer examination reveals an increasing M_S, H_C and M_R with decreasing temperature similar to the materials previously discussed.

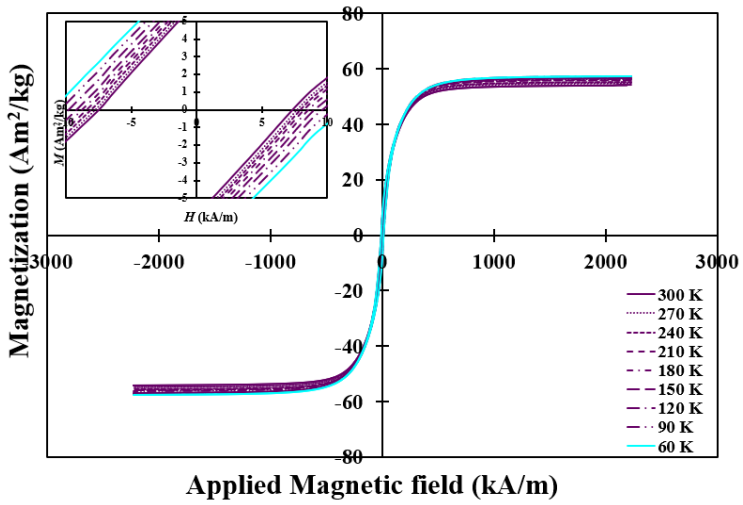

Figure 36. Magnetization (M) vs. Applied magnetic field (H) curves for elemental Ni-Flake powders at sub-ambient temperatures

Figure 35 below shows the variation of M_S, H_C and M_R concerning temperature(T).

(a)

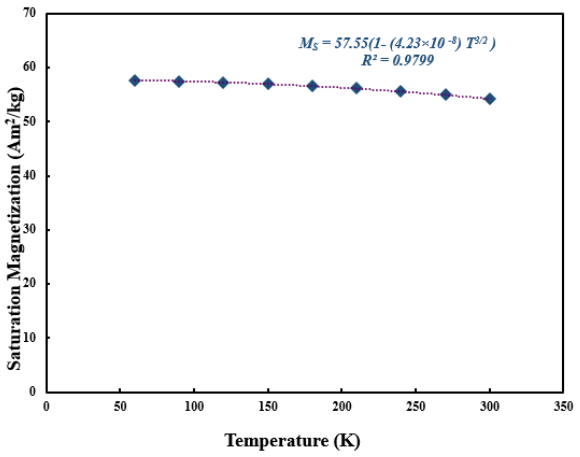

(b)

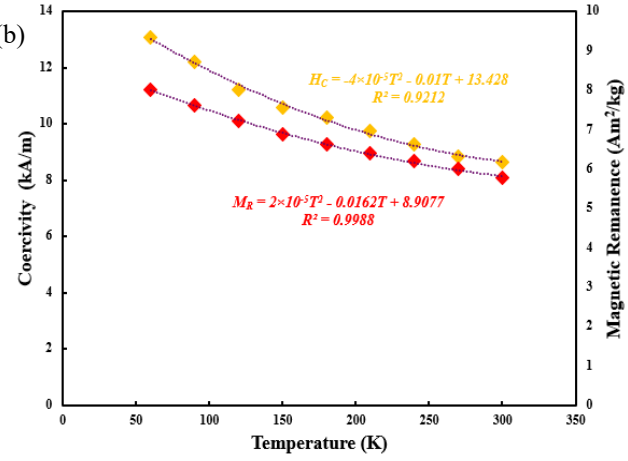

Figure 37.a)Magnetic saturation (M_S) vs Temperature (T) b) Coercivity (H_C) & Magnetic remanence (M_R) vs Temperature (T)

M_S, H_C and M_R progressively increased with decreasing temperature. M_S increased from ~54 Am^2/kg at 300 K to about ~58 Am^2/kg at 60 K, an increase of about ~7%. A similar trend in the case of H_C and M_R is noticed where H_C increased from ~9 kA/m at 300 K to ~13 kA/m at 60 K, a ~45% increase, M_R increased from ~6 Am^2/kg at 300 K to 8 Am^2/kg an increase of about 33%. Using Bloch's law $M_S\,(0)$ and A was estimated to be ~57.55 Am^2/kg and ~4.23×10^{-8} $K^{-3/2}$. In a similar fashion, using Eqn 32, taking A_W for nickel as 58.68 g/mol we calculate magnetic moment per atom (μ_H) to be ~0.56 μ_B .

Table 4.Evaluation of different variants of Law of Approach to Saturation in Ni flake powders

	LAS A				**LAS B**					**LAS C**					**LAS D**				
Temperature (K)	Magnetic saturation M_S (Am^2/kg) ±0.3	Constant $b\times10^{10}$ ±8%	Magneto crystalline Anisotropy Constant K_1 (J/m^3)×10^5 ±4%		Magnetic saturation M_S (Am^2/kg) ±0.3	Constant $b\times10^{10}$ ±9%	Constant χ	Magneto crystalline Anisotropy Constant K_1 (J/m^3)×10^5 ±4%		Magnetic saturation M_S (Am^2/kg) ±0.3	Constant $b\times10^{10}$ ±11%	Constant $a\times10^2$ *±39%*	Magneto crystalline Anisotropy Constant K_1 (J/m^3)×10^5 ±5%		Magnetic saturation M_S (Am^2/kg) ±0.3	Constant $b\times10^{10}$ ±4%	Constant $a\times10^3$ *±43%*	Constant χ	Magneto crystalline Anisotropy Constant K_1 (J/m^3)×10^5 ±2%
300	54.4	1.09	2.30		54.4	1.05	0.000	2.25		54.5	1.01	44.4	2.19		53.8	1.39	11.0	0.002	2.56
270	55.1	1.08	2.32		55.0	1.05	0.000	2.28		55.1	1.00	18.9	2.23		54.5	1.37	10.3	0.002	2.59
240	55.7	1.11	2.37		55.7	1.09	0.000	2.35		55.7	1.07	8.65	2.33		55.1	1.42	10.7	0.002	2.66
210	56.2	1.13	2.42		56.2	1.13	0.000	2.42		56.2	1.14	4.51	2.44		55.7	1.45	10.4	0.001	2.72
180	56.7	1.16	2.48		56.7	1.17	0.000	2.48		56.7	1.21	10.1	2.52		56.2	1.47	9.79	0.001	2.76
150	57.1	1.20	2.53		57.1	1.21	0.000	2.54		57.0	1.26	15.9	2.59		56.6	1.50	9.32	0.001	2.80
120	57.3	1.25	2.60		57.4	1.27	0.000	2.61		57.3	1.33	19.7	2.68		57.0	1.47	6.75	0.001	2.80
90	57.6	1.31	2.67		57.6	1.33	0.000	2.69		57.5	1.40	20.0	2.75		57.4	1.43	3.46	0.000	2.78
60	57.8	1.37	2.74		57.8	1.39	0.000	2.76		57.7	1.45	18.2	2.81		57.9	1.35	1.89	0.000	2.73

Note: R^2 values for all the above variants of Law of approach to saturation are >0.999

Magnetocrystalline anisotropy constant (K_1) analysis:

Table 4 above shows the data obtained from curve fitting different variants of LAS in the case of Ni (flake powders). Examination of constant *b* in the different variants of LAS, we see that the variation is <11%. The constant *a* shows a large variation of ~40% in both LAS C and LAS D. The constant χ shows negligible effect on K_1 in both LAS B and LAS D. The magnetocrystalline anisotropy across all the different variants of LAS show a variation of <5%. The values of M_S at room temperature in the case of all the LAS seem to closely match the M_S value of ~54 Am^2/kg inferred from the hysteresis loops. The M_S values also seem to closely mirror each other as the temperature decreases from 300 K to 60 K. As noticed in the case of Ni (spherical powders) constant *a* seems to be counteracting the discrepancy in K_1 due to variation in constant *b* in LAS C and reporting an even higher value K_1 value in the case of LAS D. Knowing the metallurgical history for these elemental powders leads us to believe that the effect of constant *a* should be minimal and constant χ appears to have minimal effect on K_1. Selecting Akulov's original equation, i.e., LAS A, appears appropriate in this case as well.

Using LAS A, the K_1 in the case of elemental Ni (flake powders) is estimated to be ~2.30×10^5 J/m^3. The figure below shows the dependence of K_1 on decreasing temperature. A trend of increasing K_1 with decreasing temperature is evident from the figure. K_1 increases from ~2.30×10^5 J/m^3 at 300 K to ~2.74×10^5 J/m^3g at 60 K, an increase of ~19%.

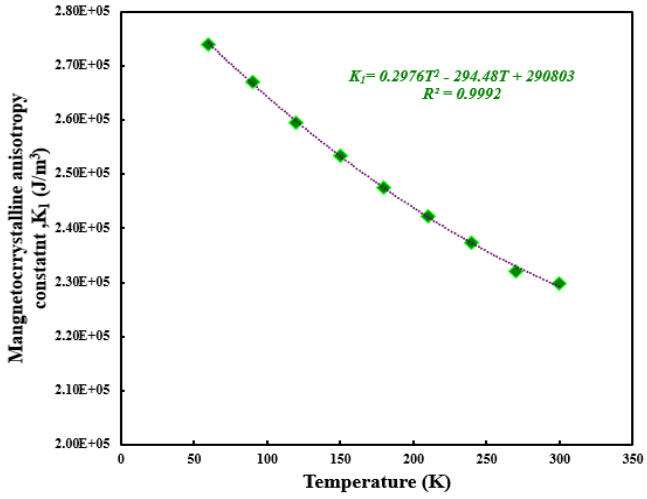

Figure 38.Magnetocrystalline anisotropy constant (K_1) vs. Temperature (*T*)

Comparison of Ni (spherical) and Ni (Flake) powders:

The figure below shows the *MvH* graphs of both Ni (spherical powders) and Ni (Flake powders) it is noticeable that there is a considerable difference in the way both these powders reach magnetic saturation.

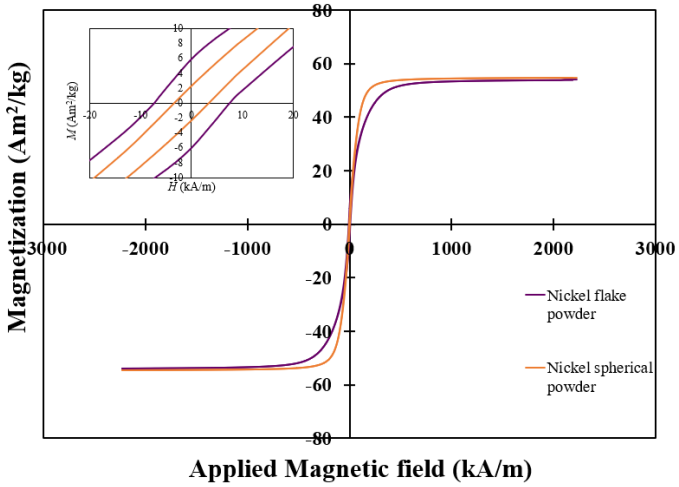

Figure 39.Magnetization (*M*) vs Applied magnetic field (*H*) curves for elemental Ni (Spherical and Flake) powders at ambient temperature

The figure indicates a similar M_S value in the case of both powders. The M_S value is ~55 Am^2/kg for the Ni (spherical powders) and ~54 Am^2/kg for the Ni (flake powders). The inset in the figure above reveals that there is considerable change in the H_C and M_R values. The H_C and M_R values for Ni (spherical) powders are~ 3 kA/m and ~2 Am^2/kg. The value of H_C and M_R for the Ni (flake) powders are ~9 kA/m and ~6 Am^2/kg. An increase in both H_C and M_R in the case of Ni (flake) powders by ~200%. This increase can be explained taking into account the shape anisotropy factor. Shape anisotropy is explained in detail in the literature review and is nothing but the preference of magnetization to the same extent in any direction in the case of a spherical solid but when the shape is non spherical (as in the case of the flake powders) the magnetization will be easier in the long axis and harder in the short axis this is because the demagnetizing field is stronger along the shorter axis. A stronger field would be required to induce the same magnetization along the shorter axis and shape alone can induce anisotropy.

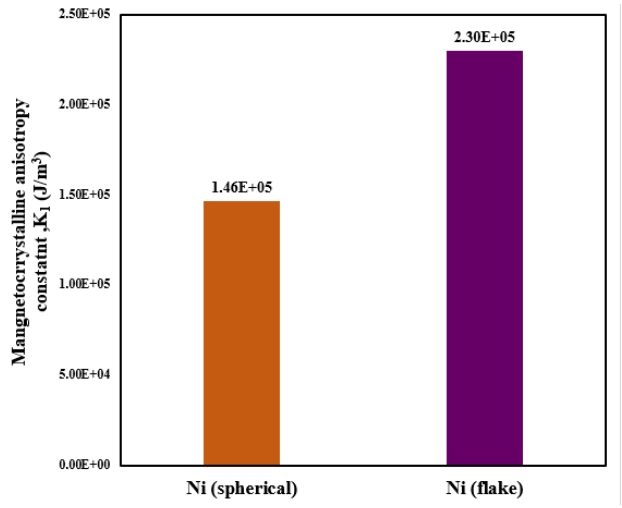

Figure 40.Comparision of the Magnetocrystalline anisotropy constant (K_1) for Ni powders

The figure above shows a comparison of the K_1 values for the Ni powders. It is clear that the K_1 values in the case of Ni (flake) powders are greater relative to the Ni (spherical) powders. The K_1 values for the Ni (flake powders) are greater in magnitude by ~60%. These increased values owing to the shape anisotropy factor can be exploited to engineer materials to fit the requirement and develop better magnets for specific applications.

5.2.4. Comparison of Elemental Powders

Figure 39 below shows the *M-H* curves for the three elemental ferromagnetic powders. The inset shows the *M-H* curves in low magnetic field realm of ± 10 kA/m.

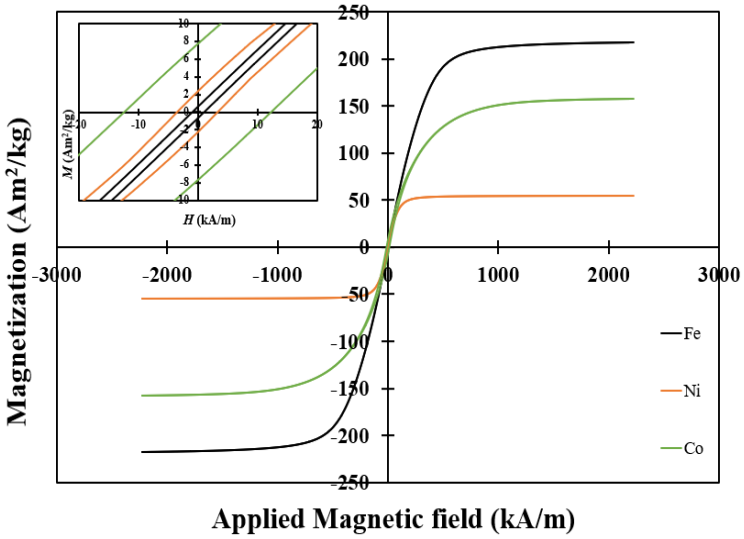

Figure 41.*M-H* curves for elemental ferromagnetic powders at 300 K

From the *M-H* curves, it is evident that Fe has superior M_S values when compared to Ni and Co. Co has intermediate M_S values but has excellent H_C and M_R values. Nickel has the lowest M_S but has better H_C and M_R values than Fe. Figure 40 below compares the K_1 values of bulk ferromagnetic materials with their powders. It is evident from the figure below that the K_1 values for the powders are at least one order above their bulk counterparts.

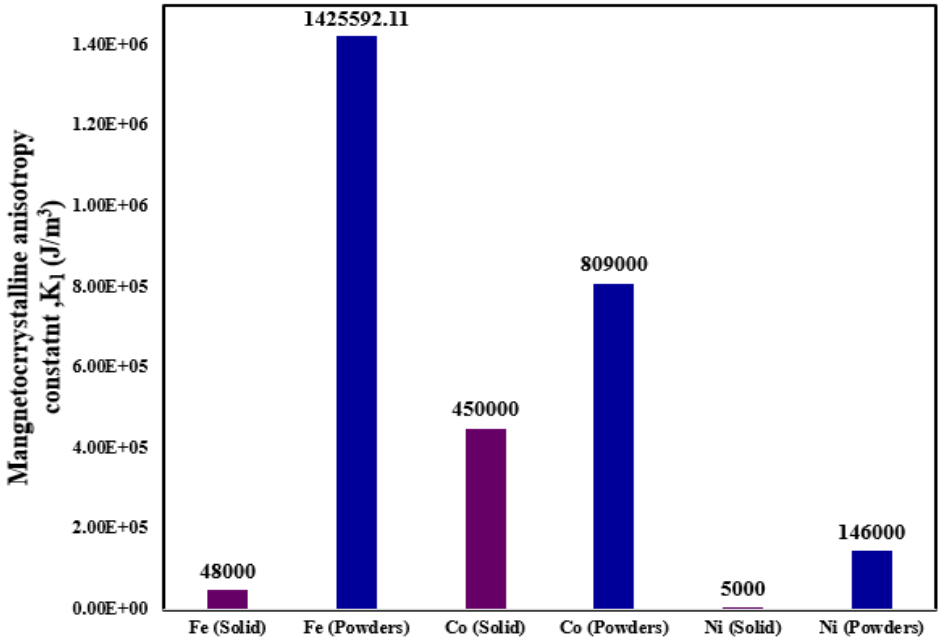

Figure 42.Comparison of K_1 for elemental ferromagnetic powders

Looking at the *M-H* curves for these three elemental powders gives us an insight regarding the magnetic properties of the various alloys that can be made with varying compositions of these materials. Such as a Fe rich alloy should give us superior M_S values while a Co rich alloy should give us superior H_C and M_R values.

5.3. Magnetic Properties of Alloy Powders

5.3.1. $Fe_{33.33}Ni_{33.33}Co_{33.33}$

Figure 41 below shows the magnetization (*M*) versus the applied magnetic field (*H*) curves for $Fe_{33.33}Ni_{33.33}Co_{33.33}$ with equiatomic composition. The M_S, H_C and M_R were estimated to be 137 ±1 Am^2/kg, ~3 ±1% kA/m, ~2 ±12% Am^2/kg, respectively.

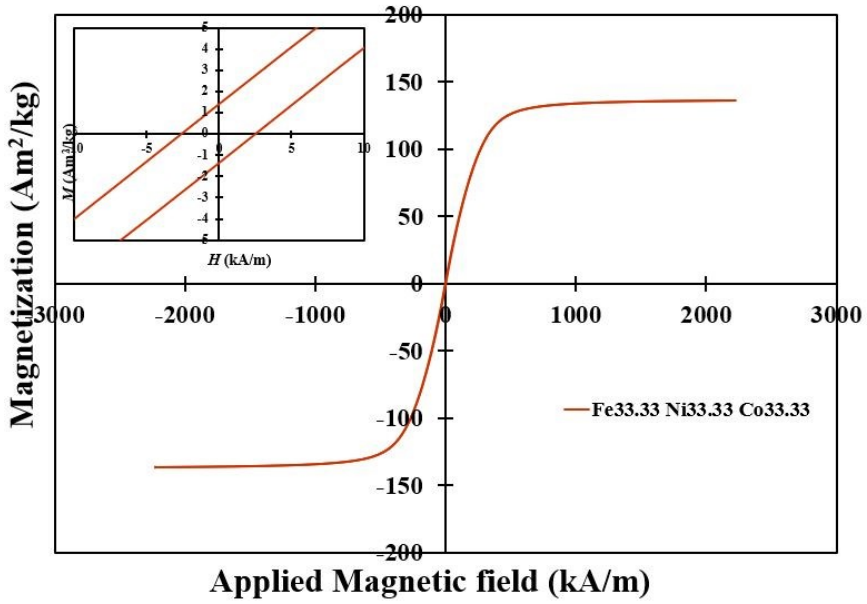

Figure 43.Magnetization (*M*) vs. Applied magnetic field (*H*) curves for $Fe_{33.33}Ni_{33.33}Co_{33.33}$ alloy powders at ambient temperature

Figure 42 below shows the *M-H* curves for the alloy $Fe_{33.33}Ni_{33.33}Co_{33.33}$ at sub-ambient temperatures.

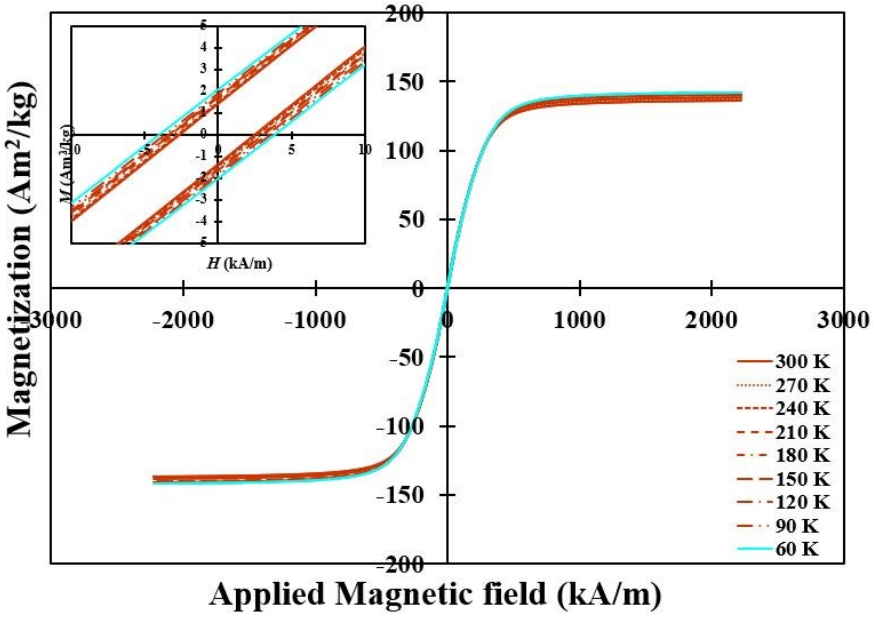

Figure 44.Magnetization (*M*) vs. Applied magnetic field (*H*) curves for $Fe_{33.33}Ni_{33.33}Co_{33.33}$ alloy powders at sub-ambient temperatures

The dependence of M_S, H_C and M_R on decreasing temperature is shown below in Figure 43.

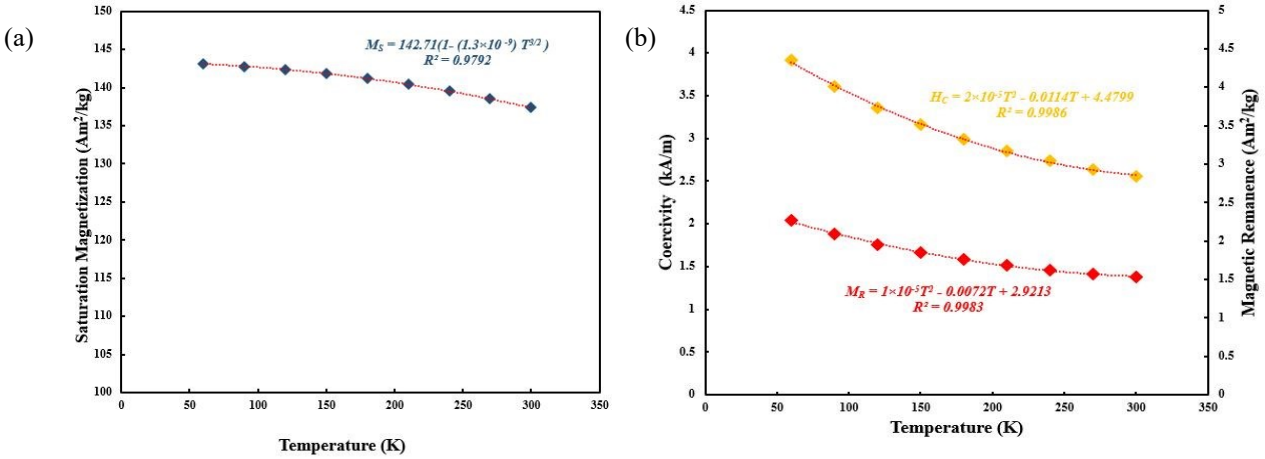

Figure 45.a)Magnetic saturation (M_S) vs Temperature (T) b) Coercivity (H_C) & Magnetic remanence (M_R) vs Temperature (T)

Similar to elemental powders, a trend of increasing M_S, H_C and M_R are noticed in the case of $Fe_{33.33}Ni_{33.33}Co_{33.33}$ equiatomic alloy. M_S increased from ~137 ±1 Am2/kg at 300K to ~143 Am^2/kg at 60 K, an increase of about ~4%. Similarly, H_C increased from ~2.5 kA/m at 300K to ~3.9 kA/m at 60K an increase of ~56% and M_R increased from ~1.3 Am^2/kg at 300K to ~2 Am^2/kg at 60 K an increase of about 53%.

The dependence of M_S on temperatures in the sub-ambient range are plotted with respect to Bloch's law as given by Eqn 31.Using Bloch's law $M_S(0)$ and A were estimated to be ~142.71 Am^2/kg and ~1.3×10^{-9} $K^{-3/2}$. Estimating magnetic moment per atom (μ_H) using Eqn 32 taking A_W for $Fe_{33.33}Ni_{33.33}Co_{33.33}$ as 57.814 g/mol, we get the value to be ~1.37 μ_B .

Table 5.Evaluation of different variants of Law of Approach to Saturation in $Fe_{33.33}Ni_{33.33}Co_{33.33}$ powders

	LAS A				**LAS B**					**LAS C**					**LAS D**				
Temperature (K)	Magnetic saturation M_S (Am^2/kg) ±0.4	Constant $b\times10^{10}$ ±18%	Magneto crystalline Anisotropy Constant K_1 (J/m^3)×10^5 ±9%		Magnetic saturation M_S (Am^2/kg) ±0.2	Constant $b\times10^{10}$ ±22%	Constant χ	Magneto crystalline Anisotropy Constant K_1 (J/m^3)×10^5 ±11%		Magnetic saturation M_S (Am^2/kg) ±0.8	Constant $b\times10^{10}$ ±34%	Constant $a\times10^3$ *±70%*	Magneto crystalline Anisotropy Constant K_1 (J/m^3)×10^5 ±17%		Magnetic saturation M_S (Am^2/kg) ±2	Constant $b\times10^{10}$ ±35%	Constant $a\times10^3$ *±97%*	Constant χ	Magneto crystalline Anisotropy Constant K_1 (J/m^3)×10^5 ±17%
300	137.4	1.63	6.58		136.9	1.55	0.002	6.37		137.8	1.36	6.49	5.96		136.0	1.75	7.62	0.004	6.68
270	138.5	1.66	6.69		138.1	1.59	0.002	6.51		138.9	1.43	5.43	6.17		137.1	1.83	8.17	0.004	6.89
240	139.6	1.69	6.80		139.2	1.63	0.002	6.64		139.9	1.50	4.90	6.36		138.0	1.91	9.14	0.005	7.08
210	140.4	1.72	6.89		140.1	1.66	0.001	6.76		140.7	1.57	4.73	6.54		138.8	1.98	9.87	0.005	7.25
180	141.2	1.74	6.98		140.9	1.70	0.001	6.88		141.4	1.63	4.58	6.72		139.5	2.05	10.9	0.005	7.41
150	141.8	1.77	7.06		141.6	1.74	0.001	6.98		142.0	1.69	4.45	6.87		140.0	2.12	12.1	0.005	7.57
120	142.4	1.79	7.13		142.2	1.77	0.001	7.07		142.4	1.75	4.41	7.01		140.5	2.18	13.0	0.005	7.70
90	142.8	1.81	7.19		142.7	1.80	0.000	7.15		142.8	1.81	4.24	7.14		140.8	2.24	13.9	0.005	7.82
60	143.1	1.82	7.23		143.1	1.82	0.000	7.22		143.1	1.87	4.24	7.28		141.1	2.30	14.9	0.005	7.94

Note: R^2 values for all the above variants of Law of approach to saturation are >0.999

Magnetocrystalline anisotropy constant (K_1) analysis:

Table 5 shows the data obtained from curve fitting different variations of LAS for the case of $Fe_{33.33}Ni_{33.33}Co_{33.33}$. Comparison of constant b shows increasing variation as we go from left to right on the table with LAS A showing the least variation ~18% and LAS D showing the highest variation ~35%. The effect of χ in the case of LAS B and LAS D seems to be negligible. A comparison of values of M_S deduced using different variants of LAS indicate a relatively close match with the M_S values inferred from the hysteresis loops. There seems to be less variation in the magnetocrystalline anisotropy constant K_1 values for LAS A and LAS B ~10% while there is a greater variation of ~17% in both LAS C and LAS D.A closer look at K_1 values from LAS C and LAS D reveals that there is a higher degree of variation in the latter case.. Also, we see a relatively similar value for the constant b in the case of LAS A, and LAS D at 300 K. LAS D seems to account for the plastic deformation undergone by these powders, and the variation might be explained by differences in the degree of deformation undergone by each individual powder particle. These powders have undergone milling for 9 hours, and a closer look at the K_1 values of LAS A and LAS D suggests that the values are relatively similar. This leads us to believe that the effect of constant a is being overemphasized in this case and the lack of sound data from LAS D leads us to choose LAS A.

Using LAS A the K_1 in the case of $Fe_{33.33}Ni_{33.33}Co_{33.33}$ is estimated to be ~6.58×10^5 J/m^3 at 300 K. The figure below shows the dependence of K_1 on decreasing temperature. A trend of increasing K_1 with decreasing temperature is evident from the figure. K_1 increases from ~6.58×10^5 Am^2/kg at 300 K to ~7.23×10^5 Am^2/kg at 60 K an increase of ~10%.

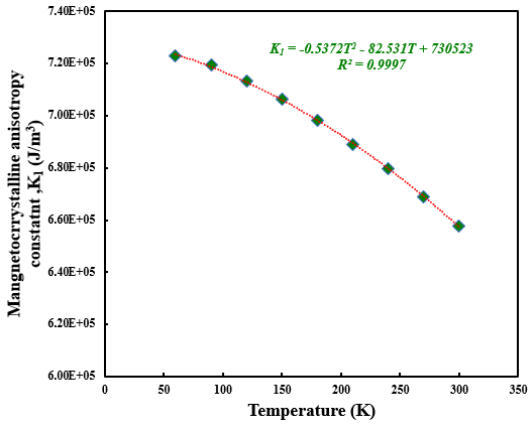

Figure 46.Magnetocrystalline anisotropy constant (K_1) vs Temperature (T)

5.3.2. $Fe_{30}Ni_{40}Co_{30}$

Figure 45 below shows the *M-H* curves for the alloy $Fe_{30}Ni_{40}Co_{30}$. The M_S, H_C, and M_R were estimated by analyzing the *M-H* curves as ~131 ±1 Am^2/kg, 2 ±1% kA/m and 1 ±13% Am^2/kg, respectively.

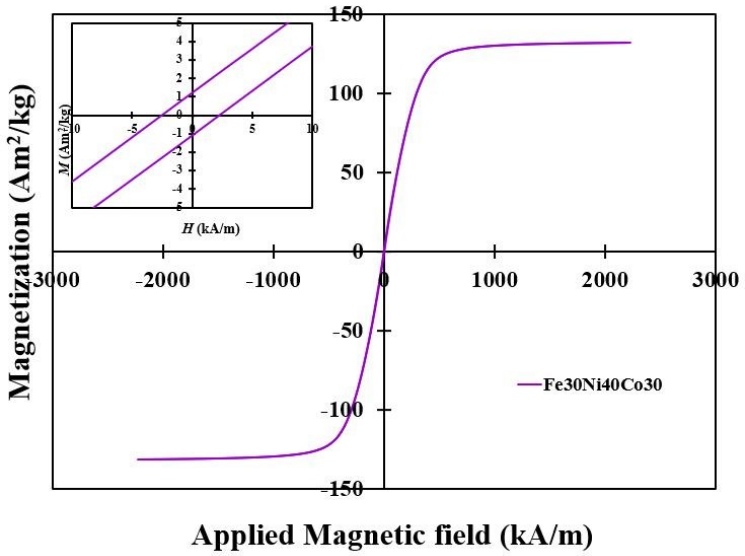

Figure 47.Magnetization (*M*) vs. Applied magnetic field (*H*) curves for $Fe_{30}Ni_{40}Co_{30}$ alloy powders at ambient temperature

Figure 46 below shows the M-H curves for the alloy $Fe_{30}Ni_{40}Co_{30}$ at sub-ambient temperatures up to 60 K.

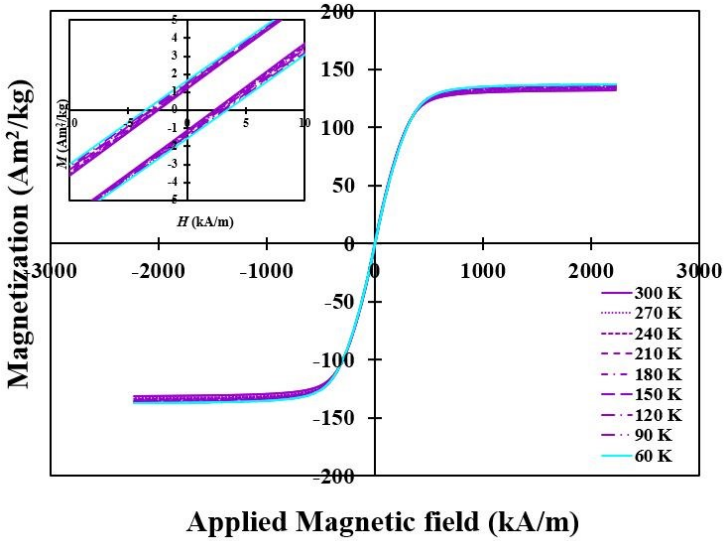

Figure 48.Magnetization (*M*) vs. Applied magnetic field (*H*) curves for $Fe_{30}Ni_{40}Co_{30}$alloy powders at sub-ambient temperatures

The variation in M_S, H_C and M_R with decreasing temperature is illustrated in the Figure 47 below.

(a)

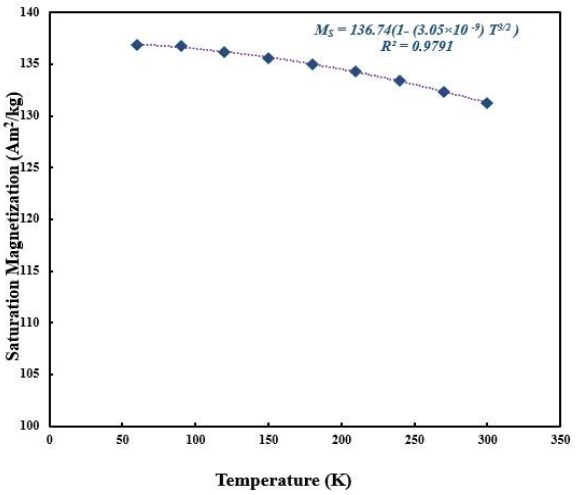

(b)

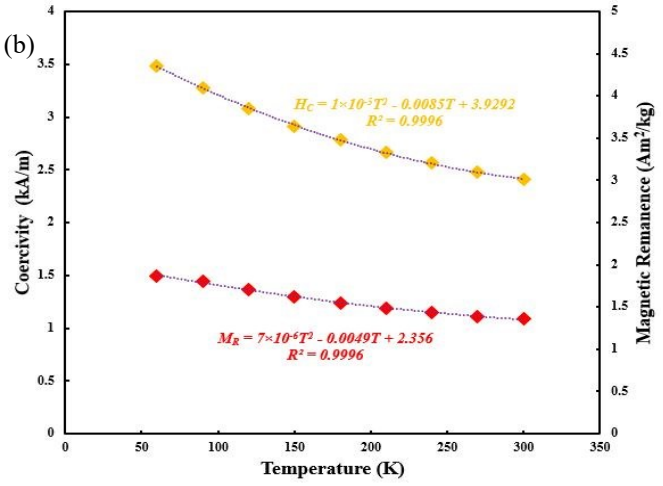

Figure 49.a)Magnetic saturation (M_S) vs Temperature (T) b) Coercivity (H_C) & Magnetic remanence (M_R) vs Temperature (T)

From Figure _, it is evident that M_S progressively increases with a decrease in temperature. M_S increased by about ~5% from about ~131 Am^2/kg to 137 Am^2/kg from 300 K to 60 K. Similarly, H_C increased by ~33% from about ~3 kA/m to ~ kA/m and M_R increased by 100% from 1 Am^2/kg to 2 Am^2/kg from 300 K to 60 K.

The dependence of M_S on temperatures in the sub-ambient temperature range is plotted with respect to Bloch's law as given by Eqn 31. Using Bloch's law $M_S(0)$ and A was estimated to be ~136.74 Am^2/kg and ~3.05×10^{-9} $K^{-3/2}$, respectively. Estimating magnetic moment per atom (μ_H) using Eqn 32 taking A_W for $Fe_{30}Ni_{40}Co_{30}$ as 57.934 g/mol, we get the value to be ~1.31 μ_B.

Table 6.Evaluation of different variants of Law of Approach to Saturation in $Fe_{30}Ni_{40}Co_{30}$ powders

	LAS A				**LAS B**					**LAS C**					**LAS D**				
Temperature (K)	Magnetic saturation M_S (Am^2/kg) ±0.6	Constant $b\times10^{10}$ ±21%	Magnetocrystalline Anisotropy Constant K_1 (J/m^3)×10^5 ±11%		Magnetic saturation M_S (Am^2/kg) ±1	Constant $b\times10^{10}$ ±27%	Constant χ	Magnetocrystalline Anisotropy Constant K_1 (J/m^3)×10^5 ±14%		Magnetic saturation M_S (Am^2/kg) ±0.3	Constant $b\times10^{10}$ ±44%	Constant $a\times10^4$ *±74%*	Magnetocrystalline Anisotropy Constant K_1 (J/m^3)×10^5 ±22%		Magnetic saturation M_S (Am^2/kg) ±2	Constant $b\times10^{10}$ ±50%	Constant $a\times10^4$ *±108 %*	Constant χ	Magnetocrystalline Anisotropy Constant K_1 (J/m^3)×10^5 ±24%
300	131.4	1.49	6.09		131.2	1.44	0.001	5.97		131.6	1.36	0.640	5.75		129.5	1.85	1.36	0.005	6.58
270	132.6	1.51	6.20		132.4	1.48	0.001	6.11		132.7	1.44	0.638	5.98		130.6	1.93	1.48	0.005	6.76
240	133.6	1.54	6.31		133.5	1.52	0.001	6.25		133.6	1.52	0.659	6.18		131.4	2.04	1.62	0.005	7.00
210	134.5	1.57	6.42		134.5	1.57	0.000	6.39		134.5	1.60	0.581	6.39		132.4	2.09	1.64	0.005	7.14
180	135.2	1.60	6.50		135.2	1.60	0.000	6.49		135.2	1.66	0.625	6.54		132.8	2.21	1.93	0.006	7.36
150	135.9	1.62	6.58		136.0	1.64	0.000	6.60		135.7	1.74	0.647	6.72		133.4	2.28	1.99	0.006	7.50
120	136.4	1.65	6.66		136.5	1.67	-0.001	6.70		136.1	1.81	0.670	6.88		133.7	2.39	2.23	0.006	7.70
90	136.9	1.68	6.73		137.0	1.70	-0.001	6.77		136.6	1.84	0.824	6.92		134.0	2.46	2.37	0.007	7.85
60	137.1	1.69	6.77		137.4	1.74	-0.001	6.87		136.7	1.94	0.797	7.16		134.3	2.52	2.43	0.006	7.94

Note: R^2 values for all the above variants of Law of approach to saturation are >0.993

Magnetocrystalline anisotropy constant (K_1) analysis:

Table 6 shows the K_1 evaluations of $Fe_{30}Ni_{40}Co_{30}$ using different variations of the law of approach to saturation. It is evident from the table that variation is constant a increase as we go from left to right on the table. Variation in constant a is high for both the cases of LAS C and LAS D. The effect of constant χ seems to be negligible in the case of both LAS B and LAS D. Similar to constant b, variation in K_1 also increases from left to right in the table with LAS A showing the least variation and LAS D showing the highest variation. The constant b values, which are related to the crystal structure in the case of LAS D show steep differences when compared to other LAS. Similarly, the M_S values also seem to off by a small margin compared to the M_S values inferred from the MvH curves. The constant a in the case of LAS D shows a variation of ~100%. While this variation can be explained as the differences in the degree of plastic deformation occurring in each powder particle, it still seems that the effect of constant a is being overemphasized in this case as the variation in K_1 values between all the LAS is negligible. The metallurgical history of these powders that have been milled for 9 hours does seem to suggest that LAS C or LAS D might be the right choice for these alloy powders but the K_1 values show no relevant differences that can justify the usage of any one of these LAS while overlooking the degree of variation from the data.

Using LAS A we estimate the K_1 value for $Fe_{30}Ni_{40}Co_{30}$ to be ~6.1×10^5 J/m^3 at 300 K. The figure below shows the dependence of K_1 on decreasing temperature. A trend of increasing K_1 with decreasing temperature is evident from the figure. K_1 increases from ~6.1×10^5 Am^2/kg at 300 K to ~6.77×10^5 Am^2/kg at 60 K an increase of ~11%.

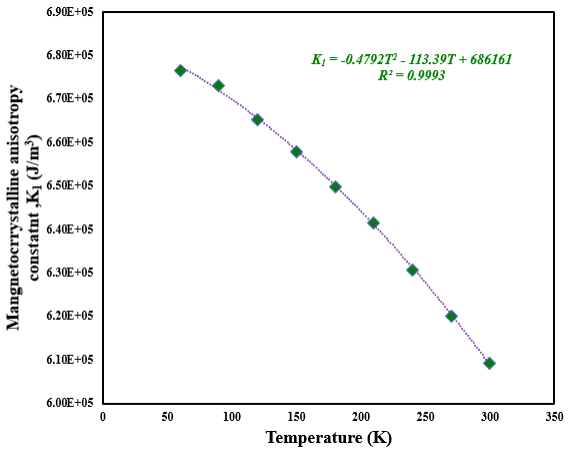

Figure 50.Magnetocrystalline anisotropy constant (K_1) vs Temperature (T)

5.3.3. $Fe_{40}Ni_{30}Co_{30}$

Figure 49 below shows the *M-H* curves for the alloy $Fe_{40}Ni_{30}Co_{30}$ at ambient temperature. The M_S, H_C, and M_R were estimated by analyzing the *M-H* curves as ~145 ±1 Am^2/kg, 5 ±1% kA/m and 3 ±19% Am^2/kg, respectively.

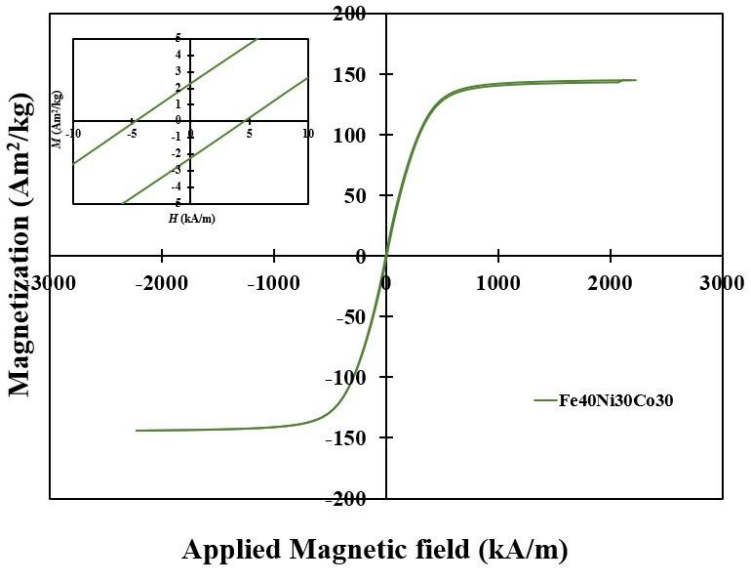

Figure 51.Magnetization (*M*) vs. Applied magnetic field (*H*) curves for $Fe_{40}Ni_{30}Co_{30}$ alloy powders at ambient temperature

Figure 50 below shows the *M-H* curves for the alloy $Fe_{40}Ni_{30}Co_{30}$ at sub-ambient temperatures.

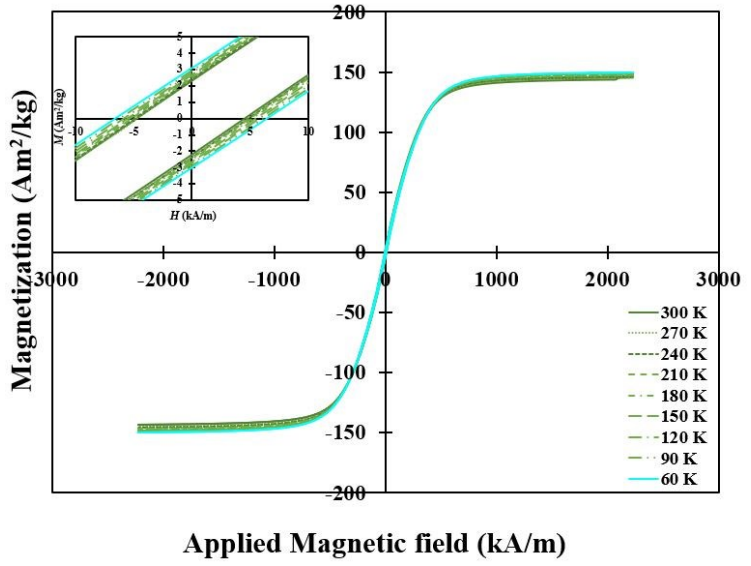

Figure 52.Magnetization (*M*) vs Applied magnetic field (*H*) curves for $Fe_{40}Ni_{30}Co_{30}$ alloy powders at sub-ambient temperatures

Figure 51 below shows the variation of M_S, H_C and M_R with decreasing temperature from 300 K to 60 K.

(a)

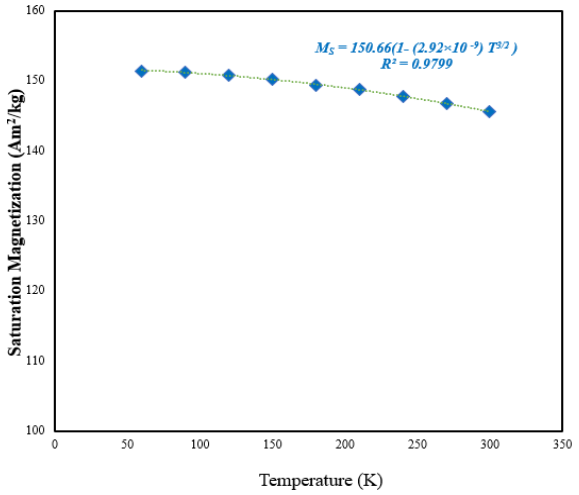

(b)

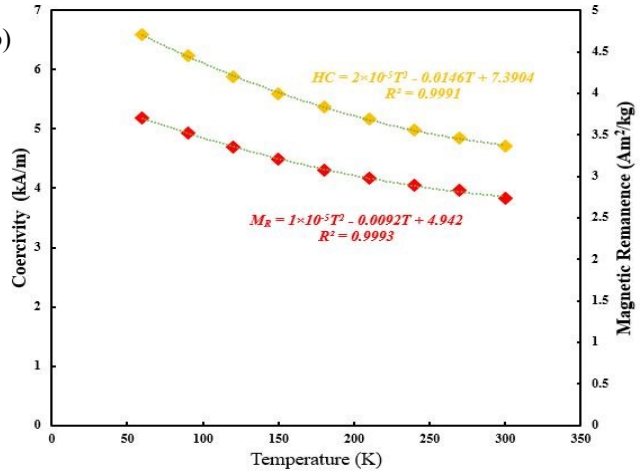

Figure 53.a)Magnetic saturation (M_S) vs Temperature (T) b) Coercivity (H_C) & Magnetic remanence (M_R) vs Temperature (T)

A trend of increasing M_S, H_C and M_R with decreasing temperature similar to the elemental powders are noticeable from the M-T curves. M_S increases by ~4% from ~145 Am^2/kg to ~151 Am^2/kg, H_C increased by ~40% from 5 kA/m to 7 kA/m and M_R increased by ~33% from 3 Am^2/kg to 4 Am^2/kg.

The dependence of M_S on temperatures in the sub-ambient temperature range are plotted with respect to Bloch's law as given by Eqn 31. Using Bloch's law $M_S(0)$ and A were estimated to be ~150.66 Am^2/kg and ~2.92×10^{-9} $K^{-3/2}$. Estimating magnetic moment per atom (μ_H) using Eqn 32 taking A_W for $Fe_{40}Ni_{30}Co_{30}$ as 57.625 g/mol, we get the value to be ~1.44 μ_B

Table 7.Evaluation of different variants of Law of Approach to Saturation in $Fe_{40}Ni_{30}Co_{30}$ powders

	LAS A				**LAS B**					**LAS C**					**LAS D**				
Temperature (K)	Magnetic saturation M_S (Am^2/kg) ±0.4	Constant $b\times10^{10}$ ±26%	Magnetocrystalline Anisotropy Constant K_1 (J/m^3)×10^5 ±13%		Magnetic saturation M_S (Am^2/kg) ±0.8	Constant $b\times10^{10}$ ±31%	Constant χ	Magnetocrystalline Anisotropy Constant K_1 (J/m^3)×10^5 ±16%		Magnetic saturation M_S (Am^2/kg) ±1.3	Constant $b\times10^{10}$ ±46%	Constant $a\times10^4$ *±244 %*	Magnetocrystalline Anisotropy Constant K_1 (J/m^3)×10^5 ±23%		Magnetic saturation M_S (Am^2/kg) ±3	Constant $b\times10^{10}$ ±50%	Constant $a\times10^4$ *±97%*	Constant χ	Magnetocrystalline Anisotropy Constant K_1 (J/m^3)×10^5 ±24%
300	145.0	2.17	8.11		145.0	2.16	0.000	8.08		144.9	2.24	-0.164	8.13		141.2	3.10	-2.86	0.009	9.16
270	146.3	2.20	8.24		146.5	2.22	-0.001	8.28		146.1	2.38	-0.416	8.44		143.2	3.02	-2.42	0.007	9.26
240	147.4	2.25	8.39		147.6	2.29	-0.001	8.47		147.0	2.49	-0.550	8.68		144.1	3.13	-2.56	0.007	9.49
210	148.3	2.30	8.53		148.7	2.35	-0.002	8.64		147.8	2.59	-0.674	8.91		145.0	3.22	-2.64	0.007	9.69
180	149.0	2.34	8.66		149.5	2.40	-0.002	8.78		148.5	2.68	-0.766	9.10		145.7	3.30	-2.71	0.007	9.86
150	149.8	2.38	8.77		150.3	2.46	-0.002	8.92		149.2	2.76	-0.863	9.28		146.4	3.37	-2.78	0.007	10.0
120	150.3	2.42	8.87		150.9	2.50	-0.003	9.04		149.6	2.83	-0.951	9.44		146.8	3.45	-2.88	0.007	10.2
90	150.7	2.45	8.95		151.4	2.54	-0.003	9.15		150.0	2.91	-1.06	9.59		147.3	3.51	-2.92	0.007	10.3
60	151.1	2.47	9.01		151.8	2.58	-0.004	9.24		150.3	2.98	-1.16	9.72		147.6	3.56	-2.96	0.007	10.4

Note: R^2 values for all the above variants of Law of approach to saturation are >0.999

Magnetocrystalline anisotropy constant (K_1) analysis:

Data obtained from evaluation of different variations of LAS for the case of $Fe_{40}Ni_{30}Co_{30}$ by curve fitting experimental data is shown above in Table 7. Comparing the constant b for all the different cases shows us that variation in constant b increases as we go from left to right on the table. Again, the effect of constant χ seems negligible. Constant a in LAS C and LAS D shows a variation of 244% and 97%, respectively. These variations also seem to be prevalent in the case of their K1 values as LAS C, and LAS D have a variation of 23% and 24%, respectively, while LAS A and LAS B only have a variation of 13% and 16%, respectively. Comparing the M_S values to the M_S values inferred from the MvH curves, the M_S values from LAS A, B and C seem to closely match with the inferred values while M_S values for LAS D seem to vary to some extent. This variation of M_S values for the case of LAS D seems to suggest a force fit. A closer comparison of the K_1 values reveal that there is barely any variation in the K_1 values for LAS A, B and C at 300 K. While these powders have been milled for 9 hours, constant a which is related to the metallurgical history of the material would be expected to have a greater effect on their K_1 values. Choosing LAS C due this is not justified as there is a lot of variation in the values and not much effect on the result. Again, LAS A seems as the right choice for this case as well.

Using LAS A we estimate the K_1 value for $Fe_{40}Ni_{30}Co_{30}$ to be ~8.11 J/m^3. The figure below shows the dependence of K_1 on decreasing temperature. A trend of increasing K_1 with decreasing temperature is evident from the figure below. K_1 increases from ~8.11×10^5 Am^2/kg at 300 K to ~9.01×10^5 Am^2/kg at 60 K an increase of ~11%.

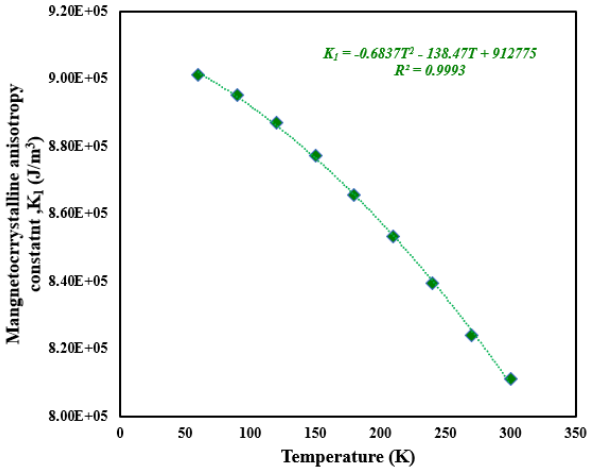

Figure 54.Magnetocrystalline anisotropy constant (K_1) vs Temperature (T)

5.3.4. $Fe_{30}Ni_{30}Co_{40}$

Figure 53 below shows the magnetic field (*M*) versus applied magnetic field (*H*) curves for the alloy $Fe_{30}Ni_{30}Co_{40}$. The M_S, H_C and M_R are estimated by analysing these *M-H* curves as ~138 Am^2/kg, ~5 kA/m and ~3 ±10% Am^2/kg respectively.

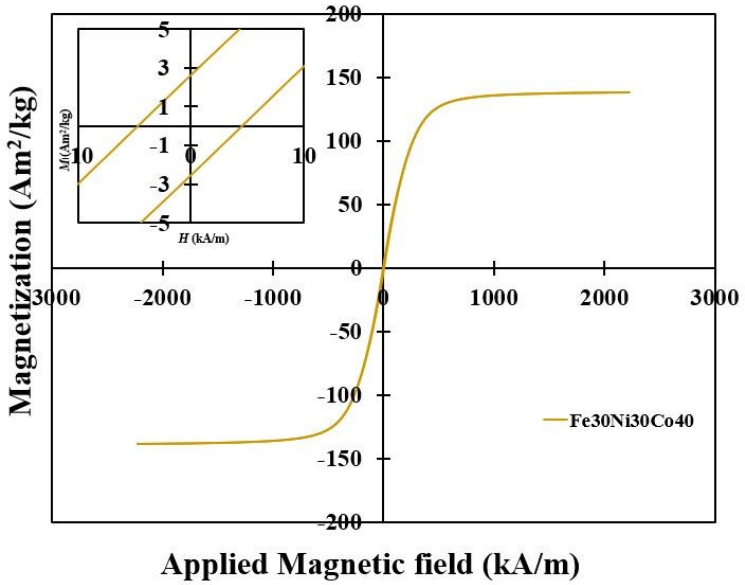

Figure 55.Magnetization (*M*) vs Applied magnetic field (*H*) curves for $Fe_{30}Ni_{30}Co_{40}$ alloy powders at ambient temperature

Figure 54 below shows the *M-H* curves for the alloy $Fe_{30}Ni_{30}Co_{40}$ at sub ambient temperatures.

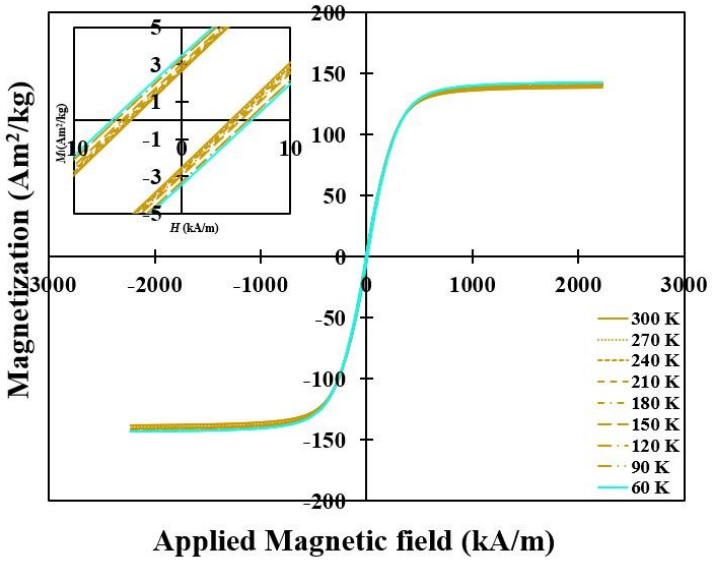

Figure 56.Magnetization (*M*) vs Applied magnetic field (*H*) curves for $Fe_{30}Ni_{30}Co_{40}$ alloy powders at sub-ambient temperatures

Figure 55 below shows the dependence of M_S, H_C and M_R of alloy $Fe_{30}Ni_{30}Co_{40}$ on decreasing temperature.

(a) (b)

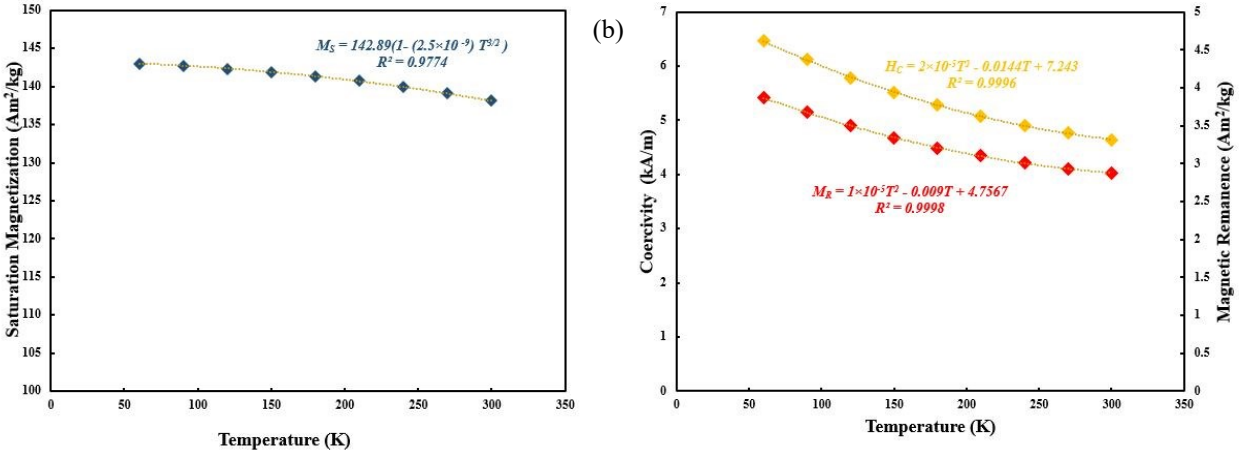

Figure 57.a)Magnetic saturation (M_S) vs Temperature (T) b) Coercivity (H_C) & Magnetic remanence (M_R) vs Temperature (T)

A trend of increasing M_S, H_C and M_R with decreasing temperature, similar to the other alloys and the elemental powders is noticed for the case of $Fe_{30}Ni_{30}Co_{40}$ alloy. The M_S increased by ~4% from ~138 Am^2/kg to ~143 Am^2/kg, H_C increased by ~20% from ~5 kA/m to ~6 kA/m and M_R increased by ~33% from 3 Am^2/kg to 4 Am^2/kg from 300 K to 60 K.

The dependence of M_S on temperatures in the sub-ambient temperature range are plotted with respect to Bloch's law as given by Eqn 31. Using Bloch's law $M_S(0)$ and A were estimated to be ~142.89 Am^2/kg and ~2.5×10^{-9} $K^{-3/2}$. Estimating magnetic moment per atom (μ_H) using Eqn 32 taking A_W for $Fe_{30}Ni_{30}Co_{40}$ as 57.91 g/mol, we get the value to be ~1.37 μ_B.

Table 8.Evaluation of different variants of Law of Approach to Saturation in $Fe_{30}Ni_{30}Co_{40}$ powders

	LAS A				**LAS B**					**LAS C**					**LAS D**				
Temperature (K)	Magnetic saturation M_S (Am^2/kg) ±0.5	Constant $b\times10^{10}$ ±14%	Magneto crystalline Anisotropy Constant K_1 (J/m^3)×10^5 ±7%		Magnetic saturation M_S (Am^2/kg) ±0.8	Constant $b\times10^{10}$ ±17%	Constant χ	Magneto crystalline Anisotropy Constant K_1 (J/m^3)×10^5 ±9%		Magnetic saturation M_S (Am^2/kg) ±0.2	Constant $b\times10^{10}$ ±26%	Constant $a\times10^3$ *±877 %*	Magneto crystalline Anisotropy Constant K_1 (J/m^3)×10^5 ±13%		Magnetic saturation M_S (Am^2/kg) ±0.5	Constant $b\times10^{10}$ ±28%	Constant $a\times10^3$ *±122 %*	Constant χ	Magneto crystalline Anisotropy Constant K_1 (J/m^3)×10^5 ±14%
300	138.4	1.87	7.15		138.0	1.82	0.001	7.03		138.6	1.71	3.78	6.82		137.1	2.04	-6.88	0.004	7.36
270	139.3	1.92	7.29		139.1	1.88	0.001	7.19		139.5	1.80	2.82	7.03		138.1	2.12	-7.67	0.004	7.55
240	140.2	1.96	7.41		140.0	1.92	0.001	7.33		140.3	1.87	1.90	7.23		138.9	2.19	-8.23	0.004	7.73
210	141.0	1.99	7.51		140.8	1.97	0.001	7.46		141.0	1.94	1.15	7.39		139.6	2.27	-8.75	0.004	7.90
180	141.6	2.02	7.60		141.5	2.01	0.000	7.57		141.6	2.00	0.489	7.53		140.2	2.32	-8.89	0.004	8.02
150	142.1	2.05	7.69		142.1	2.04	0.000	7.67		142.1	2.06	-0.140	7.67		140.8	2.36	-8.91	0.003	8.12
120	142.6	2.08	7.76		142.6	2.08	0.000	7.76		142.6	2.11	-0.648	7.79		141.2	2.41	-9.05	0.003	8.24
90	143.0	2.10	7.83		143.0	2.11	0.000	7.84		142.9	2.16	-0.995	7.90		141.5	2.46	-9.44	0.003	8.33
60	143.3	2.12	7.87		143.4	2.13	-0.001	7.91		143.1	2.22	-1.33	8.02		141.8	2.49	-9.44	0.003	8.42

Note: R^2 values for all the above variants of Law of approach to saturation are >0.999

Magnetocrystalline anisotropy constant (K_1) analysis:

The table 8 above shows the data obtained for curve fitting the experimental data with the different variations of LAS. It is evident from the table that there is higher variation in both constants *a* and *b* as we go from left to right on the table. It is also evident that the K_1 values have the least variation of ~7% in LAS A while LAS D has the highest variation of ~14%.The constant χ in the case of both LAS B and LAS D seems to have negligible effect. These powders have been milled for 9 hours in a ball mill and as such one would be expect constant *a* to have a greater effect on their K_1 values due to constant *a* being related to the metallurgical history of the powders. Constant *a* in the case of LAS D shows huge variations of ~877% and LAS D shows a variation of ~122%. These huge variations seem to indicate unreliable data in the case of LAS C and LAS D. These variations might be explained on the basis that the degree plastic deformation undergone by each individual powder could vary greatly but again selection of LAS C and LAS D based on the metallurgical history cannot be justified as the variation among the K_1 values are minimal at best.

Again using LAS A which is Akulov's original equation based on least variation and sound data seems like the correct choice. K_1 is estimated to be ~7.15×10^5 J/m^3. The figure below shows the dependence of K_1 on decreasing temperature. A trend of increasing K_1 with decreasing temperature is evident from the figure. K_1 increases from ~7.15×10^5 J/m^3 at 300 K to ~7.87×10^5 J/m^3 at 60 K an increase of ~10%.

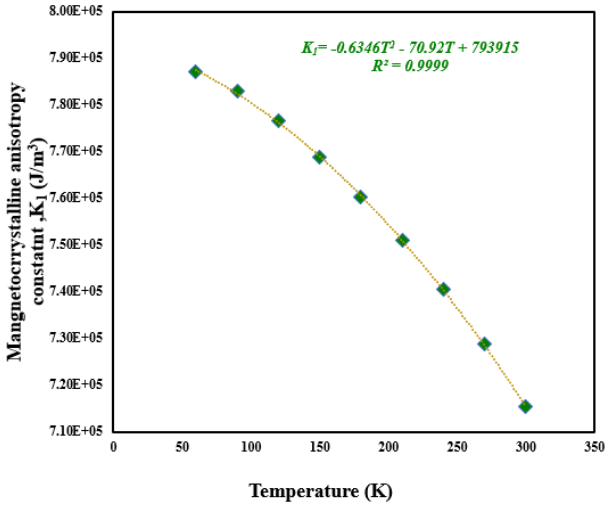

Figure 58.Magnetocrystalline anisotropy constant (K_1) vs Temperature (T)

5.3.5. Comparison of Alloy Powders

Figure 57 below shows the *M-H* curves for the three elemental ferromagnetic powders. The inset shows the *M-H* curves in low magnetic field realm of ± 10 kA/m.

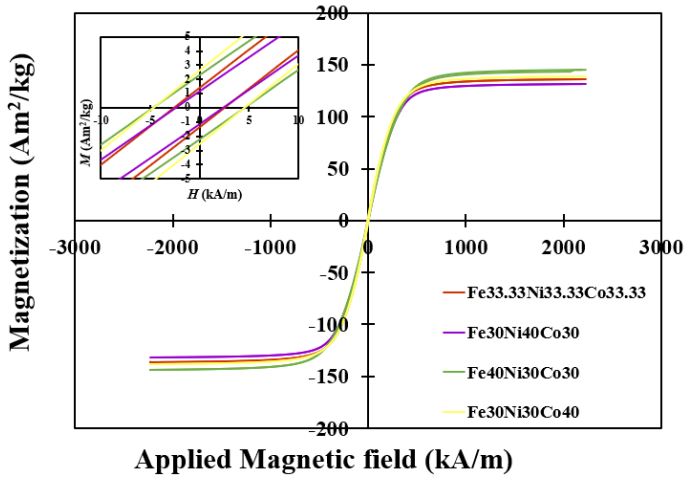

Figure 59.*M-H* curves for pure elemental ferromagnetic alloy powders at 300 K

From the *M-H* curves it is evident that the non equiatomic compositions have better hard magnetic and soft magnetic properties than the equiatomic composition of $Fe_{33.33}$ $Ni_{33.33}$ $Co_{33.33}$. $Fe_{40}Ni_{30}Co_{30}$ has the best hard magnetic properties while $Fe_{30}Ni_{40}Co_{30}$ has the best soft magnetic properties. Use of these powders as precursors for manufacturing commercial magnets can enhance the desired magnetic properties. The Figure 58 below compares the K_1 values of the pure elemental alloy powders.

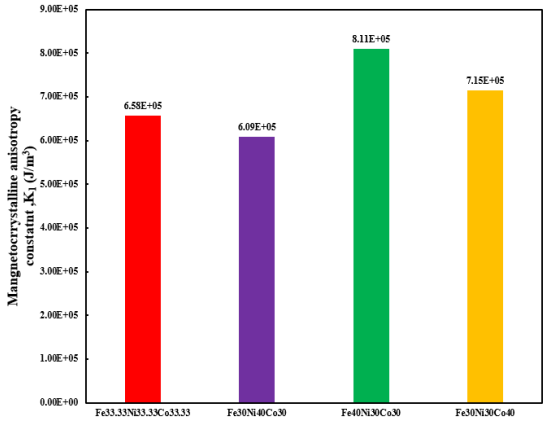

Figure 60.Comparision of K_1 for elemental ferromagnetic powders

It is evident from the figure above that the alloy with the better hard magnetic properties($Fe_{40}Ni_{30}Co_{30}$) has higher K_1 values as expected as its more difficult to magnetize and

demagnetize while the alloy with the better soft magnetic properties ($Fe_{30}Ni_{40}Co_{30}$) has lower K_1 values.

5.4. Magnetic Properties of Maraging Steel (MARS) Powders

5.4.1. MARS-AR (As Received)

Figure 59 below shows the magnetization (M) versus applied magnetic field (H) curve for maraging steel powders. The M_S, H_C and M_R were estimated to be 177±2 Am^2/kg, ~3 kA/m and 1±14% Am^2/kg respectively.

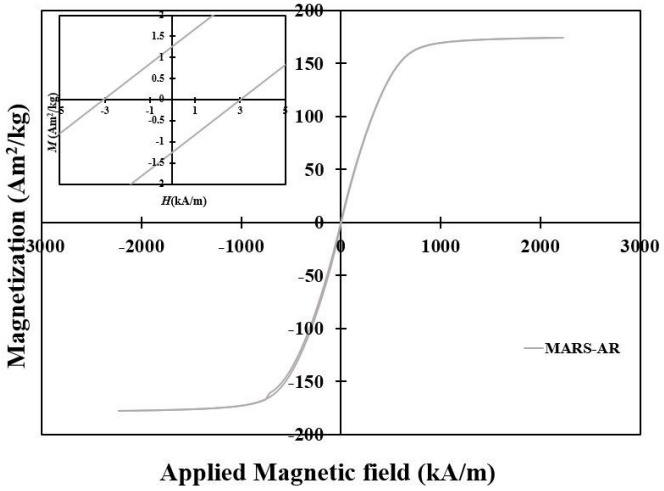

Figure 61.Magnetization (*M*) vs Applied magnetic field (*H*) curves for MARS-AR powders at ambient temperature

Figure 60 below shows the *M-H* curves for the MARS-AR powders at sub ambient temperatures.

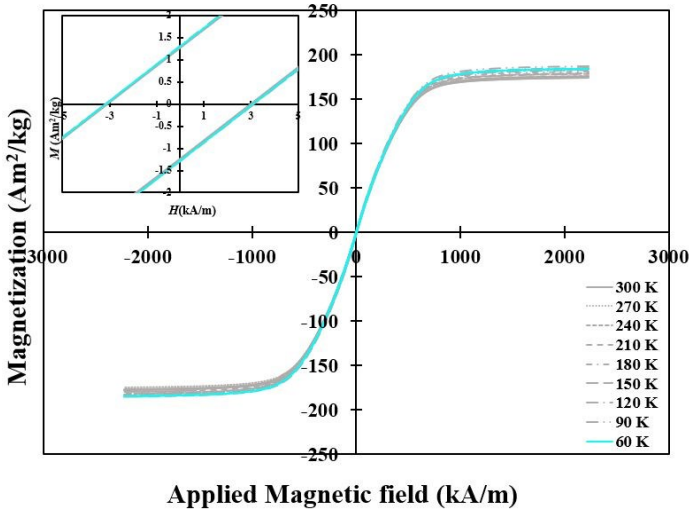

Figure 62.Magnetization (*M*) vs Applied magnetic field (*H*) curves for MARS-AR powders at sub-ambient temperatures

Figure 61 below show the dependence of M_S, H_C and M_R on decreasing temperature in the case of MARS-AR powders.

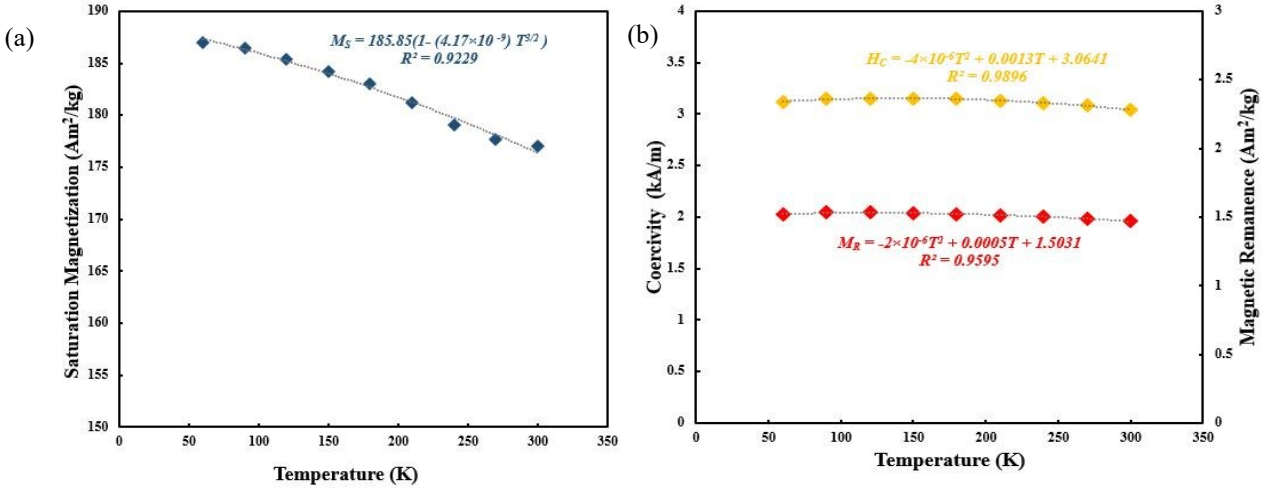

Figure 63.a)Magnetic saturation (M_S) vs Temperature (T) b) Coercivity (H_C) & Magnetic remanence (M_R) vs Temperature (T)

M_S, H_C and M_R progressively increase with decreasing temperature. M_S increased by ~6 % from ~177 Am2/kg to 187 Am2/kg, H_C increased by a modest ~3% from ~3.03 kA/m to ~3.13 kA/m and M_R increased by 100% from 1 Am2/kg to 2 Am2/kg from 300 K to 60 K.

The dependence of M_S on temperatures in the sub-ambient temperature range are plotted with respect to Bloch's law as given by Eqn 31. Using Bloch's law $M_S(0)$ and A were estimated to be ~185.85 Am^2/kg and ~4.17×10^{-9} $K^{-3/2}$. Estimating magnetic moment per atom (μ_H) using Eqn 32 taking A_W for MARS-AR as 58.177g/mol, we get the value to be ~1.79 μ_B.

Table 9.Evaluation of different variants of Law of Approach to Saturation in MARS-AR powders

	LAS A				**LAS B**					**LAS C**					**LAS D**				
Temperature (K)	Magnetic saturation M_S (Am^2/kg) ±1.4	Constant $b\times10^{10}$ ±36%	Magnetocrystalline Anisotropy Constant K_1 (J/m^3)×10^5 ±18%		Magnetic saturation M_S (Am^2/kg) ±3	Constant $b\times10^{10}$ ±37%	Constant χ	Magnetocrystalline Anisotropy Constant K_1 (J/m^3)×10^5 ±20%		Magnetic saturation M_S (Am^2/kg) ±2	Constant $b\times10^{10}$ ±45%	Constant $a\times10^5$ *±64%*	Magnetocrystalline Anisotropy Constant K_1 (J/m^3)×10^5 ±21%		Magnetic saturation M_S (Am^2/kg) ±3	Constant $b\times10^{10}$ ±33%	Constant $a\times10^5$ *±24%*	Constant χ	Magnetocrystalline Anisotropy Constant K_1 (J/m^3)×10^5 ±16%
300	176.5	3.56	11.9		180.4	4.07	-0.015	13.0		173.3	5.65	-0.443	14.6		163.1	7.81	-1.09	0.024	16.3
270	177.7	3.75	12.3		181.0	4.11	-0.015	13.1		174.1	5.68	-0.436	14.7		163.2	7.97	-1.12	0.026	16.5
240	179.1	3.83	12.5		182.5	4.20	-0.015	13.4		175.4	5.78	-0.439	14.9		165.0	7.95	-1.09	0.025	16.6
210	181.2	3.93	12.8		184.3	4.26	-0.014	13.6		177.8	5.71	-0.402	15.1		166.6	8.02	-1.09	0.026	16.9
180	183.0	3.95	13.0		186.5	4.31	-0.015	13.9		179.3	5.89	-0.436	15.4		168.5	8.10	-1.09	0.025	17.1
150	184.2	3.97	13.1		187.3	4.30	-0.014	13.9		180.8	5.74	-0.399	15.4		168.2	8.42	-1.19	0.030	17.3
120	185.4	4.01	13.3		188.9	4.38	-0.016	14.2		181.6	5.95	-0.434	15.7		171.8	7.91	-1.02	0.023	17.3
90	186.5	4.02	13.4		190.1	4.40	-0.016	14.3		182.6	6.00	-0.445	15.9		173.2	7.87	-1.01	0.022	17.4
60	187.0	4.03	13.4		190.9	4.43	-0.017	14.4		183.0	6.10	-0.465	16.0		174.0	7.88	-1.00	0.021	17.5

Note: R^2 values for all the above variants of Law of approach to saturation are >0.986

Magnetocrystalline anisotropy constant (K_1) analysis:

Table 9 above shows the evaluation of different LAS for the case of MARS-AR powders done by curve fitting experimental plots. Here unlike the pure elemental alloys LAS D has the least variation for both constant b (~33%) as well as the K_1 value itself (~16%). LAS A, B and C have variations of ~36%, 37% and ~45% for constant b and ~20% variation for the K_1 value. The effect of the constant χ in both the cases of LAS B and LAS D does seem negligible as seen prior cases. A closer comparison of the M_S values obtained from the different LAS to the M_S values inferred from the *MvH* curves shows that only M_S values from LAS A and LAS B are in agreement with the *MvH* values while both LAS C and LAS D show stark differences in the M_S values. This difference suggests that the data has been force fit and the plots are not reliable. This along with the fact that these powders have no metallurgical history of plastic deformation or any other form of induced stresses suggest that LAS A should be the correct fit for this case.

Using LAS A K_1 is estimated to be ~11.9 $\times 10^5$ J/m^3. The figure below shows the dependence of K_1 on decreasing temperature. A trend of increasing K_1 with decreasing temperature is evident from the figure below. K_1 increases from ~11.9 $\times 10^5$ Am^2/kg at 300 K to ~13.4$\times 10^5$ Am^2/kg at 60 K an increase of ~13%.

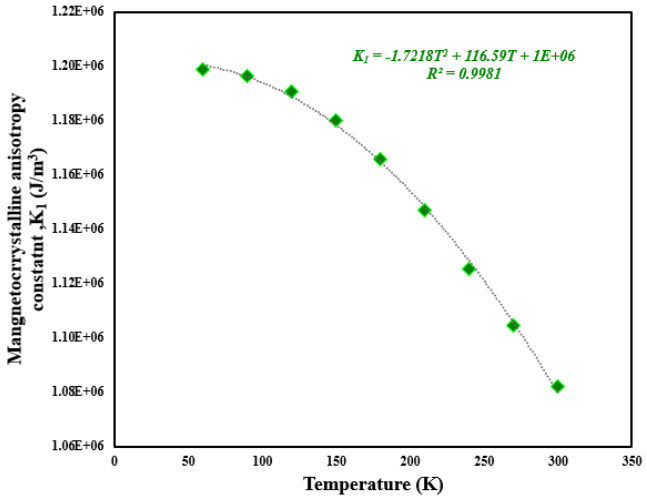

Figure 64.Magnetocrystalline anisotropy constant (K_1) vs Temperature (T)

5.4.2. MARS-5h (5h Milled)

Figure 63 below shows the *M-H* curves for maraging steel (MARS) powders milled for 5 hours. The M_S, H_C and M_R was estimated to be 165 ±1 Am^2/kg, ~5 kA/m and 3 ±10% Am^2/kg.

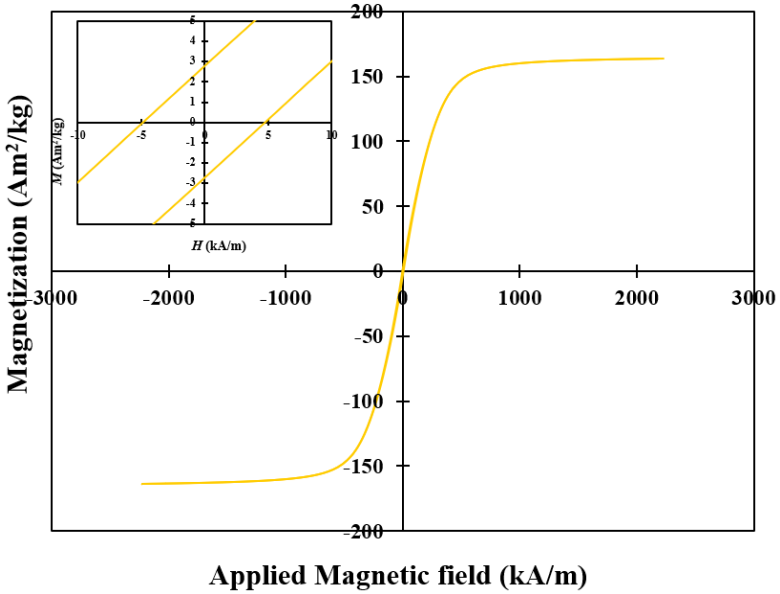

Figure 65.Magnetization (*M*) vs Applied magnetic field (*H*) curves for MARS-5h powders at ambient temperature

Figure 64 below shows the M-H curves for MARS-5h milled powders in the sub ambient temperature range from 300 K to 60 K.

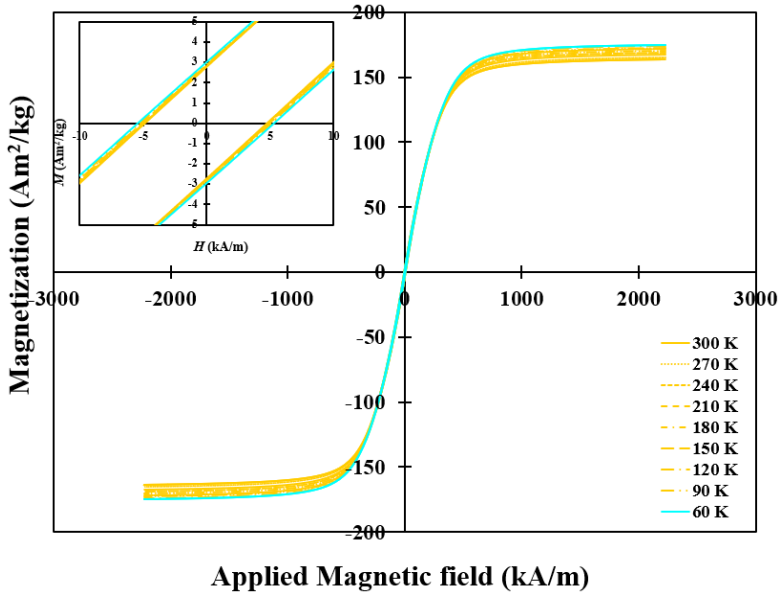

Figure 66.Magnetization (*M*) vs Applied magnetic field (*H*) curves for MARS-5h powders at sub-ambient temperatures

Figure 65 below depicts the change in M_S, H_C and M_R with decreasing temperature.

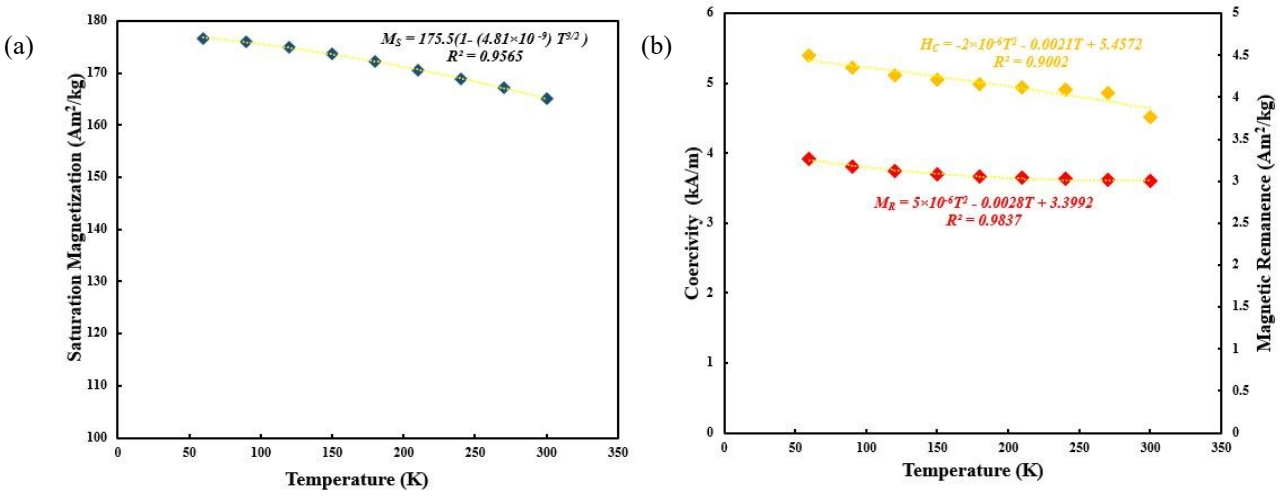

Figure 67.a)Magnetic saturation (M_S) vs Temperature (T) b) Coercivity (H_C) & Magnetic remanence (M_R) vs Temperature (T)

M_S, H_C and M_R increase in an almost linear fashion with respect to decreasing temperature. M_S increases by ~7% from ~165 Am^2/kg to ~177 Am^2/kg, H_C increases by ~12% from ~4.8 kA/m to ~5.4 kA/m and M_R increases by ~11% from ~2.7 Am^2/kg to ~3 Am^2/kg.

The dependence of M_S on temperatures in the sub-ambient temperature range are plotted with respect to Bloch's law as given by Eqn 31. Using Bloch's law $M_S(0)$ and A were estimated to be ~175.5Am^2/kg and ~$4.81\times10^{-9}\,K^{-3/2}$. Estimating magnetic moment per atom (μ_H) using Eqn 32 taking A_W for MARS-5h as 58.177g/mol, we get the value to be ~1.69 μ_B

Table 10.Evaluation of different variants of Law of Approach to Saturation in MARS-5h milled powders

	LAS A				**LAS B**					**LAS C**					**LAS D**				
Temperature (K)	Magnetic saturation M_S (Am^2/kg) ±1	Constant $b\times10^{10}$ ±15%	Magneto crystalline Anisotropy Constant K_1 (J/m^3)×10^5 ±7%		Magnetic saturation M_S (Am^2/kg) ±0.7	Constant $b\times10^{10}$ ±18%	Constant χ	Magneto crystalline Anisotropy Constant K_1 (J/m^3)×10^5 ±9%		Magnetic saturation M_S (Am^2/kg) ±1	Constant $b\times10^{10}$ ±28%	Constant $a\times10^4$ *±73%*	Magneto crystalline Anisotropy Constant K_1 (J/m^3)×10^5 ±14%		Magnetic saturation M_S (Am^2/kg) ±2	Constant $b\times10^{10}$ ±29%	Constant $a\times10^4$ *±65%*	Constant χ	Magneto crystalline Anisotropy Constant K_1 (J/m^3)×10^5 ±14%
300	165.1	2.30	9.01		164.3	2.19	0.003	8.76		165.7	1.97	0.750	8.31		161.8	2.71	-1.61	0.009	9.55
270	167.1	2.33	9.19		166.6	2.25	0.003	9.01		167.5	2.11	0.551	8.73		163.7	2.84	-1.79	0.009	9.87
240	168.9	2.37	9.38		168.5	2.32	0.002	9.24		169.2	2.23	0.505	9.05		165.4	2.95	-1.94	0.009	10.02
210	170.6	2.41	9.53		170.4	2.38	0.001	9.47		170.7	2.38	0.575	9.44		167.0	3.07	-2.14	0.009	10.04
180	172.1	2.46	9.72		172.0	2.43	0.001	9.65		172.2	2.44	0.498	9.63		168.6	3.11	-2.09	0.009	10.06
150	173.7	2.49	9.87		173.6	2.48	0.000	9.84		173.5	2.55	0.582	9.92		169.6	3.27	-2.41	0.009	10.10
120	174.8	2.53	10.00		174.9	2.53	0.000	10.00		174.7	2.61	0.566	10.01		171.0	3.30	-2.47	0.009	10.11
90	176.0	2.56	10.01		176.2	2.58	-0.001	10.02		175.7	2.73	0.653	10.04		171.8	3.45	-2.64	0.009	10.14
60	176.7	2.57	10.02		177.0	2.61	-0.001	10.03		176.3	2.79	0.679	10.06		172.3	3.52	-2.78	0.009	10.16

Note: R^2 values for all the above variants of Law of approach to saturation are >0.999

Magnetocrystalline anisotropy constant (K_1) analysis:

Table 10 above shows the data obtained through curve fitting of experimental plots for the case of MARS- 5h milled powders. The table reveals that variation in constant *b* which is related to the crystal structure increases as we go from left to right on the table. LAS A has the least variation (~15) and LAS D has the highest variation (~29%). Constant *a* which is related to the metallurgical history of the powders, in the case of LAS C and D has variations of ~73% and ~65% respectively. Constant χ which is related to internal magnetic fields seems to have negligible effect on both LAS B and LAS D. Looking at the K_1 values itself we see the least variations in LAS A (~7%) followed by LAS B (~9%), LAS C (~14%) and LAS D (~14%). Comparison of M_S values obtained from different LAS with the M_S values inferred from the *MvH* curves we find that although M_S values from LAS A.B and C are within the acceptable limits the M_S values obtained from LAS D show sharp variation this might indicate a force fit. Values of K_1 for LAS A, B and C are relatively similar and knowing that these powders have undergone milling for 5 hours we would expect a greater contribution from constant *a* but that is not the case. This along with the fact that there are huge variations in the value of constant *a* makes the data seem unreliable. Again, for this case we feel the effect of constant *a* has been overemphasized and LAS A seems to give us the most reliable data.

Using LAS A K_1 is estimated to be ~9.01×10^5 J/m^3. The figure below shows the dependence of K_1 on decreasing temperature. A trend of increasing K_1 with decreasing temperature is evident from the figure. K_1 increases from ~9.01×10^5 Am^2/kg at 300 K to ~10×10^5 Am^2/kg at 60 K an increase of ~11%.

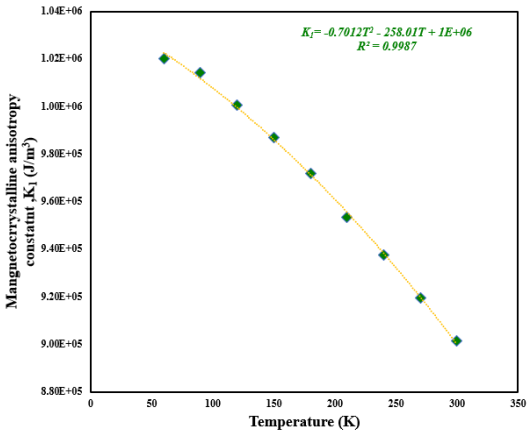

Figure 68.Magnetocrystalline anisotropy constant (K_1) vs Temperature (T)

5.4.3. MARS-56h (56h Milled)

Figure 67 below shows the Magnetization (M) versus the applied magnetic field (H) curves for the maraging steel (MARS) powders milled for 56 hours. The M_S was estimated to be ~84 Am^2/kg. The H_C and M_R were estimated to be ~7 kA/m and ~5 ±9% Am^2/kg

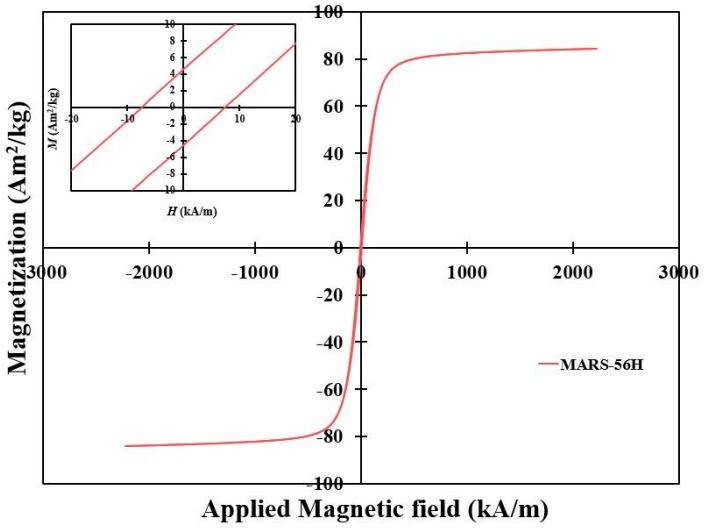

Figure 69.Magnetization (*M*) vs Applied magnetic field (*H*) curves for MARS-56h powders at ambient temperature

Figure 68 below shows the *M-H* curves for the MARS-56h milled powders at the sub ambient temperature range from 300 K to 60 K.

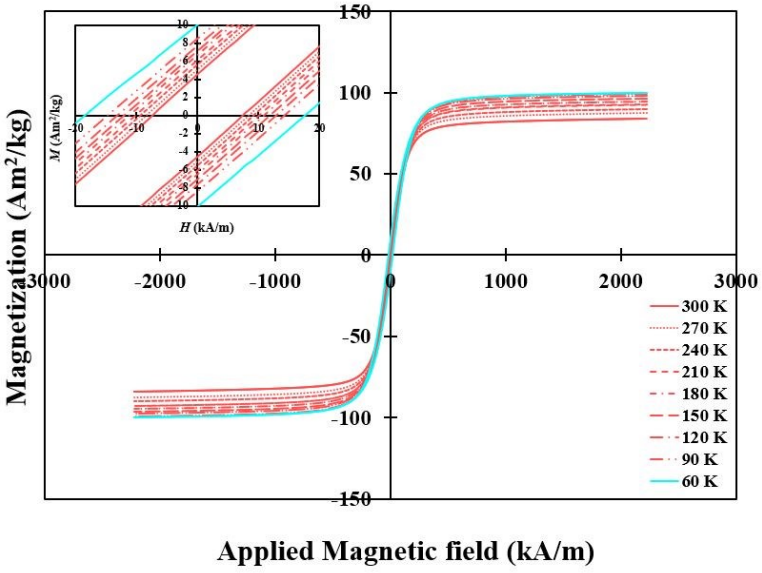

Figure 70.Magnetization (*M*) vs Applied magnetic field (*H*) curves for MARS-56h powders at sub-ambient temperatures

The dependence of M_S, H_C and M_R on decreasing temperature is illustrated below in Figure 69.

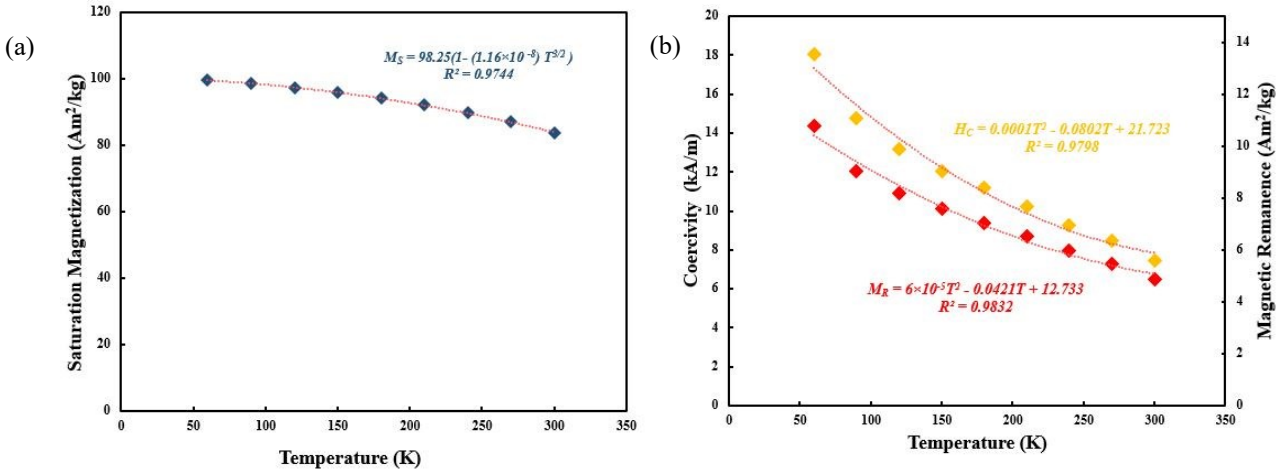

Figure 71.a)Magnetic saturation (M_S) vs Temperature (T) b) Coercivity (H_C) & Magnetic remanence (M_R) vs Temperature (T)

The graphs show a progressive increase in M_S, H_C and M_R with respect to decreasing temperature. M_S increases from ~84 Am^2/kg to ~100 Am^2/kg, an increase of ~19%. H_C increases from ~7 kA/m to ~18 kA/m, an increase of ~157%. M_R increases from ~5 Am^2/kg to ~11 Am^2/kg, an increase of ~120%.

The dependence of M_S on temperatures in the sub-ambient temperature range are plotted with respect to Bloch's law as given by Eqn 31. Using Bloch's law $M_S(0)$ and A were estimated to be ~98.25 Am^2/kg and ~4.81×10^{-9} $K^{-3/2}$. Estimating magnetic moment per atom (μ_H) using Eqn _ taking A_W for MARS-56h as 58.177g/mol, we get the value to be ~0.94 μ_B.

Table 11.Evaluation of different variants of Law of Approach to Saturation in MARS-56h milled powders

	LAS A				**LAS B**					**LAS C**					**LAS D**				
Temperature (K)	Magnetic saturation M_S (Am^2/kg) ±0.2	Constant $b\times10^{10}$ ±4%	Magnetocrystalline Anisotropy Constant K_1 (J/m^3)×10^5 ±2%		Magnetic saturation M_S (Am^2/kg) ±0.7	Constant $b\times10^{10}$ ±18%	Constant χ	Magnetocrystalline Anisotropy Constant K_1 (J/m^3)×10^5 ±9%		Magnetic saturation M_S (Am^2/kg) ±0.2	Constant $b\times10^{10}$ ±38%	Constant $a\times10^4$ *±2%*	Magnetocrystalline Anisotropy Constant K_1 (J/m^3)×10^5 ±21%		Magnetic saturation M_S (Am^2/kg) ±0.3	Constant $b\times10^{10}$ ±17%	Constant $a\times10^4$ *±12%*	Constant χ	Magnetocrystalline Anisotropy Constant K_1 (J/m^3)×10^5 ±8%
300	83.9	1.31	3.47		81.9	2.19	0.003	8.76		85.8	0.641	4.56	2.48		83.1	0.278	1.49	0.006	1.57
270	86.9	1.29	3.56		166.6	2.25	0.003	9.01		88.7	0.482	4.12	2.22		86.0	0.395	1.20	0.006	1.95
240	89.6	1.21	3.56		168.5	2.32	0.002	9.24		91.3	0.328	3.78	1.88		89.0	0.397	1.37	0.005	1.94
210	91.8	1.12	3.51		170.4	2.38	0.001	9.47		93.5	0.210	3.48	1.54		91.1	0.532	1.02	0.006	2.40
180	93.8	1.08	3.52		172.0	2.43	0.001	9.65		95.4	0.114	3.29	1.13		93.2	0.561	1.05	0.005	2.51
150	95.5	1.04	3.52		173.6	2.48	0.000	9.84		97.1	0.0463	3.05	0.749		95.1	0.606	1.02	0.005	2.67
120	96.9	1.03	3.55		174.9	2.53	0.000	10.0		98.6	0.0664	2.93	0.800		96.7	0.622	1.09	0.004	2.74
90	98.1	1.01	3.56		176.2	2.58	-0.001	10.2		99.8	0.135	2.78	1.29		97.9	0.676	0.994	0.004	2.90
60	99.1	1.00	3.57		177.0	2.61	-0.001	10.3		100.8	0.155	2.78	1.33		98.9	0.698	0.980	0.004	2.97

Note: R^2 values for all the above variants of Law of approach to saturation are >0.921

Magnetocrystalline anisotropy constant (K_1) analysis:

The table above shows the data obtained from curve fitting of experimental *MvH* plots in the case of MARS-56h milled powders. LAS A has the least amount of variation in data with ~4% variation in constant *b* values and ~2% variation in K_1 values. The M_S values also seem to closely match with the values obtained through *MvH* plots. LAS B also has relatively low variation in the data but a closer look at M_S values shows a massive jump of ~100% in M_S from 300 K to 270 K this indicates a force fit as the M_S values do not match the M_S values from the *MvH* curves. LAS C shows relatively high variation in the constant *b* value (~38%) and the K_1 value (~21%). Along with high variation in values we also witness a decrease in the K_1 value with decrease in temperature and this is not possible as we know M_S and H_C are related to K_1 and both M_S and H_C increase with decrease in temperature. LAS D also shows low variation in data with a ~17% variation in constant *b* values, ~12% variation in constant *a* values and ~8% variation in K_1 values. A low variation in constant *a* value indicates to us that there is uniform contribution to stress anisotropy from individual powders and this is supported by the metallurgical history of these powders which have been milled for 56 hours.

Using LAS D we estimate K_1 as 1.57×10^5 J/m^3 at 300 K. The figure below shows the dependence of K_1 on decreasing temperature. A trend of increasing K_1 with decreasing temperature is evident from the figure. K_1 increases from ~1.57×10^5 Am^2/kg at 300 K to ~2.97×10^5 Am^2/kg at 60 K an increase of ~90%.

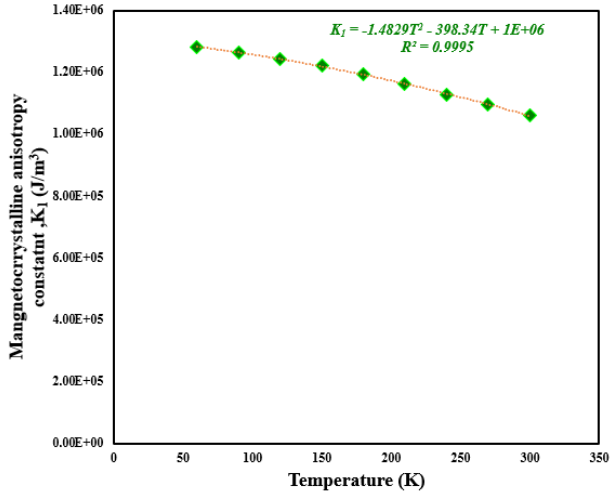

Figure 72.Magnetocrystalline anisotropy constant (K_1) vs Temperature (T)

5.4.4. Comparison of MARS Powders

Figure 71 below shows the *M-H* curves for the three elemental ferromagnetic powders. The inset shows the *M-H* curves in low magnetic field realm of ± 10 kA/m.

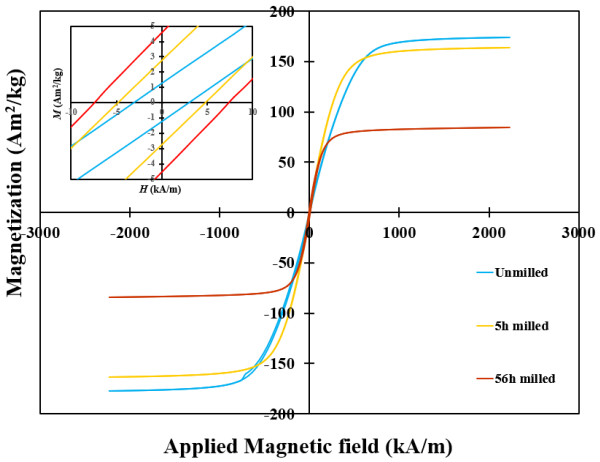

Figure 73.*M-H* curves for Maraging steel powders at 300 K

It is evident from the figure above that as the milling time increases, we see superior hard magnetic properties from the maraging steel powders. The figure below the comparison between the magnetocrystalline anisotropy constant (K_1) of different samples of MARS powders milled for increasing intervals of time.

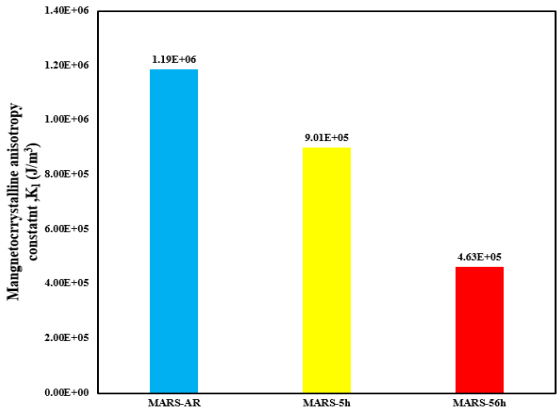

Figure 74.Comparision of K_1 of MARS powders

As K_1 is dependent on both M_S and H_C and here the M_S of the 56h milled powders here has decreased considerably, and quite similarly, the H_C value of the 5h milled powder has not increased much either, explaining the reason for the un-milled powders having the highest K_1 values. Here again, powders with considerably better hard magnetic properties have higher K_1 values than the other powders.

5.5 Relationship Between Magnetocrystalline Anisotropy Constant (K_1) Between Ferromagnetic Elemental Powders and Their Alloys

5.5.1. Pure Elemental Alloys

Figure 73 below shows the relationship between the K_1 of elemental powders and their alloys. A relationship between the K_1 of elemental powders and their alloys helps us to analyze the magnetic properties of the alloy powders having different compositions and can help characterize powders used for manufacturing of magnets with newer upcoming manufacturing technologies such as additive manufacturing.

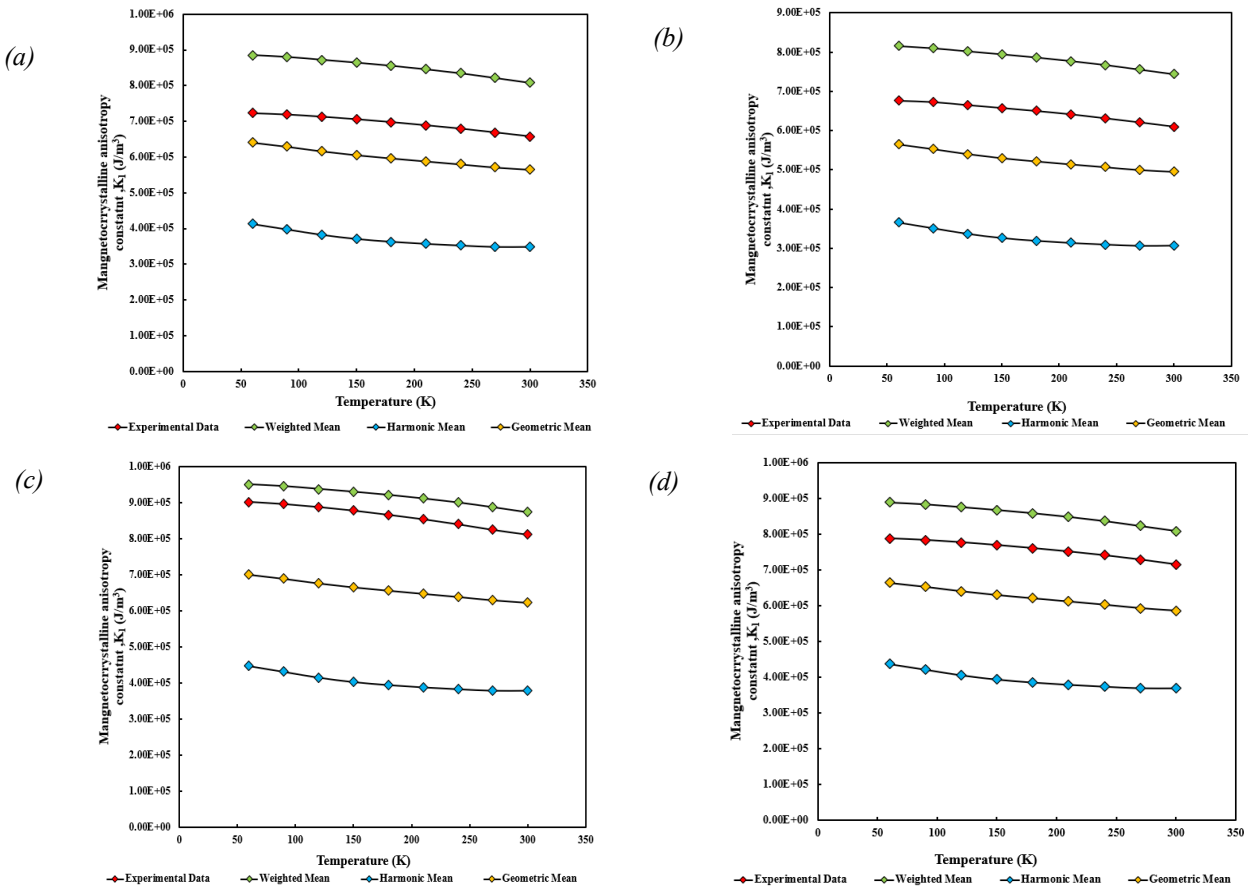

Figure 75.Relationship between K_1 of elemental powders and a)$Fe_{33.33}Ni_{33.33}Co_{33.33}$ b)$Fe_{30}Ni_{40}Co_{30}$ c) $Fe_{40}Ni_{30}Co_{30}$ d)$Fe_{30}Ni_{30}Co_{40}$

Figure 73 (a) shows the relationship between K_1 of elemental powders and the alloy having a composition $Fe_{33.33}Ni_{33.33}Co_{33.33}$ across a wide range of temperatures from 300 K room temperature cryogenic temperatures as low as 60 K. The red data plots show the magnetocrystalline anisotropy constant K_1 values obtained experimentally through *MvH* plots. The green data plots show the K_1

values obtained through weighted volumetric averages of the K_1 values of the individual elemental powders based on the composition of the alloy. The blue plots are the weighted harmonic averages of the individual elemental powders based on the composition of the alloy to account for the lower range K_1 values. The yellow plots are the weighted geometric averages of the individual elemental powders based on the composition of the alloy to account for the variation in data ranges. From figure 73 (a) it is evident that the K_1 values of the equiatomic alloy $Fe_{33.33}Ni_{33.33}Co_{33.33}$ are in close agreement to the values obtained by weighted volumetric averaging of the individual K_1 values of the elemental powders. The actual experimental value falls between the weighted mean and the geometric mean. The weighted mean acts as an upper limit for the values as it skews the data towards the higher-order terms and the geometric mean gives us a central tendency of the values, while the harmonic mean skews the values to the lower order values and gives us a lower limit this trend is visible in the case of all the alloys. The weighted volumetric mean gives a value of $\sim 8.1\times10^5$ J/m^{3,} and the actual experimental mean value gives $\sim 6.6\times10^5$ J/m^3 at 300 K. The values are lower than the calculated values, and this is expected as we see the trend of decreasing K_1 with increasing milling time in the case of maraging steel powders and is also seen throughout the literature [46]. All the alloys discussed in this section have been milled for 9 hours and we expect to see a lower actual value than the calculated value. Crystal structure which is related to the constant b in the law of approach to saturation is generally attributed as the reason for this decrease in K_1 as the crystallite size decreases as the milling time increases. It is also noticed that at lower milling times, K_1 values decrease significantly. Figure 73 (b) shows the relationship between K_1 of elemental powders and the alloy having composition $Fe_{30}Ni_{40}Co_{30}$ shows a strong similarity between the experimental values and the calculated weighted volumetric values. The weighted volumetric mean gives a value of $\sim 7.4\times10^5$ J/m^3 and the actual experimental mean value gives $\sim 6.1\times10^5$ J/m^3 at 300 K. The experimental values again are lower than the calculated value as expected. Similarly, in the case of the alloy $Fe_{40}Ni_{30}Co_{30,}$ we see a close relationship between the weighted value and the experimental value, as seen in figure 73 (c). The weighted volumetric mean gives a K_1 value of $\sim 8.7\times10^5$ J/m^3 and the actual experimental mean gives a value of $\sim 8.1\times10^5$ J/m^3 at 300 K, a lower actual value than the calculated value similar to the trend noticed for the other alloys. For the case of $Fe_{30}Ni_{30}Co_{40,}$ we see a similar trend wherein we see strong similarities between the calculated value of $\sim 8.1\times10^5$ J/m^3 and the actual experimental value $\sim 7.2\times10^5$ J/m^3 at 300 K in figure 73 (d). The plots also reveal that the trend for the K_1 values with decrease in

temperature from 300 K to 60 K is also similar to the trend of the calculated values albeit with the expected reduction in value on account of milling.

5.5.2. Maraging Steel

Figure 74 shows the graphical plots depicting the relationship between the magnetocrystalline anisotropy constant (K_1) of the elemental powders and their alloys in this case maraging steel. These powders are different from the previous cases as the maraging steel composition has other non-ferromagnetic elemental powders. The gas atomized maraging steel powders have a composition of 18.5 wt% Ni, 8.7 wt% Co, 4.9 wt% Mo, 0.7 wt% Ti, 0.1 wt% Al, 0.1 wt% Cr, 0.07 wt% Mn, 0.03 wt% Cu, 0.02 wt% Si, 0.01 wt% C. 0.01 wt% S, <0.01 wt% P and the remaining Fe (~67 wt%).

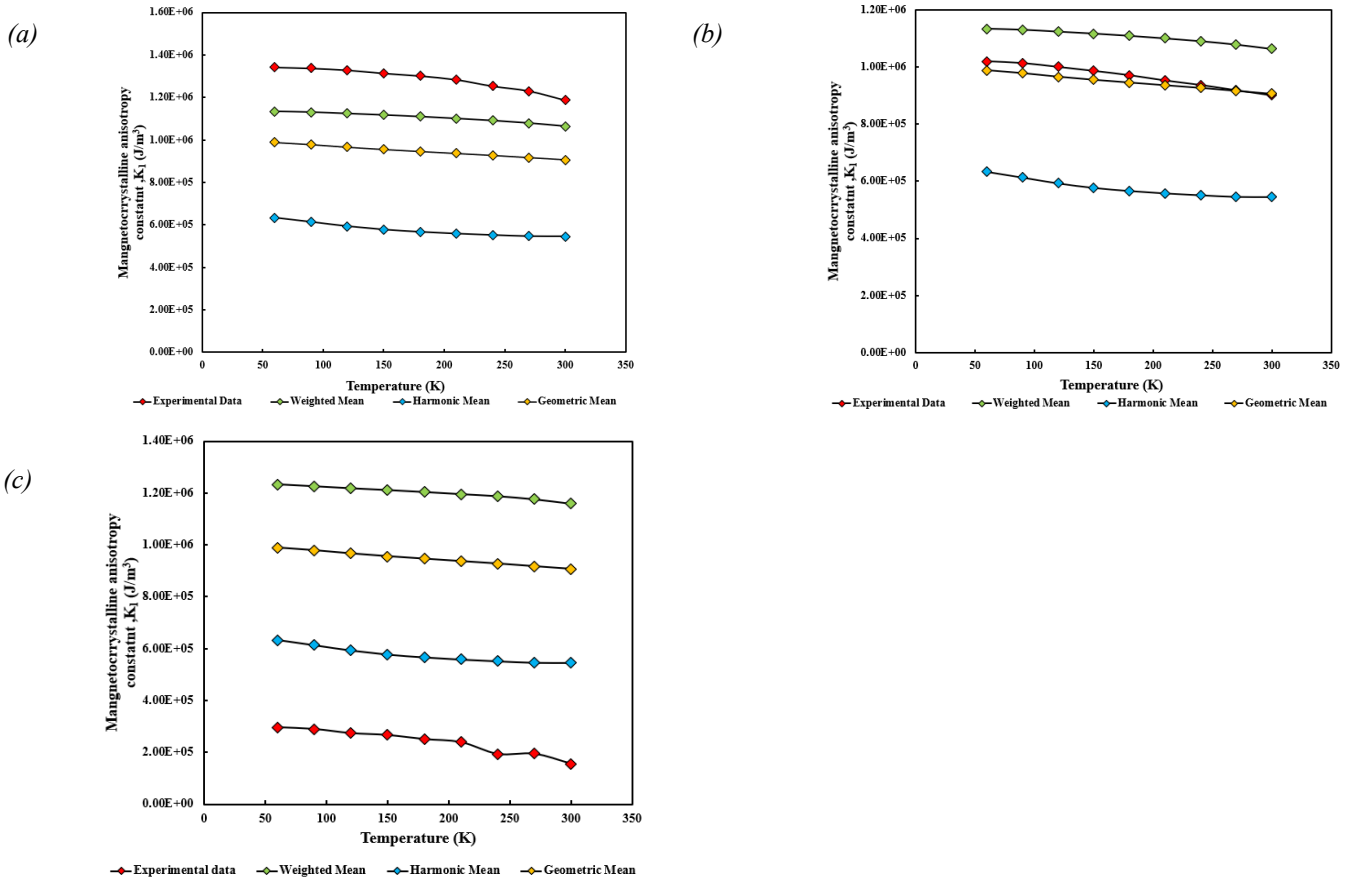

Figure 76. Relationship between K_1 of elemental powders and a) MARS-AR b) MARS-5h c) MARS-56h

Figure 74 (a) shows the varying plots of the experimental values, the weighted volumetric mean, the harmonic mean, and the geometric mean for the MARS- AR powders. These are gas atomized powders with no metallurgical history of having undergone milling, added to the fact

that these powders have a composition with other non-ferromagnetic elements. It is important to study these alloys as most commercial magnets have such compositions. It is observed from the plot that the experimental values are higher than the calculated weighted volumetric mean values. The experimental value of K_1 for the MARS-AR powder is ~12×10^5 J/m^{3,} while the calculated weighted volumetric value is ~10.6×10^5 J/m^3. The values seem to be relatively similar, but unlike the previous pure elemental alloys, the K_1 values are higher than the calculated values. This is most probably due to the effect of the presence of non-magnetic elements combined with the fact that these powders have not undergone milling.

Figure 74 (b) shows the plots for the case of MARS-5h. It is evident from the plots that the experimental values for this case are lower than the calculated value, as seen in previous pure elemental alloys. The experimental K_1 value at 300 K is ~9×10^5 J/m^3, while the calculated K_1 is ~10.6×10^5 J/m^3. The decrease in this K_1 value is as expected due to the effect of the 5h of milling on the constant *b*.

Figure 74 (c) shows the plots for MARS-56h milled powders. Here we see that there is a considerable decrease in magnetocrystalline anisotropy constant K_1 values. It is already known from the literature that an increase in milling time decreases the K_1 values as it affects the crystal structure, which is related to the constant b. In the 56h milled powders, we notice that the values are quite low compared to the weighted volumetric mean and is lower than the calculated harmonic mean. In the case of MARS-56 h powders, we have confirmed the presence of extraneous phases, and some of which may be non-magnetic and may have an influence on the magnetic anisotropy values. The plots also reveal the dependence of K_1 on decreasing temperature; similar to the previous cases, K_1 here increases with a decrease in temperature.

Chapter 6. Conclusions

The magnetic characterization of ferromagnetic elemental powders was carried out successfully. Determined M_S, H_C, and M_R. The M_S was estimated to be 217 ± 4 Am^2/kg, the H_C and M_R were approximated to ~1 ± ~1% kA/m and 1 Am^2/kg, respectively for Fe. The M_S, H_C and M_R were estimated to be 160 ±1 Am^2/kg, ~12 kA/m and 7 Am^2/kg respectively for Co, ~55 Am^2/kg, 3 ± ~1% kA/m and 2 Am^2/kg respectively for spherical Ni powders, ~54 Am^2/kg, ~9 ±1% kA/m and ~6 ±3% Am^2/kg for Ni Flake powders.

Magnetic characterization of pure elemental ternary alloys ($Fe_xCo_yNi_z$) was carried out to determine the M_S, H_C and M_R. The M_S, H_C, and M_R were estimated to be 137 ±1 Am^2/kg, ~3 ±1% kA/m, ~2 Am^2/kg respectively for $Fe_{33.33}Ni_{33.33}Co_{33.33}$, ~131 ±1 Am^2/kg, 2 ±1% kA/m and 1 Am^2/kg respectively for $Fe_{30}Ni_{40}Co_{30}$,~145 ±1 Am^2/kg, 5 ±1% kA/m and 3 Am^2/kg respectively for $Fe_{40}Ni_{30}Co_{30}$, ~138 Am^2/kg, ~5 kA/m and ~3 Am^2/kg respectively for $Fe_{30}Ni_{30}Co_{40}$.

Magnetic characterization of maraging steel powders was carried out to determine the M_S, H_C and M_R. The M_S, H_C and M_R were estimated to be 177±2 Am^2/kg, ~3 kA/m and 1 Am^2/kg respectively for MARS-AR (as received powders), ~165 ±1 Am^2/kg, ~5 kA/m and 3 Am^2/kg for MARS-5h milled powders and ~84 Am^2/kg, ~7 kA/m and ~5 Am^2/kg for MARS-56h milled powders.

Curve fitting of the experimental plots of these powders was conducted, and evaluations of different variations of Law of Approach to Saturation (LAS) were conducted to estimate the magnetocrystalline anisotropy (K_1). The K_1 at 300 K was estimated for the Fe powders as ~1.43×10^6 J/m^3, ~1.46×10^5 J/m^3 for Ni (spherical powders), ~2.30×10^5 J/m^3 for Ni (flake powders).

For the pure elemental alloys, the K_1 at room temperature (300 K) was estimated to be ~6.58×10^5 J/m^3 for $Fe_{33.33}Ni_{33.33}Co_{33.33}$, ~$6.1\times10^5$ J/m^3 for $Fe_{30}Ni_{40}Co_{30}$, ~8.11 J/m^3 for $Fe_{40}Ni_{30}Co_{30}$, ~7.15×10^5 J/m^3 $Fe_{30}Ni_{30}Co_{40}$.

For Maraging steel powders, the K_1 at room temperature (300 K) was estimated to be ~11.9 $\times 10^5$ J/m^3 for MARS-AR (As received), ~9.01×10^5 J/m^3 for MARS-5h milled, 1.57×10^5 J/m^3 for MARS-56h milled.

A relationship to estimate K_1 of alloys based of the K_1 values of elemental ferromagnetic powders was established. The use of weighted volumetric means to approximate K_1 values of un-milled powders and powders milled for less than 10 hours can be used to get a rough estimate of K_1 values of alloys.

Chapter 7. Future Work

Further work on Analysis of the magnetocrystalline anisotropy constant (K_1) of elemental powders milled for a specific duration, depending on the number of hours it takes to form an alloy and verify if values with a closer tolerance can be calculated.

Similarly a more in-depth study on the dependence of magnetocrystalline anisotropy constant (K_1) on the crystal structure, wherein simultaneous structural and magnetic characterization of the elements is carried out can help achieve a deeper understanding of K_1.

Study on how milling affects the alloy powders and analysis with shorter milling time intervals to establish a trend to predict the K_1 of the powders based on the duration of milling is another potential path to explore.

Magnetic characterization of parts manufactured using additive manufacturing and a study of how K_1 in the raw powders translates after fabrication into various magnetic components or parts would be useful in proving the practical application of this study.

Analyzing the effects of shape anisotropy and how it can be applied to manipulate and induce anisotropy in other magnetic materials other than Ni could prove to be groundbreaking.

References

[1] B. D. Cullity and C. D. Graham, "Magnetic Anisotropy," in *Introduction to Magnetic Materials*, Hoboken, New Jersey, Wiley, 2009, pp. 197-238.

[2] S. Kozawa, "Trends and problems in research of permanent magnets for motors: addressing scarcity problem of rare earth elements," *Science & Technology Trends,* no. 88, pp. 40-54, 2011.

[3] W. D. Callister Jr and D. D. Rethwisch, "Magnetic properties," in *Material Science and Engineering*, Hoboken, NJ, Wiley, 2014, pp. 804-836.

[4] R. A. McCurrie, "Soft magnetic alloys," in *Ferromagnetic Materials: Structure and Property*, San Diego, CA, Academic Press Inc, 1994, pp. 26-93.

[5] D. Jiles, "Domain processes," in *Introduction to Magnetism and Magnetic Materials*, Boca Raton,FL, CRC Press, 1991, pp. 147-194.

[6] T. M.Montazer, "Magnetic nanofinishes for textiles," in *Nano finishing of textile materials*, Woodhead Publishing, 2018, pp. 127-143.

[7] P. Weiss, "La variation du ferromagnetisme du temperature," *Comptes Rendus,* vol. 4, no. 1, pp. 847-873, 1906.

[8] D. Mukherjee, "Graduate Theses and Dissertations: Growth and characterization of epitaxial thin films and multiferroic heterostructures of ferromagnetic and ferroelectric materials," University of South Florida, Tampa, 2009.

[9] F. N. Bradley, Materials for Magnetic Functions, 1 ed., Indianapolis,IN: SAMS, 1971.

[10] R. James, "Magnetic alloys break the rules," *Nature,* vol. 521, no. 7552, p. 298–299, 2015.

[11] N.S.Akulov, "Über die magnetostriktion der eiseneinkristalle," *Zeitschrift für Physik,* vol. 52, no. 5-6, p. 389–405, 1929.

[12] G. Herzer, "The Random Anisotropy Model: A Critical Review And Update," in *NATO Advanced Research Workshop on Properties and Application of Nanocrystalline Alloys from Amorphous Precursors*, Budmerice, Slovakia, 2003.

[13] E. C. Stoner and E. P. Wohlfarth, "A mechanism of magnetic hysteresis in heterogeneous alloys," *IEEE Transactions on Magnetics,* vol. 27, no. 4, pp. 3475-3518, 1991.

[14] H. Lawton and K. Stewart, "Magnetization curves for ferromagnetic single crystals," *Proc. R. Soc. Lond. A,* vol. 193, no. 1, p. 72–88, 1948.

[15] R. Kohlhaas, W. Rocker and H. Lange, "Literaturverzeichnis," in *Magnetometrie und magnetokalorischer Effekt des Kobalts in der Umgebung der Curie-Temperatur*, vol. 15, Germany, VS Verlag für Sozialwissenschaften, 1962, pp. 14-20.

[16] N.S.Akulov, "Über den verlauf der magnetisierungskurve in starken feldern," *Zeitschrift Für Physik,* vol. 69, no. 11-12, p. 822–831, 1931.

[17] T. Holstein and H. Primakoff, "Field dependence of the intrinsic domain magnetization of a ferromagnet," *Physical Review,* vol. 58, no. 12, pp. 1098--1113, 1940.

[18] T. Holstein and H. Primakoff, "Magnetization Near Saturation in Polycrystalline Ferromagnets," *Physical Review,* vol. 59, no. 4, pp. 388--394, 1940.

[19] W. F. Brown Jr, "Theory of the Approach to Magnetic Saturation," *Physical Review,* vol. 58, no. 8, pp. 736--743, 1940.

[20] R. Polley and H. Becker, "Influence of internal strain on the law of approach to saturation for nickel," *Ann. Physik,* vol. 36, p. 625, 1940.

[21] R. Gans, "Über das magnetische Verhalten isotroper Ferromagnetika," *Annalen der Physik,* vol. 407, no. 1, pp. 28-44, 1932.

[22] J. F. Herbst and F. E. Pinkerton, "Law of approach to saturation for polycrystalline ferromagnets: Remanent initial state," *Physical Review B,* vol. 57, no. 17, pp. 10733--10739, 1998.

[23] L. Néel, "La loi d'approche en a: H et une nouvelle théorie de la dureté magnétique," *J. Phys. Radium,* vol. 9, no. 5, pp. 184-192, 1948.

[24] T. Huzimura, "Law of appraoch to saturation," *Science reports of the Research Institutes,Tohoku University. Ser. A, Physics, chemistry and metallurgy,* vol. 8, pp. 71-78, 1955.

[25] D. E. Grady, "Origin of the linear term in the expression for the approach," *Physical Review B,* vol. 4, no. 11, pp. 3982-3989, 1971.

[26] H. Zhang, D. Zeng and Z. Liu, "The law of approach to saturation in ferromagnets originating from the magnetocrystalline anisotropy," *Journal of Magnetism and Magnetic Materials,* vol. 322, no. 16, pp. 2375-2380, 2010.

[27] R. Grössinger, "A critical examination of the law of appraoch to saturation," *Physica Status Solidi (a),* vol. 66, no. 2, pp. 665-674, 1981.

[28] E. C. Devi and I. Soibam, "Law of approach to saturation in Mn–Zn ferrite nanoparticles," *Journal of Superconductivity and Novel Magnetism,* vol. 32, no. 5, p. 1293–1298, 2018.

[29] E. C. Devi and I. Soibam, "Magnetic properties and law of approach to saturation in Mn-Ni," *Journal of Alloys and Compounds,* vol. 772, pp. 920-924, 2019.

[30] J. Sternberk, "On the law of approach to saturation in manganese-magnesium ferrite," *Czech J Phys,* vol. 12, no. 6, p. 471–484, 1962.

[31] T. Utsunomiya, H. Nishizawa and K. Kaneta, "Effects of stress on the law of approach to saturation," *IEEE transactions on magnetics,* vol. 27, no. 3, pp. 3420-3425, 1991.

[32] H. Kronmuller and J. Ulner, "Micromagnetic theory of amorphous magnets," *Journal of magnetism and magnetic materials,* vol. 6, pp. 52-56, 1977.

[33] M. Fahnle and H. Kronmuller, "The Influence Of Spacially Random Magnetostatic, Magnetocrystalline, Magnetostrictive And Exchange Fluctuations On The Law Of Approach To Ferromagnetic Saturation Of Amorphous Ferromagnets," *Journal of magnetism and magnetic materials,* vol. 8, no. 2, pp. 149-156, 1977.

[34] M. Domann, H. Grimm and H. Kronmuller, "The high field magnetization curve of amorphous ferromagnetic alloys," *Journal of magnetism and magnetic materials,* vol. 2, no. 1-2, pp. 81-84, 1979.

[35] H. Grimm and H. Kronmuller, "Magnetic polarization of amorphous alloys in the approach to ferromagnetic saturation," *Journal of magnetism and magnetic materials,* Vols. 15-18, pp. 1411-1412, 1980.

[36] Z. Jin, W. Tang, J. Zhang, H. Qin and Y. Du, "Effective magnetic anisotropy of nanocrystalline Nd-Fe-Ti-N hard magnetic alloys," *The European physics journal B,* vol. 3, no. 1, p. 41–44, 1998.

[37] N. Ranvah, Y. Melikhov, I. C. Nlebedim, D. C. Jiles, J. E. Snyder and A. J. Moses, "Temperature dependence of magnetic anisotropy of germanium/cobalt cosubstituted cobalt ferrite," *Journal of applied physics,* vol. 105, no. 7, 2009.

[38] A. A. Paul, A. Rathi, G. V. Thotakura and T. V. Jayaraman, "Influence of milling atmosphere on the structure and magnetic properties of mechanically alloyed Fe40Co30Ni30," *Materials Chemistry and Physics,* vol. 258, 2020.

[39] A. Rathi, V. M. Meka and T. V. Jayaraman, "Synthesis of nanocrystalline equiatomic nickel-cobalt-iron alloy powders by mechanical alloying and their structural and magnetic characterization," *Journal of Magnetism and Magnetic Materials,* vol. 469, pp. 467-482, 2019.

[40] T. V. Jayaraman, A. Rathi and G. V. Thotakura, "Evaluation of the suitability of Fe40Co30Ni30 as a precursor for Fe-rich FeCoNi-based high-entropy semi-hard magnets," *Intermetallics,* vol. 119, 2020.

[41] T. V. Jayaraman, A. Rathi and G. V. Thotakura, "Phase evolution, structure, and magnetic characterization of mechanosynthesized Co40Fe30Ni30 medium-entropy alloy," *Intermetallics,* vol. 113, 2019.

[42] T. V. Jayaraman, G. V. Thotakura and A. Rathi, "Phase evolution, structure, and magnetic characterization of mechanosynthesized Ni40Fe30Co30 medium-entropy alloy," *Journal of Magnetism and Magnetic Materials,* vol. 489, p. 165466, 2019.

[43] G. V. Thotakura, R. Goswami and T. V. Jayaraman, "Influence on the structural and magnetic properties of the pre-alloyed gas-atomized maraging steel," in *Characterization of Minerals, Metals, and Materials 2020*, Springer, 2020, pp. 271-281.

[44] K. M. Krishnan, Fundamentals and Applications of Magnetic Materials, 1st ed., Oxford university press, 2016.

[45] R.M. Bozorth, Ferromagnetism, 3rd edn. IEEE Press, IEEE Press, 1993.

[46] J. A. Betancourt-Cantera, F. Sanchez-De Jesusb, A. M. Bolarin-Miro, G. Torres-Villasenor and L. G. Betancour-Cantera, "Magnetic properties and crystal structure of elemental cobalt powder modified by high-energy ball milling," *Journal of Materials Research and Technology,* vol. 8, pp. 4995-5003, 2019.